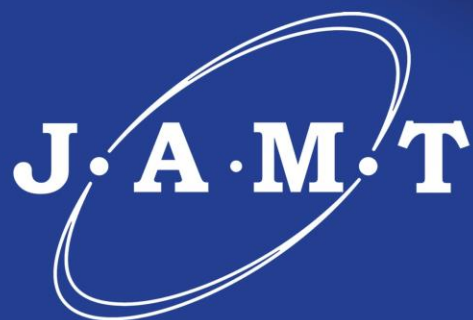


ISSN 2782-2192 (Print)

ISSN 2782-2206 (Online)

Journal of Advanced Materials and Technologies

J · A · M · T



**Vol. 6, No. 1.
2021**



ISSN 2782-2192 (Print)
ISSN 2782-2206 (Online)
DOI: 10.17277/issn.2782-2192



Journal of Advanced Materials and Technologies

**Vol. 6, No. 1.
2021**

**Том 6, № 1.
2021**

16+

© Tambov State Technical University, Tambov, Russian Federation, 2021
© Merzhanov Institute of Structural Macrokinetics and Materials Sciences of Russian Academy of Sciences,
Chernogolovka, Moscow region, Russian Federation, 2021
© Design by TSTU Publishing, 2021

Journal of Advanced Materials and Technologies

Научный журнал

«Journal of Advanced Materials and Technologies» – научный рецензируемый журнал, посвященный исследованиям в области материаловедения и примыкающих вопросов физики и механики материалов.

Журнал «Journal of Advanced Materials and Technologies» публикует оригинальные статьи, обзоры, краткие сообщения, содействующие развитию современной науки о материалах, подготовленные как известными учеными, так и молодыми специалистами.

Миссия журнала – обмен актуальной научной информацией в области теоретических и практических исследований и моделирования процессов, связанных с получением, определением свойств новых материалов, в том числе наноразмерных, и их применения.

Средство массовой информации периодическое печатное издание, журнал «Journal of Advanced Materials and Technologies» зарегистрировано Федеральной службой по надзору в сфере связи, информационных технологий и массовых коммуникаций. Регистрационный номер СМИ ПИ № ФС 77-74804 от 25.01.2019

ISSN 2782-2192 (Print), ISSN 2782-2206 (Online)

| | |
|----------------------------------|--|
| Сведения о переименовании | «Advanced materials & technologies» (2016–2021), Print ISSN 2414-4606, Online ISSN 2541-8513 |
| Журнал основан | 2016 г. |
| Периодичность | 4 раза в год |
| Учредители | Федеральное государственное бюджетное образовательное учреждение высшего образования «Тамбовский государственный технический университет» (ФГБОУ ВО «ТГТУ»), Федеральное государственное бюджетное учреждение науки Институт структурной макрокинетики и проблем материаловедения им. А.Г. Мержанова Российской академии наук (ИСМАН) |
| Адреса учредителей | ФГБОУ ВО «ТГТУ»: 392000, Тамбовская обл., г. Тамбов, ул. Советская, д. 106, ИСМАН: 142432, Московская обл., г. Черноголовка, ул. Академика Осипьяна, д. 8 |
| Адрес издателя | ФГБОУ ВО «ТГТУ»: 392000, Тамбовская обл., г. Тамбов, ул. Советская, д. 106 |
| Адрес редакции | 392000, Тамбовская обл., г. Тамбов, ул. Советская, д. 106 |
| Контакты | Тел.: +7 4752 63 03 91; amt.journal@yandex.ru |
| Типография | Издательство ФГБОУ ВО «ТГТУ»: 392032, Тамбовская обл., г. Тамбов, ул. Мичуринская, д. 112А Тел.: +7 4752 63 03 91; +7 4752 63 07 46 |
| Сайт | http://amt.tstu.ru/ |
| E-mail | amt.journal@yandex.ru |
| Телефон | +7 4752 63 92 93 |
| Подписка | Электронная версия журнала находится в свободном доступе на сайте журнала, а также в базах данных открытого доступа. Подписку на печатную версию журнала можно оформить по объединенному каталогу «Пресса России». Подписной индекс – 80453 |
| Главный редактор | Алымов Михаил Иванович, д.т.н, профессор, член-корреспондент РАН |

Journal of Advanced Materials and Technologies

Scientific Journal

“Journal of Advanced Materials and Technologies” is a peer-reviewed scientific journal of research in materials science and related issues in materials physics and mechanics.

“Journal of Advanced Materials and Technologies” publishes original articles, reviews, short reports written by both renowned scientists and young researchers that contribute to the development of modern materials science.

The journal promotes research and exchange of information in the field of theoretical and practical research into materials science, modeling of processes involved in the creation of new materials, including nanomaterials, their properties and application.

ISSN 2782-2192 (Print), ISSN 2782-2206 (Online)

| | |
|---------------------------------|---|
| Rename information | Advanced materials & technologies (2016-2021), Print ISSN 2414-4606, Online ISSN 2541-8513 |
| The journal was founded | 2016 |
| Publication frequency | 4 times per year |
| Founders | Tambov State Technical University (TSTU), Merzhanov Institute of Structural Macrokinetics and Materials Sciences of Russian Academy of Sciences (ISMAN) |
| Postal address | TSTU: 106, Sovetskaya St., Tambov, 392000 ISMAN: 8, Academician Osipyan St., Moscow region, Chernogolovka, 142432 |
| Editorial office address | 106, Sovetskaya St., Tambov, 392000 |
| Contacts | Phone +7 4752 63 03 91; amt.journal@yandex.ru |
| Printing House | TSTU Publishing, 112A, Michurinskaya St., Tambov, 392032 Phone +7 4752 63 03 91; +7 4752 63 07 46 |
| Website | http://amt.tstu.ru/ |
| E-mail | amt.journal@yandex.ru |
| Phone | +7 4752 63 92 93 |
| Subscription | The electronic version of the Journal is freely available on the journal’s website, as well as in open access databases. The subscription index for the Journal printed version in the unified catalog “Press of Russia” is 80453 |
| Editor-in-Chief | Mikhail I. Alymov, D.Sc.(Engineering), Professor, Corresponding Member of the Russian Academy of Sciences |

EDITORS

- Mikhail I. Alymov**, D.Sc. (Engineering), Professor, Corresponding Member of the Russian Academy of Sciences (RAS), Director of Merzhanov Institute of Structural Macrokineitics and Materials Sciences RAS (ISMAN), Chernogolovka, Moscow Region, Russian Federation
- Mikhail N. Krasnyansky**, D.Sc. (Engineering), Professor, Rector of Tambov State Technical University (TSTU), Tambov, Russian Federation
- Alexey G. Tkachev**, D.Sc. (Engineering), Professor, Head of Department of Technologies and Methods of Nanoproducts Manufacturing, TSTU, Tambov, Russian Federation
- Irina V. Burakova**, Ph.D., Associate Professor of Department of Technologies and Methods of Nanoproducts Manufacturing, TSTU, Tambov, Russian Federation
- Imran Ali**, PhD, FRSC, Professor, Department of Chemistry, Jamia Millia Islamia (Central University), New Delhi, India
- Vyacheslav M. Buznik**, D.Sc. (Chemistry), Professor, RAS Academician, All-Russian Scientific Research Institute of Aviation Materials, Moscow, Russian Federation
- Alexander G. Divin**, D.Sc. (Engineering), Associate Professor, Head of Department of Mechatronics and Technological Measurements, TSTU, Tambov, Russian Federation
- Tatyana P. Dyachkova**, D.Sc. (Chemistry), Professor, Director of Center for Collective Use of Scientific Equipment “Production and Application of Multifunctional Nanomaterials”, TSTU, Tambov, Russian Federation
- Yury I. Golovin**, D.Sc. (Engineering), Professor, Director of Center for Nanotechnology and Nanomaterials, Derzhavin Tambov State University, Tambov, Russian Federation
- Jesus Iniesta Valcarcel**, Ph.D., Associate Professor, Department of Physical Chemistry, University of Alicante, Alicante, Spain
- Ruslan Kh. Khamizov**, D.Sc. (Chemistry), Professor, Head of Laboratory of Sorption Methods, Vernadsky Institute of Geochemistry and Analytical Chemistry of RAS, Moscow, Russian Federation
- Mikhail L. Kheifetz**, D.Sc. (Engineering), Professor, Director of Institute of Applied Physics of National Academy of Science of Belarus, Minsk, Belarus
- Roman B. Morgunov**, D.Sc. (Physics and Mathematics), Professor, Leading Researcher, Institute of Problems of Chemical Physics RAS, Chernogolovka, Moscow Region, Russia
- Fadei F. Komarov**, D.Sc. (Physics and Mathematics), Professor, Corresponding Member of the National Academy of Sciences of Belarus, Head of Elionics Laboratory at A. N. Sevchenko Institute of Applied Physical Problems of Belarusian State University, Minsk, Belarus
- Stephane Mangin**, Ph.D., Professor, Physics of Matter and Materials Department, Institute Jean Lamour, University of Lorraine, Nancy, France
- Vladimir F. Pershin**, D.Sc. (Engineering), Professor, Professor at the Department of Technologies and Methods of Nanoproducts Manufacturing, TSTU, Tambov, Russian Federation
- Dimitar Stavrev**, D. Sc. (Engineering), Professor, Professor of Department of Materials Science at the Technical University of Varna, Varna, Bulgaria
- Alexander M. Stolin**, D. Sc. (Physics and Mathematics), Professor, Head of Laboratory, ISMAN RAS, Chernogolovka, Moscow Region, Russian Federation
- Yoshifumi Tanimoto**, Ph.D., Professor, Hiroshima University, Japan
- Vener A. Valitov**, D. Sc. (Engineering), Leading Researcher, Institute for Metals Superplasticity Problems of the Russian Academy of Sciences, Ufa, Russian Federation
- Sergey M. Arakelian**, D.Sc. (Physics and Mathematics), Professor, Head of the Department of Physics and Applied Mathematics, Vladimir State University, Vladimir, Russian Federation
- Arif A. Babaev**, D.Sc. (Physics and Mathematics), Professor, Head of the Laboratory of Optical Phenomena in Condensed Matter, Institute of Physics of Dagestan Scientific Center of Russian Academy of Sciences, Makhachkala, Republic of Dagestan, Russian Federation
- Evgeniy I. Terukov**, D.Sc. (Engineering), Professor, Deputy Director for Science of R&D Center of Thin-Film Technology for Energetics under Ioffe Institute, St. Petersburg, Russian Federation
- Valeriy Yu. Dolmatov**, D.Sc. (Engineering), Head of Research Laboratory at the “Special Construction and Technology Bureau “Technolog”, St. Petersburg, Russian Federation
- Valeriy V. Savin**, D.Sc. (Physics and Mathematics), Leading Researcher, Head of the Laboratory of Physical Materials Science, International Research Center “X-ray Coherent Optics”, Immanuel Kant Baltic Federal University, Kaliningrad, Russian Federation
- Gennady E. Selyutin**, Ph.D., Associate Professor, Senior Researcher, Federal Research Center “Krasnoyarsk Science Center” of Siberian Branch of the Russian Academy of Sciences, Krasnoyarsk, Russian Federation
- Vladimir V. Petrov**, D.Sc. (Physics and Mathematics), Professor, Saratov State University, Saratov, Russian Federation
- Yury E. Kalinin**, D.Sc. (Physics and Mathematics), Professor, Voronezh State Technical University, Voronezh, Russian Federation
- Vladimir S. Sevostyanov**, D.Sc. (Engineering), Professor, Head of the Department “Technological Complexes, Machines and Mechanisms”, V.G. Shukhov Belgorod State Technological University, Belgorod, Russian Federation
- Victor M. Mukhin**, D.Sc. (Engineering), Professor, D. Mendeleev University of Chemical Technology of Russia, Moscow, Russian Federation
- Vladimir D. Vermel**, D.Sc. (Engineering), Professor, Head of the Scientific and Technical Center of the Scientific and Production Complex, Central Aerohydrodynamic Institute, Zhukovsky, Moscow Region, Russian Federation
- Nadezhda V. Usoltseva**, D.Sc. (Chemistry), Professor, Director of the Research Institute of Nanomaterials, Ivanovo State University, Ivanovo, Russian Federation
- Lyaylya A. Abdrakhmanova**, D.Sc. (Engineering), Professor, Kazan State University of Architecture and Engineering, Kazan, Russian Federation
- Vyacheslav A. Sergeev**, D.Sc. (Engineering), Professor, Director of the Ulyanovsk branch of Kotelnikov Institute of Radioengineering and Electronics of Russian Academy of Science, Ulyanovsk, Russian Federation
- Irina V. Zaporotskova**, D.Sc. (Physics and Mathematics), Professor, Director of the Institute of Priority Technologies, Volgograd State University, Volgograd, Russian Federation
- Vladimir E. Guteran**, Ph.D., Professor, Leading Researcher, Southern Federal University, Rostov-on-Don, Russian Federation
- Stepan N. Kalmykov**, D.Sc. (Chemistry), Professor, Corresponding Member of the Russian Academy of Sciences, Dean of the Faculty of Chemistry at the Lomonosov Moscow State University, Moscow, Russian Federation
- Vladimir I. Kodolov**, D.Sc. (Chemistry), Professor, Kalashnikov Izhevsk State Technical University, Izhevsk, Russian Federation
- Valeria S. Tafintseva**, Researcher, Department of Physics, Faculty of Science and Engineering, Norwegian University of Life Sciences, Norway
- Vyacheslav M. Tyutyunik**, D.Sc. (Engineering), Professor, Director General of International Nobel Information Centre (INIC), Ltd., TSTU, Tambov, Russian Federation
- Translator:** Natalia A. Gunina, Ph.D., Associate Professor, Head of Department of International Professional and Scientific Communication, TSTU, Tambov, Russian Federation
- Computer layout:** Olga V. Mochalina, TSTU, Tambov, Russian Federation

СОВЕТ РЕДАКТОРОВ

- Альмов Михаил Иванович**, д.т.н., профессор, член-корреспондент РАН, директор Института структурной макрокинетики и материалаоведения им. А.Г. Мерджанова РАН (ИСМАН), г. Черноголовка, Московская область, Россия
- Краснянский Михаил Николаевич**, д.т.н., профессор, ректор, ФГБОУ ВО «Тамбовский государственный технический университет» (ФГБОУ ВО «ТГТУ»), г. Тамбов, Россия
- Ткачев Алексей Григорьевич**, д.т.н., профессор, заведующий кафедрой «Техника и технологии производства нанопродуктов», ФГБОУ ВО «ТГТУ», г. Тамбов, Россия
- Буракова Ирина Владимировна**, к.т.н., доцент, доцент кафедры «Техника и технологии производства нанопродуктов», ФГБОУ ВО «ТГТУ», г. Тамбов, Россия
- Али Иман**, PhD, FRSC, профессор кафедры химии, Джамя Миллия Исламия (Центральный университет), г. Нью-Дели, Индия
- Бузник Вячеслав Михайлович**, д.х.н., профессор, академик РАН, Всероссийский научно-исследовательский институт авиационных материалов, г. Москва, Россия
- Дивин Александр Георгиевич**, д.т.н., доцент, заведующий кафедрой «Мехатроника и технологические измерения», ФГБОУ ВО «ТГТУ», г. Тамбов, Россия
- Дьячкова Татьяна Петровна**, д.х.н., профессор, директор центра коллективного пользования научным оборудованием «Получение и применение полифункциональных наноматериалов», ФГБОУ ВО «ТГТУ», г. Тамбов, Россия
- Головин Юрий Иванович**, д.ф.-м.н., профессор, директор НИИ «Нанотехнологии и наноматериалы» ФГБОУ ВО «Тамбовский государственный университет имени Г. Р. Державина», г. Тамбов, Россия
- Иньеста Хесус Валькарсель**, PhD, доцент кафедры физической химии Университета Аликанте, г. Аликанте, Испания
- Хамизов Руслан Хажсетович**, д.х.н., профессор, заведующий лабораторией сорбционных методов Института геохимии и аналитической химии им. В.И. Вернадского РАН, г. Москва, Россия
- Хейфец Михаил Львович**, д.т.н., профессор, директор института, ГНУ «Институт прикладной физики НАН Беларуси», г. Минск, Беларусь
- Моргунов Роман Борисович**, д.ф.-м.н., профессор, главный научный сотрудник, Институт проблем химической физики РАН, г. Черноголовка, Московская область, Россия
- Комаров Фадей Фадеевич**, д.ф.-м.н., профессор, член-корреспондент Национальной академии наук Республики Беларусь, заведующий лабораторией эллионики, НИУ Институт прикладных физических проблем имени А. Н. Севченко Белорусского государственного университета, г. Минск, Беларусь
- Мангин Стефан**, PhD, профессор кафедры физики материи и материалов Института Жана Ламура, Университет Лотарингии, Нанси, Франция
- Першин Владимир Федорович**, д.т.н., профессор, профессор кафедры «Техника и технологии производства нанопродуктов», ФГБОУ ВО «ТГТУ», г. Тамбов, Россия
- Ставрев Димитр**, д.т.н., профессор, профессор кафедры «Материаловедения», Варненский технический университет, г. Варна, Болгария
- Столин Александр Моисеевич**, д.ф.-м.н., профессор, заведующий лабораторией, ИСМАН РАН, Московская область, г. Черноголовка, Россия
- Танимото Есифуми**, PhD, профессор, Хиросимский университет, Япония
- Валитов Венер Анварович**, д.т.н., ведущий научный сотрудник, ФГБУН «Институт проблем сверхпластичности металлов» РАН, г. Уфа, Республика Башкортостан, Россия
- Аракелян Сергей Мартиросович**, д.ф.-м.н., профессор, заведующий кафедрой физики и прикладной математики, Владимирский государственный университет им. А.Г. и Н.Г. Столетовых, г. Владимир, Россия
- Бабаев Ариф Азимович**, д.ф.-м.н., профессор, заведующий лабораторией оптических явлений в конденсированных средах ФГБУН «Институт физики им. Х. И. Амирханова» ДНЦ РАН, г. Махачкала, Республика Дагестан, Россия
- Теруков Евгений Иванович**, д.т.н., профессор, заместитель генерального директора по научной работе ООО «НТЦ тонкопленочных технологий в энергетике при ФТИ им. А.Ф. Иоффе», г. Санкт-Петербург, Россия
- Долматов Валерий Юрьевич**, д.т.н., начальник научно-исследовательской лаборатории, ФГУП «Специальное конструкторско-технологическое бюро «Технолог», г. Санкт-Петербург, Россия
- Савин Валерий Васильевич**, д.ф.-м.н., ведущий научный сотрудник, заведующий лабораторией физического материаловедения МНИЦ «Когерентная рентгеновская оптика для установок «Мегасайенс», ФГАОУ ВО «Балтийский федеральный университет имени Иммануила Канта», г. Калининград, Россия
- Селютин Геннадий Егорович**, к.ф.-м.н., доцент, старший научный сотрудник, Институт химии и химической технологии Сибирского отделения Российской академии наук ФИЦ КИХ СО РАН, г. Красноярск, Россия
- Петров Владимир Владимирович**, д.ф.-м.н., профессор, Саратовский национальный исследовательский университет имени Н. Г. Чернышевского, г. Саратов, Россия
- Калинин Юрий Егорович**, д.ф.-м.н., профессор, Воронежский государственный технический университет, г. Воронеж, Россия
- Севостьянов Владимир Семенович**, д.т.н., профессор, заведующий кафедрой «Технологические комплексы, машины и механизмы», ФГБОУ ВО «Белгородский государственный технологический университет имени В. Г. Шухова», г. Белгород, Россия
- Мухин Виктор Михайлович**, д.т.н., профессор, ФГБОУ ВО «Российский химико-технологический университет имени Д.И. Менделеева», г. Москва, Россия
- Вермель Владимир Дмитриевич**, д.т.н., профессор, начальник Научно-технического центра научно-производственного комплекса, ГИЦ ФГУП «Центральный аэрогидродинамический институт имени профессора Н.Е. Жуковского», Московская область, г. Жуковский, Россия
- Усольцева Надежда Васильевна**, д.х.н., профессор, директор НИИ наноматериалов, Ивановский государственный университет, г. Иваново, Россия
- Абдрахманова Ляйля Абдулловна**, д.т.н., профессор, Казанский государственный архитектурно-строительный университет, г. Казань, Россия
- Сергеев Вячеслав Андреевич**, д.т.н., профессор, директор Ульяновского филиала ФГБУН «Институт радиотехники и электроники имени В. А. Котельникова» РАН, г. Ульяновск, Россия
- Запороцкова Ирина Владимировна**, д.ф.-м.н., профессор, директор института приоритетных технологий, Волгоградский государственный университет, г. Волгоград, Россия
- Гутерман Владимир Ефимович**, д.х.н., профессор, главный научный сотрудник, ФГАОУ ВО «Южный федеральный университет», г. Ростов-на-Дону, Россия
- Калмыков Степан Николаевич**, д.х.н., профессор, член-корреспондент РАН, декан химического факультета Московского государственного университета имени М. В. Ломоносова, г. Москва, Россия
- Кодолов Владимир Иванович**, д.х.н., профессор, Ижевский государственный технический университет имени М. Т. Калашникова, г. Ижевск, Россия
- Тафинцева Валерия Сергеевна**, Ph.D., научный сотрудник, кафедра физики, факультет науки и технологий, Норвежский университет естественных наук, Норвегия
- Тютюнник Вячеслав Михайлович**, д.т.н., профессор, генеральный директор ООО «Международный информационный Нобелевский центр» (МИНЦ), ФГБОУ ВО «ТГТУ», г. Тамбов, Россия
- Переводчик:** Гунина Наталия Александровна, к.ф.н., заведующий кафедрой «Международная научная и профессиональная коммуникация», ФГБОУ ВО «ТГТУ», г. Тамбов, Россия
- Компьютерный дизайн и верстка:** Мочалина Ольга Викторовна, ФГБОУ ВО «ТГТУ», г. Тамбов, Россия

CONTENTS

Short communications

Nobelistics

- Tyutyunnik V.M.** Graphene breakthrough into future technology: the 2010 Nobel Prize in Physics Laureate Sir Konstantin Sergeevich Novoselov 6

Original papers

Nanostructured, nanoscale materials and nanodevices

- Kulnitskiy B.A., Perezhogin I.A., Batov D.V., Blank V.D., Alshevskiy Yu.L.** High resolution transmission electron microscopy analysis of conical carbon nanotubes formed in the high isostatic pressure apparatus..... 10

Manufacturing processes and systems

- Kheifetz M.L.** Design of mechatronic engineering systems in digitalized traditional and additive manufacturing 18

Materials for energy and environment, next-generation photovoltaics, and green technologies

- Mukhin V.M.** Anthracite-based activated carbons for the efficient solution of important environmental problems 30

- Lazarev S.I., Kovaleva O.A., Khorokhorina I.V., Khromova T.A., Kovalev S.V.** Studies of the pore space of the UPM-K, UAM-50, UAM-100 composite ultrafiltration membrane 42

Reviews

Nanostructured, nanoscale materials and nanodevices

- Dolmatov V.Yu., Shames A.I., Ōsawa E., Vehanen A., Myllymäki V., Dorokhov A.O., Martchukov V.A., Kozlov A.C., Naryzhny S.Yu., Smirnova A.Z.** Detonation nanodiamonds: from synthesis theory to application practice..... 54

СОДЕРЖАНИЕ

Краткие сообщения

Нобелистика

- Тютюнник В. М.** Графеновый прорыв к технологии будущего: лауреат Нобелевской премии по физике 2010 года Сэр Константин Сергеевич Новосёлов..... 6

Оригинальные статьи

Наноструктурированные, наномасштабные материалы и наноустройства

- Кульницкий Б. А., Пережогин И. А., Батов Д. В., Бланк В. Д., Альшевский Ю. Л.** Электронномикроскопический анализ высокого разрешения конусных углеродных нанотрубок, формируемых в аппарате высокого изостатического давления 10

Производственные процессы и системы

- Хейфец М. Л.** Проектирование мехатронных технологических комплексов при цифровизации традиционного и аддитивного производства 18

Материалы для энергетики и окружающей среды, фотоэлектрическая энергия следующего поколения и зеленые технологии

- Мухин В. М.** Активные угли на основе антрацита для эффективного решения важных экологических проблем ... 30

- Лазарев С. И., Ковалева О. А., Хорохорина И. В., Хромова Т. А., Ковалев С. В.** Исследования порового пространства композитной ультрафильтрационной мембраны УПМ-К, УАМ-50, УАМ-100 42

Обзоры

Наноструктурированные, наномасштабные материалы и наноустройства

- Долматов В. Ю., Шамес А. И., Осава Э., Веханен А., Мюллюмяки В., Дорохов А. О., Марчуков В. А., Козлов А. С., Нарыжный С. Ю., Смирнова А. З.** Детонационные наноалмазы: от теории синтеза до практики применения 54

Short communications
Nobelistics

УДК 06.068+929

DOI: 10.17277/jamt.2021.01.pp.006-009

**Graphene breakthrough into future technology:
the 2010 Nobel Prize in Physics Laureate
Sir Konstantin Sergeevich Novoselov**

Vyacheslav M. Tyutyunnik ✉

*Tambov State Technical University, 106, Sovetskaya St., Tambov 392000, Russian Federation,
International Nobel Information Centre (INIC), 30-6, Pervomaiskaya Sq., Tambov 392002, Russian Federation*

✉ vmtutyunnik@gmail.com

Abstract: The paper explores the research work of one of the youngest winners of the 2010 Nobel Prize in Physics, Konstantin Sergeevich Novoselov (born 23.08.1974). Since 2004 when the single-atom graphene was extracted and the research findings were published for the first time, the graphene breakthrough has been made. The paper focuses on the main milestones of Novoselov's biography and analyzes his publishing activity between 2004 and 2018. The data confirming the highest number of citation of Novoselov's publications in the world's leading scientific journals are presented. Novoselov's main scientific awards are listed.

Keywords: 2010 Nobel Prize in Physics; Konstantin Sergeevich Novoselov; grapheme; publishing activity; citation; technologies of the future.

For citation: Tyutyunnik VM. Graphene Breakthrough into Future Technology: The 2010 Nobel Prize in Physics Laureate Sir Konstantin Sergeevich Novoselov. *Journal of Advanced Materials and Technologies*. 2021;6(1):6-9. DOI: 10.17277/jamt.2021.01.pp.006-009

**Графеновый прорыв к технологии будущего:
лауреат Нобелевской премии по физике 2010 года
Сэр Константин Сергеевич Новосёлов**

В. М. Тютюнник ✉

*Тамбовский государственный технический университет,
ул. Советская, 106, Тамбов 392000, Российская Федерация,
Международный Информационный Нобелевский Центр (МИНЦ),
Первомайская площадь, 30-6, Тамбов 392002, Российская Федерация*

✉ vmtutyunnik@gmail.com

Аннотация: Рассмотрена деятельность одного из самых молодых лауреатов Нобелевской премии по физике 2010 г. Константина Сергеевича Новосёлова (род. 23.08.1974). Показано, что после получения одноатомной плёнки графена и первой публикации 2004 г., в мире начался графеновый прорыв к технологии будущего. Описаны основные вехи биографии Новосёлова, проанализирована его публикационная активность в период 2004 – 2018 гг., приведены данные, свидетельствующие о самом высоком уровне цитируемости публикаций Новосёлова в ведущих научных журналах мира. Перечислены основные научные награды, увлечения Новосёлова.

Ключевые слова: Нобелевская премия по физике 2010 года; Константин Сергеевич Новосёлов; графен; публикационная активность; цитируемость; технологии будущего.

Для цитирования: Tyutyunnik VM. Graphene Breakthrough into Future Technology: The 2010 Nobel Prize in Physics Laureate Sir Konstantin Sergeevich Novoselov. *Journal of Advanced Materials and Technologies*. 2021;6(1):6-9. DOI: 10.17277/jamt.2021.01.pp.006-009

Carbon in the form of two three-dimensional allotropic modifications – graphite and diamond – has been used in everyday life, in science and technology since ancient times. At the end of the 20th century, one-dimensional nanotubes and zero-dimensional fullerenes were added to them. This resulted in the rapid development of scientific research and technologies based on them [1–5]. However, it was still impossible to produce only a two-dimensional modification of carbon – graphene. Meanwhile, the research into mesoscopic physics (mesoscopy), as one of the most interesting branches of condensed matter physics, and nanotechnology showed convincingly that such a modification was possible.

Graphene consists of ultrathin layers (one atom thick) of carbon atoms linked into a hexagonal structure (consisting of hexagons with common sides). It is the thinnest and, at the same time, the most durable material with excellent conductive properties. In terms of thermal conductivity, it surpasses all materials known to date. Two-dimensional graphene layers are almost transparent, but extremely dense and impenetrable even for monoatomic helium molecules.

The theoretical study of graphene began long before the production of real samples of the material, since graphene is the basis for constructing a three-dimensional crystal of ordinary graphite. However, it was not possible to extract graphene experimentally for a long time. The discovery of carbon nanotubes revived an interest in it. Attempts to produce graphene attached to another material began with experiments using a simple pencil lead, and continued using an atomic force microscope for mechanical removing layers of graphite. Previously it had been shown theoretically that a free ideal two-dimensional film cannot be produced due to instability caused by folding or twisting). It was made possible only in 2004, when K.S. Novoselov and A.K. Geim (in collaboration with six other researchers) published an epoch-making article in the *Science* journal [6], where they reported on the production of graphene on an oxidized silicon substrate using the micromechanical lamination technology. Later, exfoliation and graphite intercalation were used most successfully. The initial reports of Novoselov and Geim about the separation of one atomic layer from the graphite crystal were not taken seriously, and the journals refused to publish their findings. It was only in October 2004, when a real graphene boom began – a breakthrough to the technology of the future. Six years had passed before the 2010 Nobel Prize in Physics was awarded to two

MIPT graduates, Novoselov and Geim, “for fundamental experiments with two-dimensional material graphene” (Fig. 1) [7, 8].

In the Nobel lecture, Novoselov compared two-dimensional graphene with E.E. Abbott’s “Flatland” and gave a detailed analysis of the properties and applications of this unusual crystal [9].



Konstantin Sergeevich Novoselov was born on August 23, 1974 in Nizhny Tagil in a typical Soviet family. His parents were well-educated; his father, Sergei Viktorovich, was an engineer at the Uralvagonzavod, and his mother, Tatyana Glebovna, was an English teacher. His passion for physics began as early as in the sixth grade of secondary school. In 1986, he took first place in the regional Olympiad in physics, and at the All-Union Olympiad for schoolchildren of the USSR he was in the top ten. After graduating with honors from Moscow Institute of Physics and Technology (specialising in nanoelectronics) in 1997, he worked at the Institute for Problems of Microelectronics Technology of the Russian Academy of Sciences (Chernogolovka) for two years, combining it with postgraduate study. However, he was awarded PhD degree at the University of Nijmegen at the end of 2004. He moved to the Netherlands in 1999, and completed his research work under supervision of Prof. Andre Geim. Since 2001 he has been affiliated with the University of Manchester (UK), where he continues his research as a professor, and combines it with work at National University of Singapore.

Novoselov is married (Fig. 2). In 2009, he and his wife had two twin daughters – Sofia and Victoria, whom they took to Stockholm to the Nobel Prize Award Ceremony. On December 31, 2011, he was awarded the knighthood and given the title of Sir.



Fig. 1. Novoselov's Nobel diploma. Copyright ©The Nobel Foundation 2010



Fig. 2. Novoselov with his wife Irina Barbolina during the reception at the Royal Swedish Academy of Sciences, 7 December, 2010.

Copyright ©The Nobel Foundation 2010

In 2014, Novoselov was included in the list of the most cited researchers. His publication activity is extremely high [11]. In the WoS database, at the beginning of 2019, 312 of his publications were recorded, of which 289 have been cited since 2004; the total number of citations is 172.525; h-index is 112; 25 publications have been cited more than 1000 times, with 4 out of them being cited more than 10000 times; the average number of citations is 597. The citation diagram by years is as follows (Fig. 3).

In the leading scientific journals of the world, Novoselov's citation is currently unattainable. For

example, in the *Science* journal, the article [6] has been cited 34,000 times, exceeding the citation of the second-place article by three times. Similar pictures are observed in the *Nature* journal and others. In the year when he was awarded the Nobel Prize he owned only 95 publications.

After the Nobel Prize Award Ceremony, Novoselov gave an interview, in which he commented on his possibility of returning to Russia and doing research there. He admitted that he was happy with his work at the University of Manchester, but if he was made an interesting job offer in Russia, perhaps he would return, although it was quite unlikely. The organization of research work in Britain is much simpler and more transparent than in Russia or in Germany. It was not just about money. However, over time, the situation has changed.

In February 2021, it became known that Novoselov is going head the Laboratory of Physics of Programmable Functional Materials at the Russian Center for the Study of the Brain and Consciousness of Moscow Institute of Physics and Technology, which is being created with a private five-year grant of 500 million rubles allocated by V.O. Potanin.

The laboratory will be engaged in interdisciplinary research at the intersection of physics, mathematics, biology, new materials, in particular, the development of ion transistor technologies. Such technologies reveal new methods of studying the brain, sensors for neurophysiological research, computer interfaces.

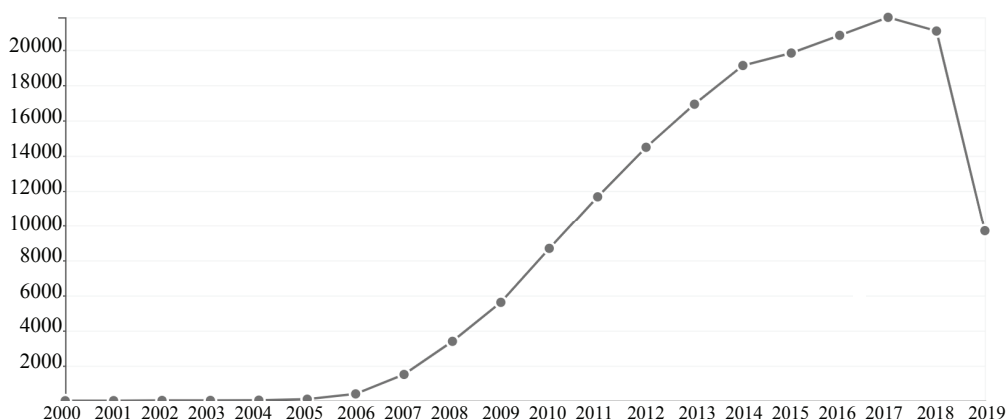


Fig. 3. The curve of Novoselov's publication activity. The ordinate is the number of citations, the abscissa is the years. The dot for 2019 takes into account citations of the first two months

Novoselov has a significant number of scientific awards. He is a member of the Royal Society of London and the US National Academy of Sciences; he has been awarded the Lars Onsager and John Dalton medals, the Otto Warburg and Europhysicist prizes. As a British-Russian citizen, Novoselov has not been included in the group of four Russian Nobel laureates who have not been elected to the Russian Academy of Sciences [12].

Novoselov is not just an outstanding researcher, but also a talented designer and artist. He led the construction project at the Manchester National Graphene Institute and is well known for his work in Chinese calligraphy and Chinese-style drawings.

References

1. Curl RF. The origins of the discovery of fullerenes: experiment and hypothesis. *Uspekhi fizicheskikh nauk = Advances in Physical Sciences*. 1998;168(3):331-342. DOI:10.3367/UFNr.0168.199803f.0331 (In Russ.)
2. Kroto H. Symmetry, space, stars and C₆₀. *Uspekhi fizicheskikh nauk = Advances in Physical Sciences*. 1998;168(3):343-358. DOI:10.3367/UFNr.0168.199803g.0343 (In Russ.)
3. Smalley RE. Opening fullerenes. *Uspekhi fizicheskikh nauk = Advances in Physical Sciences*. 1998;168(3):323-330. DOI:10.3367/UFNr.0168.199803e.0323. (In Russ.)

4. Iijima S. Helical microtubules of graphitic carbon. *Nature*. 1991;354:56-58.

5. Morozov SV, Novoselov RS, Geim AK. Electronic transport in graphene. *Uspekhi fizicheskikh nauk = Advances in Physical Sciences*. 2008;178(7):776-780. (In Russ.)

6. Novoselov KS, Geim AK, et al. Electric field effect in atomically thin carbon films. *Science*. 2004;306(5696):666-669.

7. *The Nobel Prize in Physics 2010*. Available from: <https://www.nobelprize.org/prizes/physics/2010/summary/> [Accessed 15 March 2021].

8. Lyubinin IA, Tyutyunnik VM. Nobel Prize winners in 2010. *Nauka i tekhnologii v promyshlennosti = Science and Technology in Industry*. 2011;1(4):109-116. (In Russ.)

9. Novoselov KS. Graphene: flatland materials. *Uspekhi fizicheskikh nauk = Advances in Physical Sciences*. 2011;181(12):1299-1311. DOI:10.3367/UFNr.0181.201112f.1299. (In Russ.)

10. Nobel Week 2010. Press Memo 2010-12-03 / The Nobel Foundation, p. 1.

11. Glushanovskii AV, Kalenov NE. Contemporary citation of Russian/Soviet Nobel laureates from the Web of Science database. Tyutyunnik VM (ed.) *Science, Technology, Society and the International Nobel Movement: Materials of the Nobel Congress – 12 International Conference for Nobel Prize Winners and Nobelists, 2-5 Oct. 2019, Tambov (Russia)*. Tambov: INIC Publ. House "Nobelists"; 2019. p. 31-50. (In Russ.)

12. Tyutyunnik VM. Nobel laureates, domestic and foreign members and winners of awards of the Russian Academy of Sciences. *Istoriya nauki i tekhniki = History of science and technology*. 2020;9:3-26. DOI:10.25791/intstg.09.2020.1210. (In Russ.)

Информация об авторах / Information about the authors

Тютюник Вячеслав Михайлович, доктор технических наук, профессор, Тамбовский государственный технический университет; генеральный директор, Международный Информационный Нобелевский Центр, Тамбов, Российская Федерация; ORCID 0000-0002-2099-5730; e-mail: vmtyutyunnik@gmail.com

Vyacheslav M. Tyutyunnik, D. Sc. (Engineering), Professor, Tambov State Technical University; Director General, International Nobel Information Centre, Tambov, Russian Federation; ORCID 0000-0002-2099-5730; e-mail: vmtyutyunnik@gmail.com

Received 15 January 2021; Accepted 08 February 2021; Published 21 April 2021



Copyright: © Tyutyunnik VM, 2021. This article is an open access article distributed under the terms and conditions of the Creative Commons Attribution (CC BY) license (<https://creativecommons.org/licenses/by/4.0/>).

High resolution transmission electron microscopy analysis of conical carbon nanotubes formed in the high isostatic pressure apparatus

**Boris A. Kulnitskiy^{a,b}✉, Igor A. Perezhogin^{a,b}, Dmitriy V. Batov^a,
Vladimir D. Blank^{a,b}, Yuriy L. Alshevskiy^a**

^a *Technological Institute for Superhard and Novel Carbon Materials,
7a, Tsentralnaya St., Troitsk, Moscow, 108840, Russian Federation,*

^b *Moscow Institute of Physics and Technology State University,
9, Institutskiy Lane, Dolgoprudny, Moscow Region, 141700, Russian Federation*

✉ boris@tisnum.ru

Abstract: Carbon nanotubes with “herringbone” layers structure synthesized in high isostatic pressure apparatus were studied by High Resolution Transmission Electron Microscopy (HRTEM) methods. Seven different values of semi-apex angles of graphene layers were observed in different nanotubes. It is shown that semi-apex angles approximately equal to 5°, 15°, 25° и 35° can be regarded only to the scroll structure of the nanotubes, while 10°, 20° and 30° can be regarded to both scroll either nested graphene layers curved to cones due to the embedding of the pentagon’s to them. Thus, the observation of all (seven) of these values of semi-apex angles testifies presence of scroll nanotubes in the sample under study, though it does not exclude presence of nested-cone nanotubes.

Keywords: carbon nanotube; herringbone structure; transmission electron microscopy; grapheme; pentagon; scroll; semiapex angle; cone.

For citation: Kulnitskiy BA, Perezhogin IA, Batov DV, Blank VD, Alshevskiy YuL. High resolution transmission electron microscopy analysis of conical carbon nanotubes formed in the high isostatic pressure apparatus. *Journal of Advanced Materials and Technologies*. 2021;6(1):10-17. DOI: 10.17277/jamt.2021.01.pp.010-017

Электронномикроскопический анализ высокого разрешения конусных углеродных нанотрубок, формируемых в аппарате высокого изостатического давления

**Б. А. Кульницкий^{a,b}✉, И. А. Пережогин^{a,b}, Д. В. Батов^a,
В. Д. Бланк^{a,b}, Ю. Л. Альшевский^a**

^a *Технологический институт сверхтвердых и новых углеродных материалов,
ул. Центральная, 7а, Москва 108840, Российская Федерация,*

^b *Московский физико-технический институт,
Институтский пер., 9, Долгопрудный, Московская область, 141700, Российская Федерация*

✉ boris@tisnum.ru

Аннотация: Углеродные нанотрубки со структурой слоев «елочка», синтезированные в аппарате высокого изостатического давления, были исследованы методами просвечивающей электронной микроскопии высокого разрешения. В разных нанотрубках наблюдалось семь различных значений полууглов при вершине конуса. Показано, что полууглы при вершине конуса, приблизительно равные 5°, 15°, 25° и 35°, можно отнести только к структуре нанотрубок типа «свертки», а 10°, 20° и 30° – как к «свертке», так и к структуре, образованной вложенными друг в друга конусами, состоящими из слоев графена, изогнутыми в виде конусов из-за встраивания в них пятиугольников. Таким образом, наблюдение всех (семи) из этих значений углов при вершине свидетельствует о наличии нанотрубок типа «свертки» в исследуемом образце, но не исключает наличия нанотрубок с вложенными конусами.

Ключевые слова: углеродная нанотрубка; структура типа «елочка»; просвечивающая электронная микроскопия; графен; пятиугольник; свертка; полуугол при вершине; конус.

Для цитирования: Kulnitskiy BA, Perezhogin IA, Batov DV, Blank VD, Alshevskiy YuL. High resolution transmission electron microscopy analysis of conical carbon nanotubes formed in the high isostatic pressure apparatus. *Journal of Advanced Materials and Technologies*. 2021;6(1):10-17. DOI:10.17277/jamt.2021.01.pp.010-017

1. Introduction

Carbon occupies a special position among all the elements in the periodic table because it is the only one that has isomers from zero up to three dimensions [1]. Graphene layers can transform into sphere-like structures (e.g., fullerenes, onions) [2] and cylinder-like structures (nanotubes, nanofibers) [3]. The discovery of carbon nanotubes is probably the most important in materials research at the end of 20 century. Two publications by Iijima [3, 4] have generated great interest and inspired an increasing number of researchers around the world to study tubular carbons. Among the numerous kinds of nanotubes, the “herringbone” nanotubes [5, 6] formed by conical-shaped graphene, are ones of the most interesting objects. “Herringbone” nanotubes may have nested-cone structure (when seamless conical graphene layers are placed one into another) either scroll structure (as a single wrapped graphene layer). Their electronic properties are very sensitive to the particular geometrical arrangement of atoms. It was shown by Heiberg-Andersen et al. that such nanotubes are characterized by large electrostatic dipole moments [7], and they are promising for many practical applications.

“Herringbone” nanotubes and nanofibers can be obtained by different methods [8]. Herringbone-type carbon nanofibers constructed by stacking graphitic nanocones with different cone angles from 60° to 180° have been synthesized in [9] by the CVD method (without using catalyst). Carbon nanotubes were prepared in [10] by aerosol method. The analysis of the apex angles showed that the nanotubes have a scroll-type structure. Scroll-type tubes were prepared by processing multilayer graphene nanoplatelets in a shear deformation diamond anvil high-pressure cell. The mechanism of formation of such a tube can be associated with twisting one or more of the top layers of the graphene stack [11]. Both hollow tubes and tubes containing filler were made in a continuous stream of CO in a horizontal reactor [12].

Apparently, the type of tubes formed is influenced by numerous factors. Nanofilaments with conical-shaped layers with semi-apex angles 15° – 20° and diameter about 100 nm were made in arc discharge in [13]. “Herringbone” nanotubes were made in [14] at temperature 800 K in the process of methane decomposition on Ni/SiO₂ substrate.

In [15] one of the possible causes of conical layers formation in “herringbone” nanotube is considered to be hydrogen, because it is known that hydrogen atoms can be adsorbed at dangling bonds of carbon.

Nitrogen-containing nanotubes have characteristic morphological peculiarities associated with irregular wavy and corrugated surfaces and cup-like features, consisting of compartmentalised ‘stacked cones’ or nested cone-type stacking of graphene sheets (bamboo-like structure) [16].

In the present work we analyze “herringbone” nanotubes prepared in high isostatic pressure apparatus (HIP). The mechanisms of their formation are discussed taking into consideration high resolution transmission electron microscopy (HRTEM) data.

2. Methods and materials

Carbon nanotubes were prepared in water cold HIP apparatus under nitrogen pressure of 26 MPa [17]. It is known that variations in the thermodynamic conditions in the HIP apparatus affect the size and shape of the grown carbon nanostructures. The heater, made of graphite, were conducting a current of 220 A under tension 7–10 V. The carbon heater temperature did not exceed (2250 ± 50) K. The carbon vapour was transported from the hottest zone by convection to the cold zone and was deposited as soot product in the upper part of the heater. Melamine (C₃N₆H₆) and ferrocene (Fe(C₅H₅)₂) were placed apart in different areas of HIP-chamber. Temperature measurement was performed by means of thermoelectric couple. The maximum temperature in HIP-chamber did not exceed 1100 °C. The temperature in a crucible with ferrocene was about 580°–600°C. The temperature in crucible with melamine was about 980°–1000°C, as at the lateral surface of the heater, where the carbon has deposited. Iron contained in ferrocene served as a catalyst. It is assumed that carbon deposit was yielded not only from the graphite heater but also from melamine (C₃N₆H₆). The duration of the experiment was less than 9 minutes. Details concerning the HIP construction can be found in [18]. Electron microscopy analysis was performed by JEM-2010 (TEM) and JSM-7600F (SEM). The specimen was extruded by the needle from the upper part of the heater on the slide plate and then deposited on the grid.

3. Results and discussion

One of the specific features of carbon nanostructure synthesis in HIP is drastic increase of convection, which favors activation of chemic reactions and transfer of the reagents into the areas with different temperature values, which, in its turn, provides a big variety of kinds of synthesized nanostructures. According to the SEM analysis, nanotubes with a diameter of up to 200 nm and a length of several hundred microns were formed as a result of the experiments (Fig. 1).

The TEM analysis has shown the presence of carbon nanotubes with both cylindrical and conical graphene layers. In spite of the fact, that ferruginous material (ferrocene) was used in our experiment, only few nanotubes contained catalyst particles. Fig 2 shows the microphotograph of the fragments of seven carbon nanotubes with conical layers, obtained by high resolution transmission electron microscopy. It can be seen that the semi-apex angles of graphene cones represent a sequence of values between 5° and 35° with 5°-step.

Fig. 3 shows fragments of the edges of the two tubes. This is evidenced by the angles between the fringes at the edges of the nanotubes, which are 50° and 70°, respectively. The catalytic particles appear to have fallen out during the preparation of the sample. The semi-apex angles are 25° and 35°, respectively.

The catalytic particles fell out during the preparation of the sample.

As a result of the growth, the cap of the tube was severely deformed, but the corners were preserved. All four angles, shown in the photo, are equal.

Fig. 4 shows a deformed cap of a nanotube in which all four marked angles between the fringes are 40°. As a result of the growth, the cap of the tube underwent severe deformation, but the angles were preserved. The possibility of the existence of internal deformations during the growth of such structures

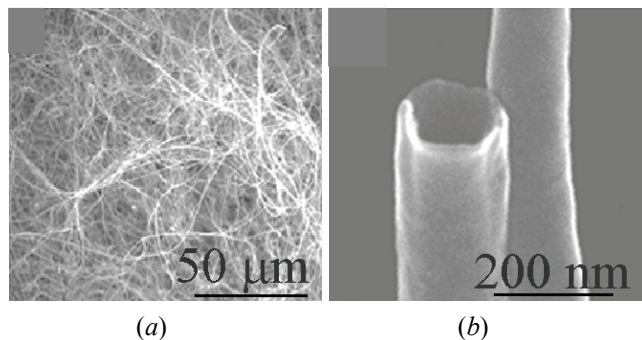


Fig. 1. Carbon nanotubes synthesized in HIP apparatus: a – main view; b – multiwalled hollow nanotube

was assumed in [19]. This can be explained by strong longitudinal deformations that could result from the formation of sp³-bonds along the fiber axis [20]. In some conical tubes, the number of graphene layers varies along the length of the tube.

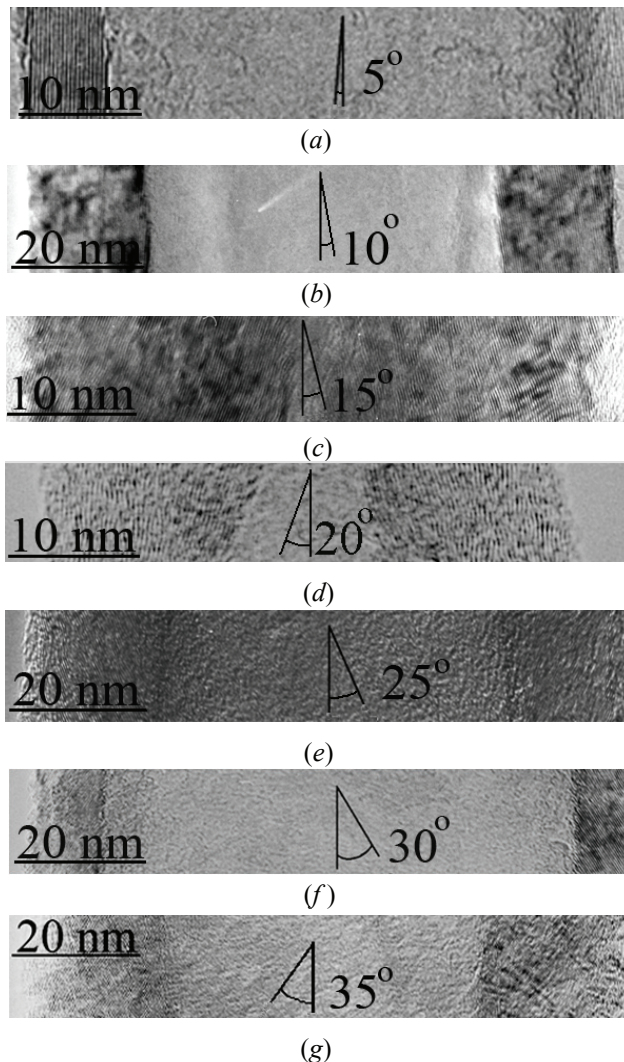


Fig. 2. Fragments of seven carbon nanotubes with layers. The semi-apex angles of graphene cones represent a sequence of values between 5° and 35° with 5°-step

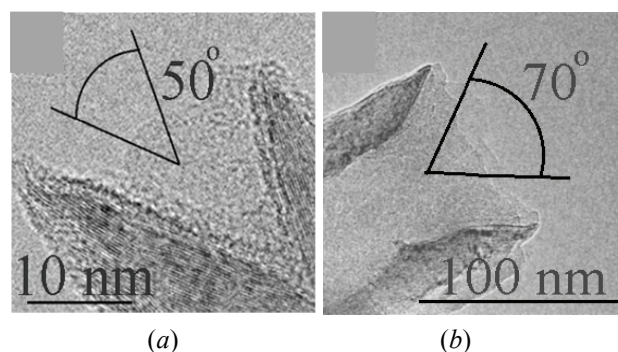


Fig. 3. Angles of 50° and 70° between the fringes at the edges of the nanotubes

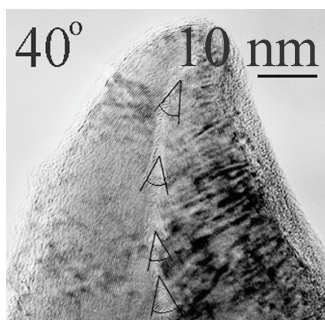


Fig. 4. The cap of the nanotube in which the fringes form an angle of 40°

As can be seen from Fig. 5, a different number of layers are located to the left and right of the tube axis at the same level (20 and 17). This cannot be due to electron microscopic contrast. Figure 6 shows a cylindrical carbon nanotube (right-hand side) that turns twice into a conical one. Arrows indicate areas in which there is a change in angle in the cross section of the tube. The question under consideration is what mechanism of formation of carbon nanotubes with conical graphene layers is. Three models are known to explain the formation of conical nanotubes: the introduction of pentagons into the hexagonal graphene plane, scroll and the disclination model. The disclination model works in the case of wrapping and “overlapping” of graphite surfaces around the disclination. In this case, the adjacent graphene layers differ from each other by the same declination angle. This mechanism gives a wide range of angles, but these angles are not found in the present work.

The symmetry of the graphite planes was considered in [21]. It is known that the nanotube cap can be formed by the pentagons embedding into the structure of graphite (002) plane during the process of nanocarbon synthesis. This effect leads to the bending of the graphite (002) plane and formation of a cone.

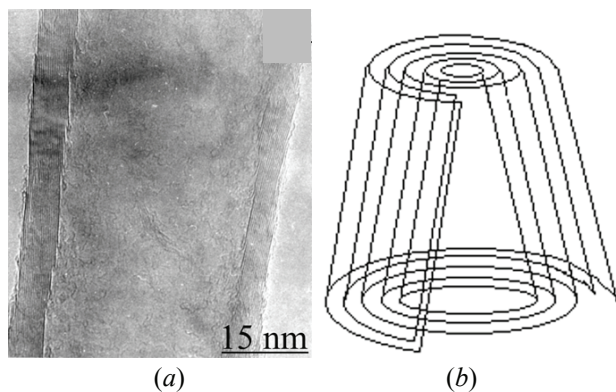


Fig. 5. The fragment of conical nanotube:
a – different number of layers to the left and right of the tube axis (20 and 17, respectively);
b – scheme from (a)

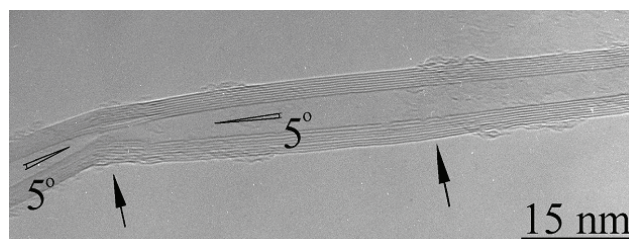


Fig. 6. Cylindrical carbon nanotube twice turning into a conical one. Arrows indicate areas in which there is a change in angle in the cross section of the tube

This is the way of formation of “herringbone” nanotube or nanofiber, consisting of nested cones of graphene. Also “herringbone” nanotube can originate from single graphene layer wrapped as a cone scroll. Such a mechanism was proposed in [22]. The dependence of the semi-apex angle of the graphene cone on the amount of the pentagons embedded in it was determined as $\sin \varphi = 1 - p/6$, where φ is the semi-apex angle and p is the amount of the pentagons. The amounts of pentagons 5, 4, 3, 2, 1 correspond to angles 9.59° , 19.47° , 30° , 42.3° and 56.5° [23]. The reasons of formation of pentagons can be different. For example, the atoms of the catalyst material placed into carbon can cause the formation of the pentagons [24], as well as the deformation or changes of temperature and/or pressure during the nanotube growth. If the amount of the pentagons in a nanotube cap attains 6, the cap becomes a hemisphere and further cylindrical nanotube growths. Twelve pentagons leads to the formation of the fullerenes (C_{60} , C_{70} , etc.) or nanotubulens with hemisphere caps at both ends. Seamless cylindrical nanotubes can be formed as a result of symmetrical wrapping of the graphene sheet in such a way, that carbon hexagons at the edges of the sheet totally coincide after wrapping. Graphene cones can be obtained in the same way, but in this case wrapping occurs asymmetrically, so, that the hexagons at the edge appear to be rotated at certain angle relatively to the ones at the other edge (in previous coil in case of scroll), and this results in formation of conical structure.

Conical scroll can be formed in case of multiple wrapping of single graphene sheet, when edges of the sheet are not connected to one another. New atoms of carbon, depositing on a free edge of a scroll constitute new coil of a scroll. The transversal section of this structure is a helix. In [24] it was shown that the transformation of a graphene sheet into a scroll requires to take into account elastic energy (due to the curvature of the wrapped plane) and Van-der-Vaals bending energy between the neighbor coils in a scroll.

The calculations of these energies shows, that scroll is more stable object than a plane and more stable than the graphene layer [24].

The time of a scroll formation is about picoseconds and the formation of this structure requires energy, which can be received by the temperature treatment, ultrasonic treatment and by other ways. Carbon hexagons of neighbor layers in a scroll cannot be oriented arbitrarily with respect to one another: the angle of rotation of the hexagons after each coil in scroll relatively to the previous layer should be a multiple of 30°. The dependence of the cone semi-apex angle θ on the angle of rotation of the hexagons α is given by the formula $\theta = 2\pi \sin \alpha$. The same result is valid for the seamless cones with pentagons [22]. As it can be seen from Table 1, semi-apex angles take only certain values. Only some of these values are the same for both types of structure: scroll and nested cones, formed by pentagons. Such coincidence occurs for angles which are multiple of 60°.

Table 1. Angle of rotation of carbon hexagon relatively to the neighbor layer in conical scroll α , semi-apex angle in conical scroll θ , semi-apex angle in cone with embedded pentagons φ , amount of pentagons p

| $\alpha, ^\circ$ (hexagon rotation) | Scrolls, $\theta = 2\pi \sin \alpha$ | Cones, made by pentagons, $\sin \varphi = 1 - p/6$ | |
|--|---|---|------------------------------|
| | $\theta, ^\circ$ (semi-apex angle in scroll) | $\varphi, ^\circ$ (semi-apex angle in cone with pentagons) | p (amount of pentagons) |
| 30 | <u>4.78</u> | | |
| 60 | <u>9.59</u> | <u>9.59</u> | 5 |
| 90 | <u>14.47</u> | | |
| 120 | <u>19.47</u> | <u>19.47</u> | 4 |
| 150 | <u>24.62</u> | | |
| 180 | <u>30</u> | <u>30</u> | 3 |
| 210 | <u>35.68</u> | | |
| 240 | 41.81 | 41.81 | 2 |
| 270 | 48.59 | | |
| 300 | 56.44 | 56.44 | 1 |
| 330 | 66.44 | | |
| 360 | 90 | | |

Fig. 2, *b* shows “herringbone” nanotube with a semi-apex angle approximately equal 10°. This value (9.59°) can be observed in both types of structure, scroll and nested cones, and the same for 20° and 30°. But 5° (4.78°) at Fig. 2, *a* can be attributed only to the scroll, and not to the nested cones (as well, as 15°, 25° and 35°). In case of 5°-semi-apex angle in scroll, hexagons in neighbor layers are rotated at 30° relatively to one another. This means that the orientation of hexagons in all odd (even) layers is the same.

Apex-angles of 50° and 70° between the fringes in the two nanotubes, shown in Fig. 3, *a, b* correspond to the scroll structure. Fig. 4 shows a deformed cap of a nanotube in which all four marked angles between the fringes are 40°, which can be explained by two growth mechanisms. The structure of the nanotube shown in Figure 5 does not agree with the scroll model, at least in its pure form, and suggests a more complex model. The concentric cones in Fig. 5 were most likely formed initially. But as a result of the fact that it is difficult to achieve equilibrium synthesis conditions in the HIP apparatus, more carbon atoms were deposited from the chemical vapor on one side of the tube than on the other; in addition, small changes in temperature and pressure could prevent the formation of pentagons, as a result of which the outer part of this structure turned out to be a scroll. In this case, the number of layers on different sides of the longitudinal centerline could be different. The different lengths of the truncated cones could also lead to the same phenomenon. In this case, it is possible to form a different number of layers along the length of the cone. Under equilibrium synthesis conditions, a multi-walled carbon nanotube, which is a set of nested cones, is a more stable structure than a scroll. In [25], when carbon nanostructures grow under controlled conditions, changes in the growth mechanisms for the same tube were observed from a concentric structure for the inner parts to a scroll for the outer parts of the tube. The angle of 5° ($\approx 4.78^\circ$), in the nanotube shown in Fig. 6, can only correspond to the scroll structure. On the other hand, you can get a cone with an angle of 4.78° by inserting a heptagon into a structure consisting of hexagons. Thus, the formation of a fragment consisting of a set of hexagons and one heptagon can be a precursor to both a scroll-cone and an ordinary cone, and an angle of 4.78° can correspond to two different structures.

Hence, every cone appears to consist of not only hexagons, but also pentagons and heptagons, and possibly more complex structures. In the case of concentric cones, all the features of the structure of

one of them must be repeated for the others. In the case of a scroll cone with an angle of 4.78° , the hexagons in the adjacent layers will be disoriented by an angle of 30° . Hence, the orientations of the hexagons in all even (odd) layers coincide. Heptagon can be formed, for example, by introducing atoms of other elements into the hexagon.

As mentioned earlier, a nested cylinder nanotube is, under equilibrium conditions, the more stable configuration compared to a scroll structure, and the energy difference decreases with increasing diameter and number of graphene layers per wall. In [25] the dynamic change of growth mechanism from nested cylinders for inner part to scroll for outer part was observed during the controllable growth process of carbon nanostructures. The authors suggest that the acceleration of the complete growth kinetics, including decomposition of the ethylene precursor gas, diffusion of carbon atoms through the catalyst, and precipitation of new graphene layers at the surface of catalyst particle, provides the conditions for the change in growth characteristics of one and the same tube. The transition region is characterized by a concentric structure towards the inside of the tube and a scroll-type structure at the outside. In [26] authors considered TEM images of nanotubes, where the amount of graphene layers at the one side of the tube projection was one layer more, than at the left side, and this was explained by the defect in sliding plane. The mechanism of formation of cones by the microclaster embedding in their structure was proposed in [27].

The observation of both types of structures (scroll and nested cones) in our experiment testifies the nonequilibrium of growth conditions. Straight cylindrical nanotubes originate through the catalytic growth and they are always seen in a deposit. The formation of these structures is favored by the small size of the graphene sheets, whereas large graphene sheets are more suitable for formation of scrolls. The formation of the cap with pentagons for the conical scroll is not possible because of incoincidence of semi-apex angles. Discussing the possible mechanisms of the formation of conical nanotubes in the HIP apparatus, we can exclude the disclination model, which assumes a wide range of angles not found in our work. As for the other two models, it is possible to form nanotubes under non-equilibrium conditions in accordance with both models. Scroll whiskers were first reported by Bacon in 1960 [28]. Scrolls possess unusual chemical, mechanical and electronic properties, and they are promising material for many practical applications. They were synthesized under different conditions: in arc discharge [29], by CVD method [9] (with apex angle from 30° to 110°). In [30] carbon nanotubes

having a structure of scrolls were formed by polymerization in the interlayer of graphite and the subsequent removal of the polymer. In [31] there were observed nanofibers with conical structure and semi-apex angles 15° , 25° and 35° . Authors explained their formation in terms of an open cone model.

Because of scroll topology, their properties should differ from those of single- or multiwall cylindrical carbon nanotubes. Scroll and nested cone structures can be distinguished by the following way: the studies of nanotube thermal expansion in 20–320 K temperature range [29] have shown that the radial expansion of the nanotubes is almost the same as in graphite along the c-axis of the graphite crystal. Authors have explained this in terms of scroll model. Other distinction of the nested cylinders from the scrolls is the intercalation capability of the last ones [32]: scrolls can be intercalated by K, FeCl_3 and other substances. In [32] it was determined by means of electron spin resonance that the sample powder consisted of both types of structures. Interlayers galleries in scrolls can be intercalated with donors and acceptors, and the nanotube diameter can expand to accommodate the volume of intercalant. This feature is potentially important for a rich variety of applications, from hydrogen storage to energy storage in supercapacitors or batteries. Nanoscrolls have chemical surface reactivity due to large number of edge sites.

At the same time, all the “herringbone” nanotubes with catalyst particles, observed in our experiments always have semi-apex angle which was multiple of 10° . Probably, both of the nanotube formation mechanisms took place in our experiment. In this case, scrolls were originating without catalyst as nanohorns did [33]. The carbon conical nanotubes may have complex band structures and fascinating charge transport properties, from insulating at the apex to metallic at the base. The electronic properties of carbon nanocones were investigated systematically in [35]. The authors described locally the electronic properties as a function of size and symmetry. It was found that the symmetry of the edge sites plays a crucial role in the determination of the electronic structure.

They might be used as building units in future nano-scale electronics devices [34].

4. Conclusion

Carbon nanotubes, where graphene layers of shape were obtained in HIP apparatus in mixed atmosphere of argon and nitrogen at temperature 1450 K and under pressure from 80 to 100 MPa. In the process of the TEM studies the nanotubes of the seven different values of the semi-apex angles

were observed, these values are 5°, 10°, 15°, 20°, 25°, 30° and 35°. Our considerations have shown that the nanotubes with semi-apex angles 10°, 20° and 30° in the graphene layers in their structure can be attributed to both conical scroll and nested cone structure, originated due to the embedding of the pentagons, whereas nanotubers with semi-apex angles 5°, 15°, 25° and 35° can be attributed only to cones. The empty cone-shaped structure of graphene walls may be of particular interest for some applications, for example, because of its simplicity for intercalation reactions.

5. Funding

This study did not receive external funding.

6. Conflict of interests

The authors declare no conflict of interest.

References

1. Saito R, Dresselhaus G, Dresselhaus MS. *Physical properties of carbon nanotubes*. London: Imperial College Press; 1998. p. 35-58. DOI:10.1142/9781860943799_0003.
2. Iijima S. Direct observation of the tetrahedral bonding in graphitized carbon black by high resolution electron microscopy. *Journal of Crystall Growth*. 1980;50(3):675-683. DOI:10.1016/0022-0248(80)90013-5
3. Iijima S. Helical microtubules of graphitic carbon. *Nature*. 1991;354:56-58. DOI:10.1038/354056a0
4. Iijima S, Ichihashi T. Single-shell carbon nanotubes of 1-nm diameter. *Nature*. 1993;363:603-605. DOI:10.1038/363603a0
5. Endo M, Takeuchi K, Kobori K, Takahashi K, Kroto HW, Sarkar A. Pyrolytic carbon nanotubes from vapor-grown carbon fibers. *Carbon*. 1995;33(7):873-881. DOI:10.1016/0008-6223(95)00016-7
6. Terrones H, Hayashi T, Munoz-navia M, Terrones M, Kim YA, Grobert N, Kamalakaran R, Dorantes-Davila J, Escudero R, Dresselhaus MS, Endo M. Graphitic cones in palladium catalysed carbon nanofibres. *Chemical Physics Letters*. 2001; 343:241-250. DOI:10.1016/S0009-2614(01)00718-7
7. Heiberg-Andersen H, Skjeltorp AT, Sattler K. Carbon nanocones: A variety of non-crystalline Solids. *Journal of Non-Crystalline Solids*. 2008;354:5247-5249. DOI:10.1016/j.jnoncrysol.2008.06.120
8. Schaper A. Carbon Nanoscrolls. In: Blank VD, Kulnitskiy BA. *Carbon nanotubes and related structures*. Kerala, India: Research Signpost; 2008. p. 2-51.
9. Lin CT, Chen WC, Yen MY, Wang LS, Lee CY, Chin TS, Chiu HT. Cone-stacked carbon nanofibers with cone angle increasing along the longitudinal axis. *Carbon*. 2007;45:411-415. DOI:10.1016/j.carbon.2006.09.002
10. Kulnitskiy B, Karaeva A, Mordkovich V, Urvanov S, Bredikhina A. TEM studies of scroll carbon nanotubes formed by aerosol synthesis. *IOP Conference Series: Materials Science and Engineering*. 2019;693:012017. DOI:10.1088/1757-899X/693/1/012017
11. Blank VD, Kulnitskiy BA, Kirichenko AN, Memetov NR, Dyachkova TP, Tkachev AG. Features of structures obtained by grapheme nanoplatelets treatment in a diamond anvil high pressure cell. *Fullerenes, nanotubes and carbon nanostructures*. 2017;25(8):488-492. DOI:10.1080/1536383X.2017.1339694
12. Kulnitskiy BA, Blank VD. Iron carbide formation inside carbon nanotubes. *Advanced Materials & Technologies*. 2017;3:34-39. DOI: 10.17277/amt.2017.03.pp.034-039
13. Fitzgerald JD, Tailor GH, Brunckhorst LF, Pang LSK, Wilson MA. Filaments with microstructures formed during fullerene production. *Carbon*. 1993;31(1):240-244. DOI:10.1016/0008-6223(93)90181-9
14. Takenaka S, Kobayashi S, Ogihara H, Otsuka K. Ni/SiO₂ catalyst effective for methane decomposition into hydrogen and carbon nanofiber. *Journal of Catalysis*. 2003;217:79-87. DOI: 10.1016/S0021-9517(02)00185-9
15. Zhuxin Yu, De Chen B, Totdal B, Holmen A. Effect of catalyst preparation on the carbon nanotube growth. *Catalysis today*. 2005;100(3-4):261-267. DOI:10.1016/j.cattod.2004.09.060
16. Nath M, Satishkumar BC, Govindaraj A, Vinod CP, Rao CNR. Production of bundles of aligned carbon and carbon-nitrogen nanotubes by the pyrolysis of precursors on silica supported iron and cobalt catalysis. *Chemical Physics Letters*. 2000;322:333-340. DOI:10.1142/9789812835734_0027
17. Blank VD, Polyakov EV, Batov DV, Kulnitskiy BA, Bangert U, Gutierrez-Sosa A, Harvey AJ, Seepujak A. Formation of N- containing C-nanotubes and nanofibres by carbon resistive heating under high nitrogen pressure. *Diamond and Related Materials*. 2003;12:864-869. DOI:10.1016/S0925-9635(02)00378-3
18. Blank VD, Polyakov EV, Kulnitskiy BA, Nuzhdin AA, Alshevskiy YL, Bangert U, Harvey AJ, Davock HJ. Nanocarbons formed in a hot isostatic pressure apparatus. *Thin solid films*. 1999;346:86-90. DOI: 10.1016/S0040-6090(98)01453-9
19. Bernaerts D, Zhang XB, Zhang XF, Amelinckx S, Van Tandeloo G, Van Landuyt J, Ivanov V, Nagy JB. Electron microscopy study of coiled carbon tubules. *Philosophical Magazine A*. 1995;71(3):605-630. DOI:10.1080/01418619508244470
20. Blank VD, Kulnitskiy BA. Proposed formation mechanism for helically coiled carbon nanofibers. *Carbon*. 2004;42:3009-3012. DOI:10.1016/j.carbon.2004.06.004
21. Krishnan A, Dujardin E, Treacy MMJ, Huggdahl J, Lynam S, Ebbesen TW. Graphitic cones and the nucleation of curved carbon surfaces. *Nature*. 1997;388:451-454. DOI:10.1038/41284
22. Amelinckx S, Devouard B, Baronnet A. Geometrical aspects of the diffraction space of serpentine rolled microstructures: their study by means of electron diffraction and microscopy. *Acta Crystallographica*. 1996;A52:850-878.
23. Boellard E, DeBokx PK, Kock AJHM, Geus JW. The formation of filamentous carbon on iron and nickel catalysts. *Journal of Catalysis*. 1985;96:481-490. DOI:10.1016/0021-9517(85)90316-1
24. Braga SF, Coluci VR, Legoas SB, Giro R, Galvao DS, Baughman RH. Structure and dynamics of

carbon nanoscrolls. *Nano Letters*. 2004;4:881-884. DOI:10.1021/nl0497272

25. Sun X, Li R, Stansfield B, Dodelet J-P, Menard G, Desilets S. Controlled synthesis of pointed carbon nanotubes. *Carbon*. 2007;45:732-737. DOI:10.1016/j.carbon.2006.11.033

26. Lavin P, Subramoney S, Ruoff R, Berber S, Tomanek D. Scrolls and nested tubes in multiwall carbon nanotubes. *Carbon*. 2002;40:1123-1130. DOI:10.1016/S0008-6223(02)00050-7.

27. Lozovik YuE, Popov AM. Formation and growth of carbon nanostructures: fullerenes, nanoparticles, nanotubes and cones. *Physica-Uspeski*. 1997;40(7):717-737. DOI:10.3367/UFNr.0167.199707d.0751

28. Bacon R. Growth, structure, and properties of graphite whiskers. *Journal of Applied Physics*. 1960;31:283-290. DOI:10.1063/1.1735559

29. Bandow S. Radial thermal expansion of purified multiwall carbon nanotubes measured by X-ray diffraction. *Japanese Journal of Applied Physics*. 1997;36:L1403-L1405. DOI:10.1143/JJAP.36.L1403

30. Shioyama H, Akita T. A new route to carbon nanotubes. *Carbon*. 2003;41:179-181. DOI:10.1016/S0008-6223(02)00278-6

31. Terrones H, Hayashi T, Munoz-Navia M, Terrones M, Kim YA, Grobert N, Kamalakaran R, Dorantes-Davila J, Escudero R, Dresselhaus M, Endo M. Graphitic cones in palladium catalysed carbon nanofibers. *Chemical Physics Letters*. 2001;343:241-250. DOI:10.1016/S0009-2614(01)00718-1

32. Mordkovich VZ, Baxendale M, Yoshimura S, Chang RPH. Intercalation into nanotubes. *Carbon*. 1996;34(10):1301-1303. DOI:10.1016/0008-6223(96)82802-8

33. Harris PJF, Tsang SC, Claridge JB, Green MLH. High resolution electron microscopy studied of a microporous carbon, produced by arc evaporation. *Journal of the Chemical Society, Faraday Transactions*. 2010;90:2799-802. DOI:10.1002/chin.199504005

34. Ge M, Sattler K. Observation of fullerene cones. *Chemical Physics Letters*. 1990;220:192-196. DOI: 10.1016/0009-2614(94)00167-7

35. Muñoz-Navia M, Dorantes-Dávila J, Terrones M, Terrones H. Ground-state electronic structure of nanoscale carbon cones. *Physical review B*. 2005;72:235403:1-7. DOI:10.1103/PhysRevB.72.235403

Информация об авторах / Information about the authors

Кульницкий Борис Арнольдович, доктор физико-математических наук, главный научный сотрудник, Технологический институт сверхтвердых и новых углеродных материалов (ТИСЧУМ), Троицк, Москва, Российская Федерация; ORCID 0000-0001-5482-3123; e-mail: boris@tisnum.ru

Пережогин Игорь Анатольевич, кандидат физико-математических наук, старший научный сотрудник, ТИСЧУМ, Троицк, Москва, Российская Федерация; ORCID 0000-0002-8930-4806; e-mail: Iap1@mail.ru

Батов Дмитрий Викторович, кандидат физико-математических наук, ученый секретарь, ТИСЧУМ, Троицк, Москва, Российская Федерация; AuthorID (Scopus) 36828098100; e-mail: d.batov@tisnum.ru

Бланк Владимир Давыдович, доктор физико-математических наук, научный руководитель, ТИСЧУМ, Троицк, Москва, Российская Федерация; AuthorID (Scopus) 7005096766; e-mail: vblank@tisnum.ru

Альшевский Юрий Львович, кандидат физико-математических наук, научный сотрудник, ТИСЧУМ, Троицк, Москва, Российская Федерация; AuthorID (Scopus) 6504159622; e-mail: Alshev.Yura38@mail.ru

Boris A. Kulnitskiy, D. Sc. (Physics and Mathematics), Chief Research Officer, Technological Institute for Superhard and Novel Carbon Materials (TISNCM), Troitsk, Moscow, Russian Federation; ORCID 0000-0001-5482-3123; e-mail: boris@tisnum.ru

Igor A. Perezhogin, Cand. Sc. (Physics and Mathematics), Senior Researcher, TISNCM, Troitsk, Moscow, Russian Federation; ORCID 0000-0002-8930-4806; e-mail: Iap1@mail.ru

Dmitriy V. Batov, Cand. Sc. (Physics and Mathematics), Academic Secretary, TISNCM, Troitsk, Moscow, Russian Federation; AuthorID (Scopus) 36828098100; e-mail: d.batov@tisnum.ru

Vladimir D. Blank, D. Sc. (Physics and Mathematics), Research Supervisor, TISNCM, Troitsk, Moscow, Russian Federation; AuthorID (Scopus) 7005096766; e-mail: vblank@tisnum.ru

Yuriy L. Alshevskiy, Cand. Sc. (Physics and Mathematics), Research Associate, TISNCM, Troitsk, Moscow, Russian Federation; AuthorID (Scopus) 6504159622; e-mail: Alshev.Yura38@mail.ru

Received 18 November 2020; Accepted 20 January 2021; Published 21 April 2021



Copyright: © Kulnitskiy BA, Perezhogin IA, Batov DV, Blank VD, Alshevskiy YuL, 2021. This article is an open access article distributed under the terms and conditions of the Creative Commons Attribution (CC BY) license (<https://creativecommons.org/licenses/by/4.0/>).

Design of mechatronic engineering systems in digitalized traditional and additive manufacturing

Mikhail L. Kheifetz✉

*Institute of Applied Physics of the National Academy of Sciences of Belarus,
16, Akademicheskaya St., Minsk, Belarus*

✉ mlk-z@mail.ru

Abstract: The paper presents the analysis of the steps and stages of designing process equipment for traditional manufacturing. The features of building process equipment using energy flows and consumables are studied. Structural synthesis of mechatronic systems in digitalized manufacturing make it possible to add new stages to the process of creating process equipment for both traditional automated subtractive and new additive manufacturing. The processes of manufacturing parts without forming equipment described by the algorithms according to the proposed structural diagram of connections provide an opportunity to analyze the existing equipment and develop new equipment for laminate synthesis of products.

The paper illustrates the use of methods and procedures for laminate synthesis and fabrication of parts from composite materials using process equipment based on the application of energy flows and material components for new additive and traditional subtractive manufacturing. Also, methods and diagrams for automation and computer-aided process control over product manufacturing are shown.

Keywords: process equipment; additive and subtractive manufacturing; laminate synthesis; product fabrication.

For citation: Kheifetz ML. Design of mechatronic engineering systems in digitalized traditional and additive manufacturing. *Journal of Advanced Materials and Technologies*. 2021;6(1):18-29. DOI: 10.17277/jamt.2021.01.pp.018-029

Проектирование мехатронных технологических комплексов при цифровизации традиционного и аддитивного производства

М. Л. Хейфец✉

*ГНУ Институт прикладной физики Национальной академии наук Беларуси,
ул. Академическая, 16, Минск, Республика Беларусь*

✉ mlk-z@mail.ru

Аннотация: Проведен анализ стадий и этапов проектирования технологического оборудования для традиционного производства, изучены особенности формирования технологического оборудования, использующего потоки энергии и расходных материалов. Структурный синтез мехатронных комплексов в цифровизированном производстве позволил дополнить новыми этапами процесс создания технологического оборудования как для традиционного автоматизированного субтрактивного, так и нового аддитивного производства. Описанные алгоритмами по предложенной структурной диаграмме связей процессы изготовления деталей без формообразующей оснастки, предоставляют возможность анализировать существующее и разрабатывать новое оборудование для послойного синтеза изделий.

Показано, как при проектировании технологического оборудования для его использования в новом аддитивном и традиционном субтрактивном производстве, применяются методы и схемы послойного синтеза и формообразования деталей из композиционных материалов, построенные на использовании различных потоков энергии и компонентов материала, а также методы и схемы автоматизации и компьютерного управления процессами производства изделий.

Ключевые слова: технологическое оборудование; аддитивное и субтрактивное производство; послойный синтез; формообразование изделий.

Для цитирования: Kheifetz ML. Design of mechatronic engineering systems in digitalized traditional and additive manufacturing. *Journal of Advanced Materials and Technologies*. 2021;6(1):18-29. DOI: 10.17277/jamt.2021.01.pp.018-029

1. Introduction

When designing process equipment for digitalization of both traditional subtractive and new additive manufacturing, it is possible to apply the existing methods and new ones for fabrication and laminate synthesis of products, as well as their automation and computerization, intensive modification of materials and surfaces with concentrated and distributed flows of energy and components of substances [1–5].

Traditionally, the initial data for the design of process equipment contains the technical design specification for a specific customer, including [6, 7]: (1) the data on materials and finished products; (2) the equipment performance; (3) the nature and type of manufacturing; (4) the level of automation and integration into modern high-tech industry.

However, this information is not sufficient when designing process equipment using distributed fields and concentrated flows of energy and components of substances [1–3] for computer-aided subtractive and additive manufacturing [4, 5, 8]. This is due to the fact that both for traditional types of subtractive [9, 10] and new types of additive [11, 12] manufacturing, which consist in layer-by-layer build-up of the surface of products, it is required to additionally consider the supply and distribution of energy and material [13, 14].

In this regard, **the aim of the paper** is to develop the existing methodology for the design of process equipment facilities with computer-aided control of processes, both for traditional methods of

combined electro-physicochemical fabrication of parts, and for new methods of laminate synthesis of products from composite materials in additive manufacturing.

2. The analysis of the steps and stages in the design of process equipment for traditional manufacturing

The design process, including structural synthesis and parametric optimization of equipment used in traditional subtractive and new additive manufacturing covers various methods and procedures for formation and synthesis of products, as well as their automation and computerization.

2.1. Structural synthesis

The sequence of design of process equipment for traditional-type manufacturing includes 8 enlarged stages based on the design diagrams (Fig. 1) [4, 6, 7]:

1. Layout and selection of the kinematic diagram (see Fig. 1, a).
2. Modular design for a limited set of units and assemblies [15, 16].
3. Calculations of static elastic displacements, the selection of the diagram and strength calculations (see Fig. 1, b).
4. Dynamic calculations of the stability of system movements and static deviations of elements, the selection of the diagram and dynamic calculations (see Fig. 1, c).

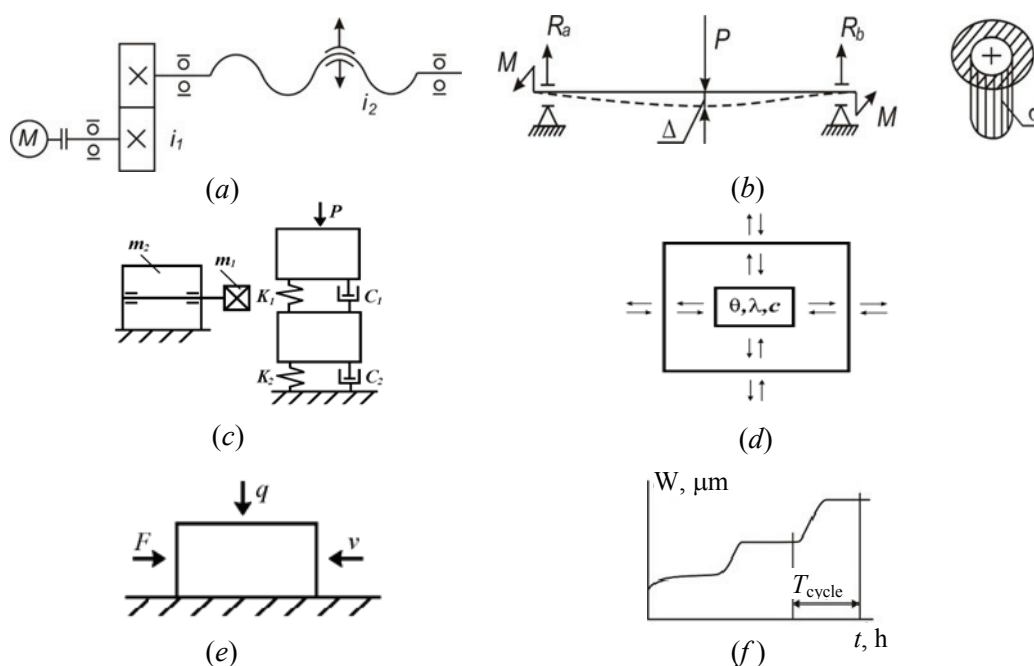


Fig. 1. Diagrams for the main systems of process equipment:

a – kinematic; b – strength; c – dynamic; d – thermodynamic; e – contact-and-friction; f – wear-and-reliability

5. Thermal calculations, the selection of thermodynamic scheme and calculation of temperatures (see Fig. 1, *d*).

6. Precision calculations, including the determination of the accuracy of geometric and kinematic connections (see Fig. 1, *a*), taking into account deformations: general (see Fig. 1, *b, c*), thermal (see Fig. 1, *d*) and contact-and-friction (see Fig. 1, *e*).

7. Calculations of reliability and durability, including determination of the reliability of units and assemblies (see Fig. 1, *a – c*), taking into account thermal and deformation processes (see Fig. 1, *d, e*) friction and wear (see Fig. 1, *f*), and in conclusion, the economic justification of the resource.

8. The analysis of the human-machine system, which also includes occupational health and safety requirements [6].

Further, by stages for process equipment, the calculations are made for the main systems: (1) bearing systems; (2) guiding movements; (3) drives of movements and others.

The design and calculation of the main systems is carried out according to the technical requirements for mechanical units, process equipment and automation equipment; lubrication systems, electrical equipment and programmable systems; diagnostic systems, taking into account safety, ergonomics and manufacturability of the machine [4, 6, 7].

For this, system diagrams are constructed, taking into account the limiting sets of units and assemblies: (1) kinematic (see Fig. 1, *a*); (2) process modules [15, 16]; (3) strength (see Fig. 1, *b*); (4) dynamic (see Fig. 1, *c*); (5) thermodynamic (see Fig. 1, *d*); (6) contact-and-friction (see Fig. 1, *e*); (7) wear-and-reliability (see Fig. 1, *f*); (8) the man-machine system as a whole [6].

2.2. Parametric optimization

Having completed the structural synthesis, parametric optimization is carried out [17, 18]; it determines the main parameters of process equipment systems. Determination of the parameters of the kinematic module is often associated with the optimization of its structure, in particular, due to the rational placement of adjustment elements in it [19]. This task relates to structural-parametric synthesis and optimization, as a result of which a rational structure of the object is formed and the values of the parameters of its elements are found in order to satisfy the requirements of synthesis with optimization during adjustment.

Let me consider the way of solving this problem using the example of a differential mechanical

module with two driving links 1 and 3, output link 6 and two adjustments i_x and i_y (Fig. 2), which can be used for parallel connection of two kinematic groups [19].

The kinematic connections of the modules $1 \rightarrow 2 \rightarrow \Sigma \rightarrow 5 \rightarrow 6$ and $3 \rightarrow 4 \rightarrow \Sigma \rightarrow 5 \rightarrow 6$ have a common area 5–6 and autonomous areas 1–2 and 3–4 connected to it through a summing mechanism Σ . The adjustment element i_x of the first kinematic group can be located either in its autonomous area 1–2 (see Fig. 2, *a*) or in the common area 5–6 (see Fig. 2, *b*). Similarly, the adjusting element i_y of the second kinematic group can also be located either in its autonomous area 3–4 or in the common area 5–6. Therefore, let me analyze various options for the placement of adjustment elements i_x и i_y [19]. If they are in the indicated autonomous areas of internal connections from the beginning, the structure of these connections can be represented as follows:

$$\begin{array}{c} \alpha \rightarrow 1 \rightarrow i_x \rightarrow 2 \rightarrow \Sigma \rightarrow 5 \rightarrow 6 \rightarrow \varphi + \theta \\ \uparrow \\ \beta \rightarrow 3 \rightarrow i_y \rightarrow 4. \end{array}$$

When one of the adjustment elements is in the common area 5–6, and if the element i_x is located in it, the following structure of the module's internal links is obtained:

$$\begin{array}{c} \alpha \rightarrow 1 \rightarrow 2 \rightarrow \Sigma \rightarrow 5 \rightarrow i_x \rightarrow 6 \rightarrow \varphi + \theta \\ \uparrow \\ \beta \rightarrow 3 \rightarrow i_y \rightarrow 4. \end{array}$$

When placing the adjustment elements according to the first option, it is necessary to reconfigure both adjustment elements, which is associated with an increase in labor intensity; it is also often impossible

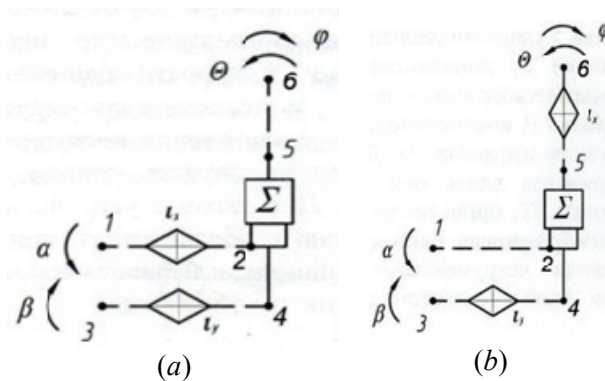


Fig. 2. Kinematic diagrams of the connection of the internal bonds of links 1–6 of the kinematic chain with the arrangement of the adjustment elements i_x and i_y in autonomous areas (*a*) and in a common area (*b*)

to ensure the same gear ratio values of the adjustment element and, therefore, the identity of the processed products for a certain parameter x . Since in the second option the value of i_y does not depend on the parameter x , then when proceeding to processing a product with a different value of this parameter, it is required to change the gear ratio of the element i_x .

Each option of the structure of the kinematic module is characterized by certain values of the parameters of the adjustment elements, which have a different effect on the functional properties of the designed object, in this case, the forming system of the process equipment [19]. Thus, the synthesis of the designed object is reduced to analyzing possible options of its structure and selecting the option with rational values of the adjusted parameters.

2.3. Supply and distribution of material and energy

It should be noted that when creating process equipment for automated subtractive and additive manufacturing, using concentrated and distributed flows of energy and material (Fig. 3) [1–3], it is not sufficient to have enlarged 8 stages involving the selection of system parameters, the procedures and the corresponding diagrams [4, 5, 8]. This is due to the fact that for traditional types of subtractive manufacturing and new types of additive manufacturing, consisting in layer-by-layer build-up of the surface of products, at the subsequent additionally introduced design stages, it is required to consider procedures and determine the parameters of process equipment modules describing the supply and distribution of material and energy [13, 14].

3. Design of process equipment using energy flows

The technologies widely used in manufacturing lead to the conclusion that the use of equipment for building-up layers and forming the surfaces of products using various combinations of energy and material flows is quite promising (see Fig. 3). This, in turn, poses the problem of distributing the components of the material and energy sources not only along a given contour or surface, but also in depth from the surface of the product, as well as taking into account the nature of the pulses of material and energy supply [4, 5, 8, 13, 14].

3.1. Heat and mass transfer criteria

The problems of distribution of material and energy flows help to solve the criteria of heat and mass transfer, which establish the sequence of

structure formation in the processed material and on the formed surface with an increase in the power of impacts [4, 8, 13, 20]:

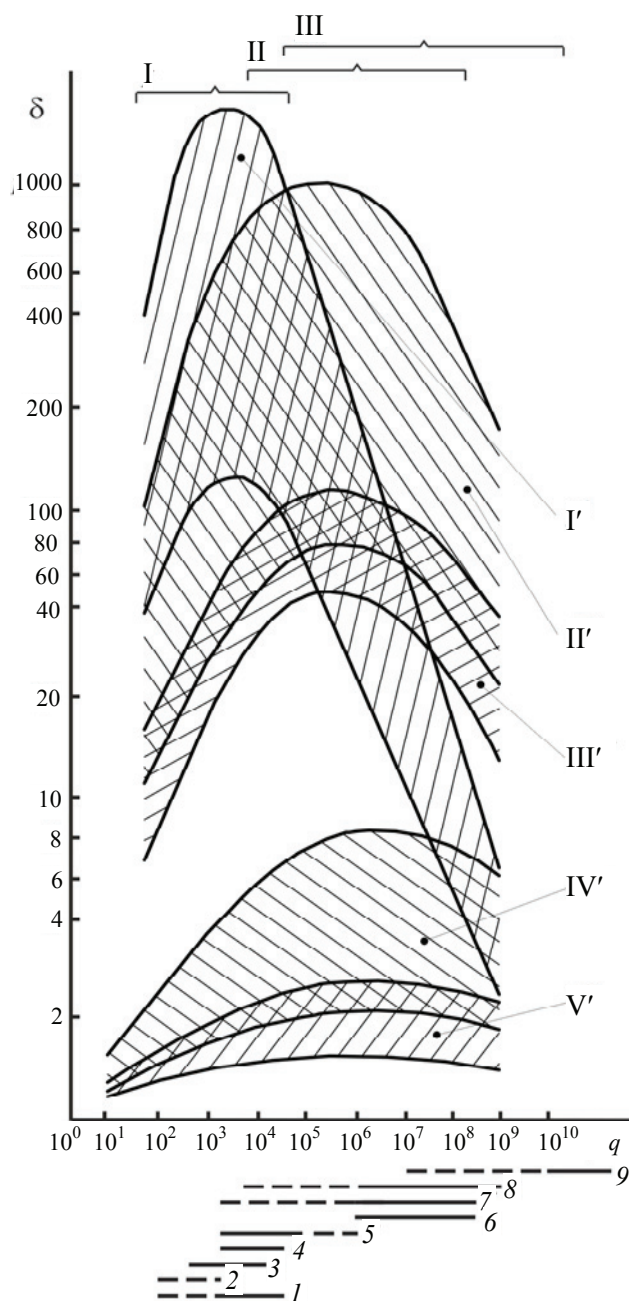


Fig. 3. Distribution of treatment methods according to the accuracy of surface formation:

I' – material separation; II' – coating; III' – heat treatment; IV' – cutting with a tool; V' – deformation; depending on the level of concentration in the zones of energy release: I – surface-distributed; II – set of localized; III – focused; for sources: 1 – induction heating; 2 – gas flame; 3 – plasma arc; 4 – electric contact heating; 5 – welding arc; 6 – spark discharge; 7 – electron, ion beam; 8 – continuous laser; 9 – pulse-periodic laser

$$\begin{array}{c}
 \boxed{\begin{array}{c}
 \text{(Re In)} \quad \overbrace{\text{(Re In)}} \\
 \text{Pe}(1/\text{Pr}) \Rightarrow \text{Re}(\text{Pr } D_s) \Rightarrow \text{Mr}(\text{Re}/\text{Pr}) \cdot (\text{In}/D_s) \Rightarrow \text{Gr}(\text{Pr}) \Rightarrow \text{Rl}, \\
 \text{(D}_s) \quad \underbrace{\text{(Re In}/D_s)}
 \end{array}} \\
 (1)
 \end{array}$$

in which $\text{Pe} = \upsilon t / \omega$ is the Peclet criterion; $\text{Pr} = \upsilon / \omega$ is the Prandtl criterion; $\text{Re} = \upsilon t / \nu$ is the Reynolds criterion; $\text{In} = \beta g \nabla T t^2 / \upsilon^2$ is the ratio of buoyancy to inertial force; $D_s = \sigma_k \nabla T t / (\upsilon \rho / \nu)$ is the ratio of the forces of capillarity and viscosity; $\text{Mr} = \sigma_k \nabla T t^2 / (\rho \omega \nu)$ is the Marangoni test; $\text{Gr} = \beta g \nabla T t^4 / \nu^2$ is the Grashof test; $\text{Rl} = \beta g \nabla T t^4 / (\omega \nu)$ is the Rayleigh criterion; where t is the characteristic dimension; ω is the coefficient of thermal diffusivity; υ is the velocity; ν is the coefficient of kinematic viscosity; β is the coefficient of volumetric expansion; g is the acceleration of gravity; T is the absolute temperature; σ_k is the thermocapillarity coefficient; ρ is the density of the process medium.

3.2. Electrical power criteria

The criteria characterizing energy flows during electro-physical-chemical processing have a significant impact on the sequence of spatial phenomena and help to control the formation of the properties of the processed material [4, 8, 13, 20]:

$$\text{Sm}(E_m/S_e) \Rightarrow \text{Si}; \quad \text{Mr}(E_k) \Rightarrow E(T_k/E_k) \Rightarrow \text{Rl}, \quad (2)$$

in which $\text{Sm} = IB / (\upsilon^2 \rho t)$ is the magnetic impact criterion; $E_m = \upsilon E_1 / (H'B)$ is the ratio of the flow velocity to its heat content and the electric field strength to its magnetic induction; $S_e = E_1 t^2 / (IR)$ is the electric field intensity criterion; $\text{Si} = I^2 R / (\nu \rho H t^3)$ is the energy criterion; $E_k = \varepsilon \gamma^2 \nabla T / \sigma_k$ is the ratio of thermoelectric and capillary forces; $E = \varepsilon \gamma^2 \nabla T t^2 / (\rho \omega \nu)$ is the thermoelectric criterion; $T_k = \rho \beta g t^2 / \sigma_k$ is the ratio of buoyancy to capillary lift; where I is the current strength; B is the magnetic induction; H' is the flow enthalpy; R is the electrical resistance; ε is dielectric factor; γ is the thermoelectromotive force coefficient E_1 is the electric field strength.

The use of sequences of transfer criteria (1) and (2) to analyze the processes of formation of structures and phases of a material greatly reduces the volume of experimental studies of the technology of formation of a surface layer with combined methods of thermomechanical and electro-physical-chemical treatment [4, 8, 13, 20].

3.3. Feedback in the process system

When unstable structures of surface layers are formed, it is advisable to measure the turbulence of flows and flows of the treated material, using the Reynolds criterion $\text{Re} = \upsilon t / \nu$, and describe the waviness and roughness of the forming surface relief R . The thickness of the formed layer t determines the increase or decrease in its mass Q , and taking into account the continuity or porosity of the laminate material or coatings change their relative hardness $H_\varepsilon = \Delta H / H$. Therefore, the layer thickness t is proportional to the expression $Q / (1 - H_\varepsilon)$ [3, 4, 8, 20].

As a result, when controlling energy flows, it is advisable to use ratios proportional to the transfer criteria to optimize the geometric characteristics of the surface relief:

$$R \approx \frac{\upsilon_S [Q / (1 - H_\varepsilon)]}{(B/I) \cdot (\upsilon/S)} = \frac{\upsilon_S S I Q}{\upsilon B (1 - H_\varepsilon)}, \quad (3)$$

and to optimize the physical and mechanical parameters of the relative hardening of the material of the surface layer from relation (3) we obtain:

$$H_\varepsilon \approx 1 - \frac{\upsilon_S S I Q}{\upsilon B R}, \quad (4)$$

where υ_S is the total velocity of the main υ and additional S of motions.

Relations (3) and (4) show a positive feedback of the relief R and a negative feedback of hardening H_ε with the treatment performance $\upsilon_S Q$, as well as with the adjustable components of the kinematic characteristics of the equipment (S/υ) and the power of the energy source (I/B) [3, 4, 8, 20]. The analysis of relations (3) and (4) allows finding the basic principles of organizing feedback in an open process system.

In the case when, first of all, it is necessary to form the surface (3), and then to strengthen it (4), as, for example, during deformation and cutting, a positive feedback is created in the process system under thermomechanical impacts. Excessive degrees of freedom of the tool and the process environment, suppressing the scattering of energy and substance

flows in the shape-changeable allowance, create strengthening structures in the surface layer and increase the processing efficiency [3, 4, 8, 14]. In the case when first it is required to strengthen (4) and then to form the surface relief (3), as, for example, when applying coatings, a negative feedback is organized in the process system under electro-physical-chemical influences. Additional impacts by energy sources and substances, forming strengthening structures in the surface layer, do not allow the development of process instability during the formation of the surface relief and, when it is stabilized, do not allow to increase the treatment performance [3, 4, 8, 14].

Taking into account the contours of direct and feedback links in the process system, it is also required to study numerical control schemes and consider the complex of process equipment as a mechatronic system [1, 3, 4, 21].

4. Design of process equipment for additive manufacturing of products

If, in the process of digitalization of production, process equipment is considered from the standpoint of computerization of manufacturing; the equipment for the implementation of additive technologies, its nodes and parts should be designed as computer peripheral devices built on the same architecture as a computer.

To designate the processes of additive manufacturing of products in the process system, the terms that have historically formed in the course of its evolution are most often used: direct manufacturing of products of complex shape – “growing” (*Solid Freeform Fabrication*); layer-by-layer manufacturing – “synthesis” (*Laminate Synthesis*); rapid prototyping – “prototyping” (*Rapid Prototyping*); the formation of three-dimensional objects – “printing” (*3D Component Forming*). Therefore, it is necessary to determine the relationship of the forming processes and make a distinction between the terms used [4, 5, 8, 22, 23].

4.1. Finite state machines and the self-reproduction model

For *Solid Freeform Fabrication*, self-reproduction of products by the von Neumann model [22, 23], the following machines are required: C is “a copier of the design plan”; O is “an executor of the design plan”; S is “a starting device” (including C and O at the appropriate time); B_{C+O+S} is “a plan for building the automaton” (describing all the elements of the model). As a result, the entire automaton is expressed symbolically $C+O+S+B_{C+O+S}$. After the

initial launch, S gets at its disposal the plan for building the automaton as a whole B_{C+O+S} , C copies it, and O, in turn, follows it to build C, O and S.

Then, one can represent [4, 5, 8, 22, 23] the launch of S as a direct access to the flows of matter and energy; getting the B_{C+O+S} plan as self-adjustment of the reproduction program; copying of the plan by C as translation of the information stream; building the automaton O as self-organization of its structure.

The study of the production processes of parts without the use of forming equipment [4, 5, 8, 22, 23], depending on the state of aggregation of the initial material, the dimension of the flows of the forming medium and the sequence of process operations made it possible to present a set of methods for “growing” parts in the form of a structural diagram of connections (Fig. 4, a).

The structural diagram of connections is a directed closed graph and describes an automaton with a finite number of states [4, 5, 8, 22, 23]. The vertices of the graph depict the processes of fabrication of parts without forming tools and represent logical operations: translation of information, flows of matter and energy; starting and stopping an automatic cycle.

The edges of the graph reflect changes in the states ($1-6$ and $1', 2', 4'$) of the material of the process environment, and the routes provide for various combinations of changes depending on the choice of the initial process and the order of execution of subsequent processes.

Thus, different options for process routes have the form of different sequences when selected as the initial process (see Fig. 4, a):

- direct production of parts of complex shape: $1 \rightarrow 2 \rightarrow 3; 4 \rightarrow 3; 1 \rightarrow 5; 4 \rightarrow 2' \rightarrow 5; 6;$
- layer-by-layer production: $1' \rightarrow 4 \rightarrow 3; 2 \rightarrow 3; 1' \rightarrow 6; 2 \rightarrow 4' \rightarrow 6; 5;$
- fast prototyping: $2' \rightarrow 1' \rightarrow 6; 4' \rightarrow 6; 2' \rightarrow 5; 4' \rightarrow 1 \rightarrow 5; 3.$

Considering the replacement in the self-reproduction model of processes (direct access to the flows of matter and energy S; self-adjustment of the reproduction program B_{C+O+S} ; translation of the information flow C; self-organization of the structure of the automaton O) by providing them with elements of the traditional non-adaptive process system (part, tool, device, machine), we come to the conclusion that it is impossible to create a finite automaton only when using a forming equipment, since it must exist for the manufacture of a part, and in turn, the equipment must also be made to produce it, etc.

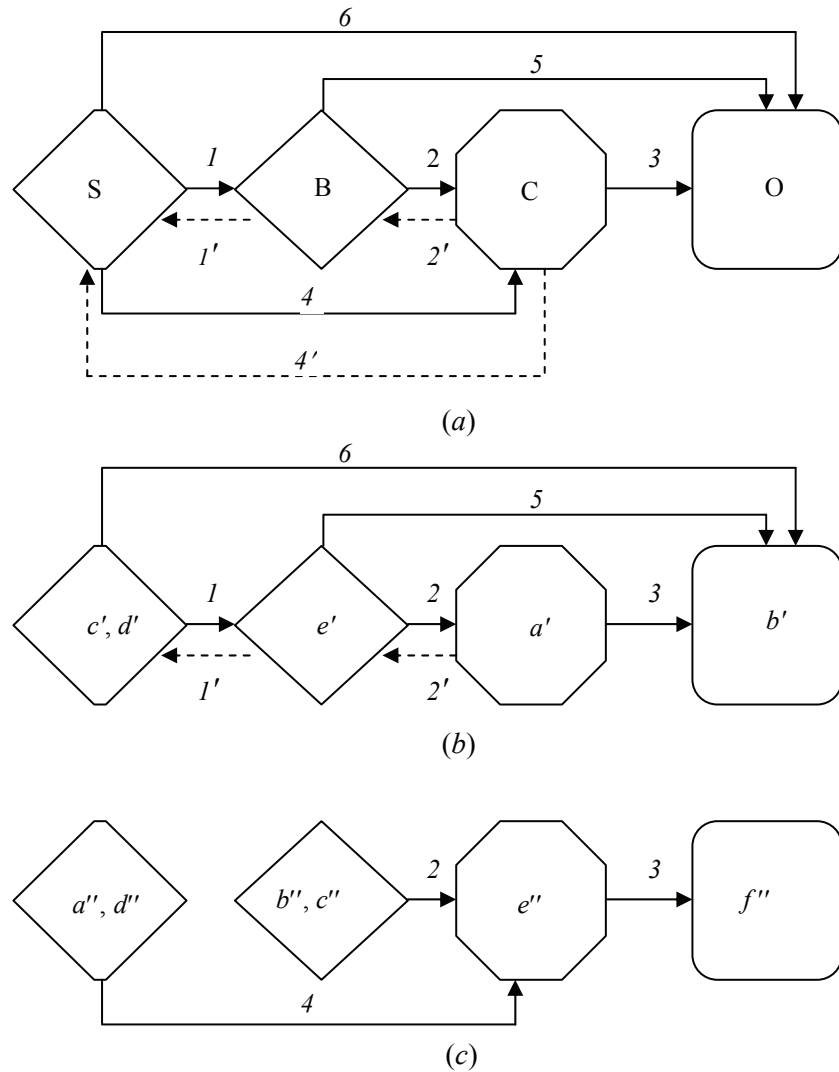


Fig. 4. Structural diagram of connections in the methods of manufacturing machine parts without forming equipment (a), joining sheet materials (b), sintering and fusing powder layers (c)

Thus, the algorithms proposed according to the von Neumann self-reproduction model [4, 5, 8, 22, 23] make it possible to describe the methods of manufacturing machine parts without forming equipment, and the inverse sequences, using non-adaptive tooling methods, are not representable as a finite automaton.

In accordance with the existing terms, the description of the processes of manufacturing parts without forming tools with algorithms in compliancy with the proposed structural diagram of connections provides an opportunity to analyze the existing equipment and develop new process equipment for direct solid freeform fabrication of products [4, 5, 21, 24].

Let me consider traditional additive methods of manufacturing machine parts described in the review [25] without forming tools [26–29].

4.2. Laminate Synthesis

The process equipment for the manufacture of parts from sheet materials [28] generally includes (Fig. 4, a) installation a' , containing a laser and a scanning device for coordinating cutting and cutting of sheet blanks, manipulator b' , which ensures the movement of the cut sheet contours and their stacking, press c' and oven d' for molding and volumetric sintering of the formed parts. The computer-based system e' provides control of the process equipment and optimal cutting of the sheet.

Having matched the flows of matter and energy S – the part formed on the press c' and in the furnace d' , the prototyping program B – the control computer e' , the information translation C – scanning by the laser a' , we connect the elements of the structure O of the process equipment by the movements of the manipulator b' (Fig. 4, b), repeating all the connections indicated in [25] on the generalized diagram (Fig. 5, a).

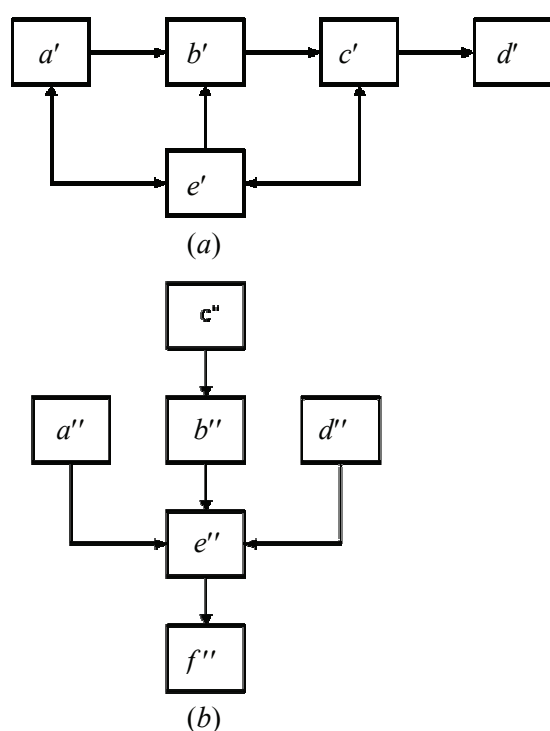


Fig. 5. Generalized diagrams of process equipment for the manufacture of parts by joining sheet materials (a), sintering and fusion of powder layers (b)

From the algorithm for manufacturing parts from sheet materials (Fig. 4, b) obtained on the basis of the generalized diagram of the process equipment (Fig. 5, a), it can be seen that there are no operations 4 and 4' connecting c' and d' with a' , and the direction of connection 6 (Fig. 4, a) is reversed. Connection 4 of the press and the furnace – c' and d' with the cutting machine a' and feedback 4' (Fig. 4, b) will be required in the case when sheets of low-melting materials are connected to create a prototype or sheets of dissimilar materials, different by thickness and physical and mechanical properties. Such connections will provide a change in the intensity of radiation and will allow you to control the depth of cut and melting. In this case, for the press and the furnace – c' and d' earlier than the feedback, direct link 6 with the manipulator b is required.

Thus, the study of the algorithm for manufacturing parts from sheet materials (Fig. 4, b) makes it possible to propose measures to expand the process capabilities of the equipment by creating layered parts from dissimilar materials.

4.3. Sintering and fusion of powder layers (Rapid Prototyping)

The process equipment for manufacturing parts by laser, electron-beam or other sintering and fusion of powder layers [29-31] contains the following main

functional units (Fig. 5, b): a device for layer-by-layer powder feeding a'' , a scanning device b'' of an emitting source c'' , a device for layer-by-layer pressing of the powder d'' and a substrate e'' equipped with a vertical drive f'' .

The analysis of the structure of links noted [25] in the generalized diagram (Fig. 5, b) demonstrates the correspondence of the devices for layer-by-layer feeding and pressing of the powder a'' and d'' – to the flows of matter and energy S, scanning device b'' and c'' – the software for reproducing B of the formed part, substrate e'' , moved by the drive f'' – translation of information C, which provides self-organization of the structure O of the process equipment (Fig. 4, c). The obtained algorithm for manufacturing parts by sintering and fusing powder layers (Fig. 4, c) shows the presence of a minimum number of links between devices that ensure rapid prototyping of a model and production of a product. There are no operations 1, 5 and 1', 2' associated with the prototyping software B (Fig. 4, a), operation 6, which ensures the connection of the vertical movement f'' of the formed part with the devices for layer-by-layer feeding and pressing of the powder a'' and d'' , as well as feedback 4' of the substrate e'' with a'' and d'' .

Therefore, the process equipment must be supplemented with a system that controls beam scanning b'' and c'' [25], providing selective sintering and fusion of various layers of the powder by means of specified displacements and beam intensity. The use of the control system will make up for the missing connections in the structure of the algorithm (Fig. 4, a).

Thus, the study of the structure of links when obtaining parts by laser, electron beam or other sintering and fusion of powder layers (Fig. 4, c) indicates the need to use an additional control device for the part prototyping program.

As a result of the analysis of the methods of direct solid freeform fabrication of machine parts, the expediency of developing processes of laminate synthesis with controlled formation of material properties by energy flows is shown.

5. Design of mechatronic process equipment in digital manufacturing

Mechatronic systems include mechanical, electromechanical, electronic and control parts [3, 4, 21, 24, 32, 33]. They include sensors of the state of the external environment and the control system itself; energy sources; executive mechanisms; amplifiers; computing elements (computers and microprocessors).

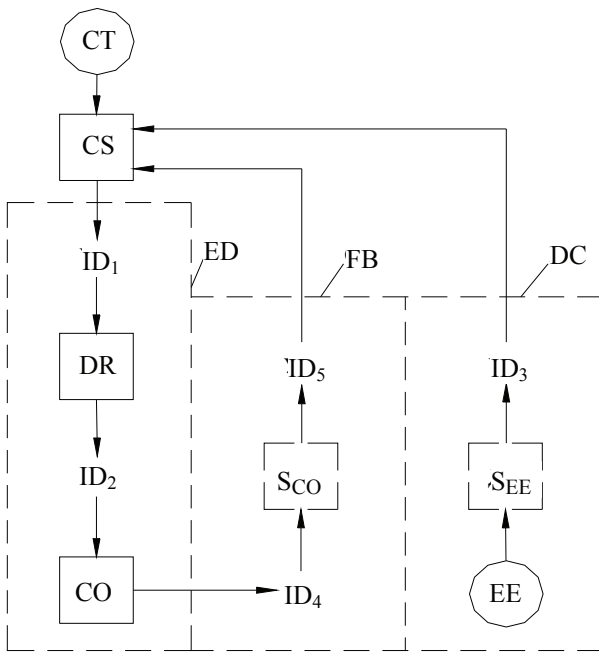


Fig. 6. Components of the mechatronic system of the technological complex:

ED – executive devices; FB – feedback; DC – direct connection; CT – control task; CS – control system; ID – interface device; DR – drives; CO – control object; S_{CO} – sensors of the state control object; S_{EE} – sensors of the state of the external environment; EE – external environment

5.1. Components of the mechatronic system

A mechatronic system is a single set of electromechanical and electronic elements and computer facilities, between which there is a continuous exchange of energy and information. A functionally simple mechatronic system of a technological complex can be subdivided into the following components (Fig. 6): executive devices (control object and drives), information devices (sensors of the internal state of the system and sensors of the external environment) and a control system (computer and microprocessors).

The interaction between these parts, realizing direct connections and feedback in the system, is carried out through the interface device. The control system includes hardware and software that ensures the coordinated operation of the hardware and ensures synchronization of the processes of collecting and processing data from information devices with the processes that control actuators. As a result, the mechatronic production module for combined processing is structurally divided into electrical and mechanical components, as well as a control system.

5.2. Structural diagram of the mechatronic system

The generalized diagram of the production module of the process equipment (Fig. 7) must contain all the necessary components of the mechatronic

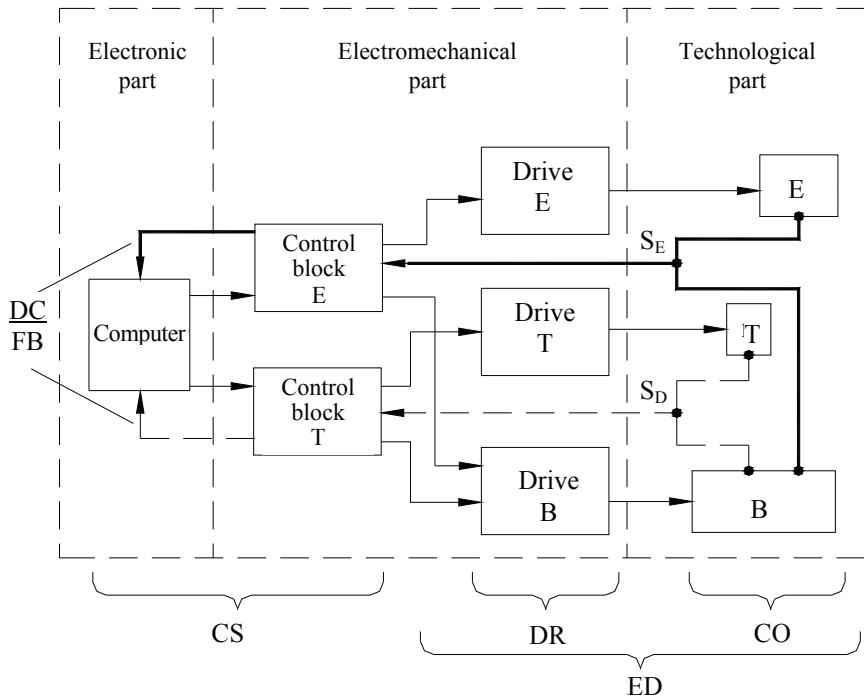


Fig. 7. Structural diagram of the mechatronic system:

B – billet; T – tool; E – concentrated energy source; S_D – displacement sensor; S_E – energy flow intensity sensor; CS – control system; DR – drives; CO – control object; ED – executive devices; DC – direct connection; FB – feedback

system: control objects; drives; sensors; control devices coupled to each other; software system.

The flexibility of the functioning of the mechatronic system in digitalized production is ensured by the use of universal working bodies capable of performing various operations (tools and energy sources), as well as by changing the modules of the replaceable tool, which are selected by the control system in accordance with the operations performed or the selection and management of energy sources.

In such process systems it is impossible to determine in advance the number and type of required actuators and sensors [3, 4, 21, 24, 30, 31]. Therefore, it becomes necessary to solve two problems: 1) to process and systematize the information coming from the sensors; 2) to ensure synchronization between this information and the movement of the actuators.

This is achieved by software that controls the operation of the corresponding computing facilities. Consequently, algorithmic and software tools play a key role in ensuring the multifunctional operation of the mechatronic system. As a result, the structural diagram of any flexible production module using concentrated energy sources must have the considered elements in order to provide the module with a long time of stable operation in an autonomous mode using a minimum amount of control actions.

6. Conclusion

Thus, the analysis of the steps and stages of the design of process equipment for the production of traditional type and the study of the features of the formation of process equipment using flows of energy and consumables, the study of the structural synthesis of mechatronic complexes in digitalized production, made it possible to supplement the process of designing complexes of automated process equipment with new stages as for traditional subtractive and new additive manufacturing.

First of all, the design of mechatronic technological complexes in digitalized production, when creating a product, should be preceded by an analysis of information flows describing the movement of material and energy flows:

- from the working area of treatment with energy flows and the introduction of consumables in process equipment;

- through tools, equipment and drives of intensive treatment process equipment;

- to computers and their peripherals, access to local production and global networks of information resources.

Additional stages in the design of technological complexes include:

- first – the choice of energy sources and consumables for the intensification of processes with the analysis of the technological environment using flows of energy and material;

- then – the allocation of direct connections and feedback in a computerized process system under electro-physical-chemical and thermomechanical influences;

- in conclusion – the analysis of the adaptation processes of the equipment facilities in the manufacturing system, including the self-adjustment of the program and the self-organization of the structure of the automated equipment.

As a result of attracting additional design stages, based on tracing information flows, the following are produced:

- structural analysis of an open production system and synthesis of process equipment using energy sources and consumables;

- parametric optimization of modules and installations, tools and equipment for the process facility;

- layout of production modules and synthesis of an adaptive mechatronic system for highly efficient treatment.

7. Funding

The presented research is currently partly funded by grants for the Project 7.3.10 and others included the National Program of Scientific Research of the Republic of Belarus for 2021–2025 “Mechanics, metallurgy and technical diagnostics in mechanical engineering”; since 1999, it has been supported continually as part of the projects of the Belarusian Republican Foundation for Fundamental Research.

8. Acknowledgments

The author expresses gratitude to his numerous co-authors and colleagues, namely to his mentor, Academician of the National Academy of Sciences of Belarus P.I. Lashcheritsyn (Belarusian National Technical University) for giving support in the design of technological facilities for machine-building industry, Academicians of the National Academy of Sciences of Belarus P.A. Vityaz (United Institute of Mechanical Engineering of the National Academy of Sciences of Belarus) and S.A. Chizhik (A.V. Lykov Institute of Heat and Mass Transfer of the National Academy of Sciences of Belarus) for their contribution of ideas related to the problems under discussion and their assistance in developing a methodology for the design of equipment for nano-

and additive technologies, and to Professor B.M. Bazrov (A.A. Blagonravov Institute of Mechanical Engineering RAS) for his ideas regarding the specifics of designing equipment on a modular basis for various types of industry and many others.

9. Conflict of interests

The authors declare no conflict of interest.

References

1. Yashcheritsyn PI, Kheifets ML, Kozhuro LM, Chemisov BP. Designing technological complexes of high-effective treatment of products on the basis of products multifactorial optimization. *Doklady Natsional'noy akademii nauk Belarusi*. 1997;41(3):112-118. (In Russ.)
2. Yashcheritsyn PI, Averchenkov VI, Kheifets ML, Kukhta SV. Analysis of the properties of ratios of technological solutions in designing combined methods of the treatment of materials. *Doklady Natsional'noy akademii nauk Belarusi*. 2001;45(3):106-109. (In Russ.)
3. Yashcheritsyn PI, Kheifets ML, Zeveleva EZ, Akulovich LM. Designing of mechatronic technological complexes of high-performance processing. *Doklady Natsional'noy akademii nauk Belarusi*. 2003;47(6):120-124. (In Russ.)
4. Rusetsky AM. *Theoretical bases of technological systems designing*. Minsk: Belaruskaya Nauka; 2012. 239 p. (In Russ.)
5. Vityaz PA, Kheifetz ML, Chizhik SA. "Industry 4.0": from information and communication and additive technologies to self-reproduction of machines and organisms. *Vesti Natsyonal'noy akademii nauk Belarusi. Seriya fiziko-tekhnicheskikh nauk*. 2017;2:54-72. (In Russ.)
6. Cherpakov BI. Metal-cutting machines and woodworking equipment; vol. IV-7. In: Frolov KV. (ed.) *Mechanical engineering: Encyclopedia*; Moscow: Mashinostroenie; 2002. 864 p. (In Russ.)
7. Pronikov AS, Averyanov OI, Apollonov YuS. Design of metal-cutting machine tools and machine-tool systems. Vol. 1. *Machine tools design*. Moscow: Mashinostroenie; 1994. 444 p. (In Russ.)
8. Vityaz PA, Kheifetz ML, Koukhta SV. *Laser-plasma techniques in computer-controlled manufacturing*. Minsk: Belarusskaya nauka; 2011. 164 p. (In Russ.)
9. Kheifets ML. Self-organization of structure formation processes in intense treatment and operation of materials. *Advanced Materials and Technologies*. 2016;3:14-20. DOI:10.17277/amt.2016.03.pp.014-020
10. Kheifetz ML. Self-organization of structure formation processes in intense treatment of materials. In: Dasic P. (ed.) *Modern Manufacturing Process and Systems; vol.1: Fundamentals. Collective monograph*. Moscow-Belgrade-Vrnjacka Banja: SaTCIP Publisher Ltd.; 2018. p. 53-73. (In Russ.)
11. Kheifetz ML. From information and additive technologies to self-reproduction of machines and organisms. *Advanced Materials and Technologies*. 2018;1:22-35. DOI:10.17277/amt.2018.01.pp.022-035
12. Vityaz PA, Kheifetz ML, Chizhik SA Synergetic Technologies of Direct Layer Deposition in Aerospace Additive Manufacturing. In: Fores F, Boyer R. (eds.) *Additive Manufacturing for the Aerospace Industry*. Cambridge: Elsevier; 2019. p. 427-448.
13. Vasil'ev AS, Dal'sky AM, Klimenko SA, Polonsky LG, Kheifetz ML. *Technological fundamentals of machine quality management*. Moscow: Mashinostroenie; 2003. 256 p. (In Russ.)
14. Kheifetz ML. *Design process of combined processing*. Moscow: Mashinostroenie; 2005. 272 p. (In Russ.)
15. Bazrov BM. *Modular technology in mechanical engineering*. Moscow: Mashinostroenie; 2001. 368 p. (In Russ.)
16. Bazrov BM, Kheifetz ML. Method of presenting a product as an object of digitalization of manufacturing by a structured set of modules. *Doklady Natsional'noy akademii nauk Belarusi*. 2019;63(3):377-384. (In Russ.)
17. Artobolevskiy II, Il'inskiy DYa. *Bases of the automatical systems of cars synthesis*. Moscow: Mashinostroenie; 1983. 280 p. (In Russ.)
18. Vragov YuD. *Analysis of configurations of metal-cutting machines: Komponentika bases*. Moscow: Mashinostroenie; 1978. 208 p. (In Russ.)
19. Rusetsky AM (ed). *Design and equipment of technological systems*. Minsk: Belaruskaya Nauka; 2014. 316 p. (In Russ.)
20. Gordienko AI, Kozhuro LM, Kheifetz ML, Kukhta SV. Use of analogy parameters for development of combined physical-chemical material processing methods. *Doklady Natsional'noy akademii nauk Belarusi*. 2004;48(4):107-110. (In Russ.)
21. Rusetsky AM. *Automation and control in technological complexes*. Minsk: Belaruskaya Nauka; 2014. 375 p. (In Russ.)
22. Kheifets ML. Analysis of the algorithms of production of machine parts by models of von Neumann's self-reproduction. *Doklady Natsional'noy akademii nauk Belarusi*. 2001;45(5):119-122. (In Russ.)
23. Kheifetz ML. *Formation of materials properties at the synthesis of layered components*. Novopolotsk: Polotsk State University; 2001. 156 p. (In Russ.)
24. Kheifetz ML. *Quality assurance of products in technological complexes*. Minsk: Belaruskaya Navuka; 2019. 248 p. (In Russ.)

25. Tolochko NK, Sobolenko NV, Mozsharov SE. Laminate synthesis technology – a new method of shaping powder products. *Vestnik mashinostroyeniya = Russian Engineering Research*. 1995;4:22-25. (In Russ.)

26. Feygin M. *Apparatus and method for forming an integral object from laminations*. United States Patent 4,752,352. 21 June 1988.

27. Deckard CR. *Method and apparatus for producing parts by selective sintering*. United States Patent 4,863,538. 5 September 1989.

28. Beaman JJ, Deckard CR. *Selective laser sintering with assisted powder handling*. United States Patent 4,938,816. 3 July 1990.

29. Bourell DL, Marcus HL, Barlow JW, Beaman JJ, Deckard CR. *Multiple material systems for selective beam sintering*. United States Patent 4,944,817. 31 July 1990.

30. Kheifetz ML. Design of mechatronic technological complexes for traditional and additive manufacturing. *Doklady Natsional'noy akademii nauk Belarusi*. 2020;64(6):744-751. (In Russ.)

31. Chizhik SA, Kheifetz ML, Filatov SA. Prospects for the development of technological systems of composite materials additive synthesis and products shaping. *Mekhanika mashin, mekhanizmov i materialov*. 2014;4(29):68-74. (In Russ.)

Информация об авторах / Information about the authors

Хейфец Михаил Львович, доктор технических наук, профессор, директор, ГНУ Институт прикладной физики НАН Беларуси, Республика Беларусь, Минск; AuthorID (Scopus) 57214720034; e-mail: mlk-z@mail.ru

Mikhail L. Kheifetz, D. Sc. (Engineering), Professor, Director of Institute of Applied Physics of the National Academy of Sciences of Belarus; Minsk, Republic Belarus; AuthorID (Scopus) 57214720034; e-mail: mlk-z@mail.ru

Received 30 November 2020; Accepted 18 January 2021; Published 21 April 2021



Copyright: © Kheifetz ML, 2021. This article is an open access article distributed under the terms and conditions of the Creative Commons Attribution (CC BY) license (<https://creativecommons.org/licenses/by/4.0/>).

Anthracite-based activated carbons for the efficient solution of important environmental problems

Victor M. Mukhin✉

*JSC "Elektrostal Scientific and Production Association "Neorganika",
4, K. Marx St., Elektrostal, 144001, Russian Federation*

✉ VictorMukhin@yandex.ru

Abstract: This article examines the issues of environmental pollution as a result of man-made activities and determines the most effective ways to protect the biosphere with the help of carbon-adsorption technologies. Due to their physical and chemical properties, activated carbons are an ideal adsorbent and allow solving a wide range of environmental safety issues.

Based on the theoretical assumptions expressed by Academician M. M. Dubinin, it is shown that anthracite is an excellent raw material for producing activated coal. A technology for obtaining CAS (Crushed Anthracite Sorbent) grade activated carbons from anthracite has been developed and its adsorption properties have been studied. Tests of CAS activated carbon in the purification of drinking water and wastewater, protection of the atmosphere from harmful gases and vapors, and detoxification of soils from herbicide residues were carried out. The necessity and requirements for the creation of new production facilities for active coals based on anthracite in Russian coal basins are substantiated.

Keywords: anthracite; activated carbon; adsorption properties; environment; drinking water purification; atmosphere protection; soil detoxification.

For citation: Mukhin VM. Anthracite-based activated carbons for the efficient solution of important environmental problems. *Journal of Advanced Materials and Technologies. 2021;6(1):30-41. DOI: 10.17277/jamt.2021.01.pp.030-041*

Активные угли на основе антрацита для эффективного решения важных экологических проблем

В. М. Мухин✉

*АО «Электростальское научно-производственное объединение «Неорганика»,
ул. К. Маркса, д. 4, Электросталь 144001, Российская Федерация*

✉ VictorMukhin@yandex.ru

Аннотация: Данная статья рассматривает вопросы загрязнения окружающей среды в результате техногенной деятельности и определяет наиболее эффективные пути защиты биосферы с помощью углеадсорбционных технологий. В силу своих физико-химических свойств активные угли являются идеальными сорбционными материалами, которые позволяют решать большой круг вопросов экологической безопасности.

На основании теоретических предпосылок, высказанных академиком М. М. Дубининым, показано, что антрацит является отличным сырьем для получения активных углей. Разработана технология получения активных углей марки ДАС (дробленый антрацитовый сорбент) из антрацита и исследованы его адсорбционные свойства. Проведены испытания активного угля ДАС в очистке питьевой и сточных вод, защиты атмосферы от вредных газов и паров и детоксикации почв от остатков пестицидов. Обоснована необходимость и потребность в создании новых производств активных углей на основе антрацита российских угольных бассейнов.

Ключевые слова: антрацит; активный уголь; адсорбционные свойства; экология; очистка питьевой воды; защита атмосферы; детоксикация почв.

Для цитирования: Mukhin VM. Anthracite-based activated carbons for the efficient solution of important environmental problems. *Journal of Advanced Materials and Technologies. 2021;1(21):30-41. DOI:10.17277/jamt.2021.01.pp.030-041*

1. Introduction

The progressive pollution of the environment has made environmental safety an important component of national security in general. Today, almost the entire planet and, especially, areas of mass population of people are subject to serious environmental threats, the main of which are radiation contamination of territories, soil oppression by acid rain, soil pollution with chemicals and pesticides, oil spills on land and sea and the destruction of the atmosphere. Biosphere pollution dramatically reduces the quality of life of people. According to the WHO (2002), factors affecting human health depend on diet and lifestyle (51 %), environment (39 %), medicine (10 %) [1].

The problems of global pollution of the environment were raised even earlier by N.V. Keltsev, the Russian scientist, Professor at Mendeleev Moscow Institute of Chemical Technology, who proposed the main way to resolve the situation. As he wrote, since not only the army was faced with the question of life and death, but all the humanity was concerned about the pollution of the biosphere, it was time to turn again for help to adsorption – one of the most effective methods of protecting the environment from pollution. [2].

Due to their physicochemical properties, carbon adsorbents (activated carbons) are unique and ideal sorption materials that allow solving a wide range of issues related to ensuring the ecological safety of humans, the environment and infrastructure.

Activated carbons (ACs) are highly porous materials obtained in the form of grains or powder based on various carbon-containing raw materials, which have a developed inner surface (up to $2500 \text{ m}^2\text{g}^{-1}$) and have high absorption characteristics for impurities in the purified media (air, gases, water and other liquids, soil) [3, 4].

Various carbon-containing materials, such as coal, peat, wood, nut shells and seeds of fruits, various crop wastes (straw of various crops, etc.), can be used as a raw material for obtaining such ACs [5]. In the porous structure of activated carbon (micropores 1.2–3.0 nm and mesopores 3.1–100 nm), any types of organic microimpurities are absorbed due to adsorption forces (surface interaction forces).

Activated carbon is the second most widely used material on earth (not by tonnage, but by fields of application). The first is iron and the second is active carbon. But according to the size of its surface, activated carbon is the first material on Earth. If you roll 1 ton of iron into a sheet, then its surface area will be about 100 m^2 , and in 1 ton of active

carbon the interface is about $1,000 \text{ km}^2$. In a tablespoon of active carbon, the interface is equal to the area of a football field.

ACs is widely used in many areas of the economy, ecology and defense of the country. In the economy, this is oil and gas production and gas processing, mining (flotation of non-ferrous metal ores), metallurgical industry (including gold hydrometallurgy), chemical, chemical and pharmaceutical industries (suffice it to say that ACs is used in the production of millions of medicines), food industry (including vodka production) and many other branches of the Russian Federation.

The role of ACs is also irreplaceable in the country's defense: from gas-mask equipment to life support systems for spaceships, orbital and (in the future) interplanetary stations.

But the most outstanding role of ACs is in ensuring environmental safety and protecting the environment from man-made pollution. The meaning of the word "ecology" is incomplete without the word "activated carbon".

Table 1 shows the main environmental technologies for ACs application in the protection of all parts of the biosphere: the atmosphere, hydrosphere, lithosphere and man himself as the main object of the biosphere [6].

The description of all environmental technologies necessary for the ACs application, it might need to publish a monograph, equivalent in size to an encyclopedia. Partially ecological technologies for using ACs are described in our monographs [5, 7].

To assess the significance of ACs in environment protection, it is worth highlighting the most vital area that ensures the environmental safety of the population – the purification of drinking water and wastewater.

Despite the huge reserves of fresh water on our planet, the shortage of drinking water on Earth is constantly growing. Currently, out of 6 billion people of the world's population, 1.5 billion (i.e., one quarter) lack drinking water (there is evidence that by 2,025 this number will reach 2.5 billion). Even if water purification is carried out, yet, due to the lack of quality water, 36 million people will die, which is comparable to the number of people dying from AIDS [8].

According to the most recent information, 40 % of the Russian population drink water that is undesirable for consumption, leading to chronic diseases and poisoning. The reason is the pollution of water supply sources with industrial wastewater and agricultural wastewater (Radio Echo of Moscow, February 9, 2021).

Table 1. Environmental technologies for the use of active coals

| Component of the biosphere | Carbon-adsorption technology |
|----------------------------|--|
| Atmosphere | Recovery of solvents, sanitary cleaning of waste gases, incl. desulfurization, gas cleaning system of nuclear power plants (NPP), capture of gasoline vapors emitted by vehicles, destruction of chemical weapons and solid household waste, purification of air in living and working premises (air conditioning) |
| Hydrosphere | Drinking water treatment, wastewater disposal, liquid radioactive waste processing, gold and non-ferrous metal mining |
| Lithosphere | Soil protection from xenobiotics, incl. pesticides, soil remediation, zones of sanitary protection of water sources |
| Person | Means of individual and collective protection of the filtering type, production of chemical and pharmaceutical preparations, vitamins, antibiotics, entero- and hemosorption, obtaining environmentally friendly food |

Russia's water resources account for 20 % of all world fresh water reserves, including the cleanest water on the planet of Lake Baikal (depth 1,600 m, length about 800 km, width 80 km). Forecasts of futurists say that the third world war may start not because of energy resources (oil and gas), but because of fresh water. The total intake of fresh water from natural sources in Russia per year is 80–85 km³, or 2 % of the total reserves. In Moscow, the consumption is ~ 1 million m³ per day of water, that is, 400 liters per person, while in the countries of Europe, the USA and Canada, this consumption is much more economical – 120–150 liters per day [9, 10].

To provide cities and large settlements with drinking-quality water, surface water supply sources must be purified, and active coal cannot be dispensed with. Most often, such waters are polluted with oil products, pesticides and other very stable (including volatile) substances, as a rule, of organic origin. They are mainly represented by humic acids with a molecular weight of 1,300–1,500, petroleum products, organochlorine substances, dioxins and some other carcinogens (compounds with a molecular weight of 200–300), phenols, ammonia and residual chlorine (substances with a molecular weight of 70–80). In some cases, this pollution causes not only an unpleasant odor and taste of water (dung, earthy, chemical, etc.), but also the danger (and even impossibility) of its direct (without treatment) use for drinking.

In order to remove the bulk of pollutants from natural waters, a wide range of technological methods are used, including carbonation

(for deodorization), flotation, coagulation, oxidation, sedimentation, filtration, and final sorption on granular active carbon [11].

However, final sorption on AC, which ensures 100 % safety of drinking water, is implemented in Russia at only a few waterworks.

The Decree of the President of Russia V.V. Putin No. 204 of 05 July 2018 (p. 7) of May 2018 focuses on the need to improve the quality of drinking water by modernizing water supply systems using promising water treatment technologies, including those developed by the organizations of the military-industrial complex. It stresses the need to improve the quality of drinking water for the population, including that for settlements not equipped with modern centralized water supply systems [12].

As mentioned above, it is impossible to create an effective water treatment system without ACs. Currently, only six sources are used as raw materials for ACs production: bituminous coal, brown coal, coconut shells, oil residues, waste from pulp mills, and charcoal [13, 14]. However, the search for new sources of raw materials reasonably led to the choice of anthracite. It can be assumed that ACs from anthracite will have properties that are not found in other types of activated carbons [13].

2. Materials and methods

Anthracite is widely represented in various regions of Russia as a fossil coal raw material. Table 2 shows the potential reserves and volumes of this type of coal raw materials. Of greatest interest are the anthracites of the Donetsk Basin, Kuznetsk Basin and Magadan Region, that is, to organize new production

of active coals on their basis, no more than $2 \cdot 10^{-3}$ of their reserves per year will be consumed [15]. Table 3 shows the characteristics of the original anthracite of the Gorlovskoye deposit in Kuzbass. As follows from Table 3, the initial anthracite is characterized by a low ash content (3 %) and high strength (over 85 %), which makes it, of course, a promising raw material for the production of carbon adsorbents. It is especially important to note the low content of volatile substances (less than 5 %), which allows such material to be directly activated without carrying out the operation of carbonization and de-volatilization.

In 1976, Academician M.M. Dubinin [16] said that in order to ensure a high adsorption capacity of the ACs in a cubic capacity (filters, adsorbers, etc.), the development of the volume of micropores per unit volume ($\text{cm}^3 \cdot \text{cm}^{-3}$) is important, rather than that per unit of weight ($\text{cm}^3 \cdot \text{g}^{-1}$). It follows from this that in order to ensure a high adsorption capacity, and, consequently, a high service life (filters, adsorbers, etc.), it is necessary to prepare ACs with a high bulk density. Then, even with a low development of the

volume of micropores in $\text{cm}^3 \cdot \text{g}^{-1}$, there will be a high development of the volume of micropores in $\text{cm}^3 \cdot \text{cm}^{-3}$. The conversion of the volume of micropores from $\text{cm}^3 \cdot \text{g}^{-1}$ to $\text{cm}^3 \cdot \text{cm}^{-3}$ is carried out by multiplying the first value ($\text{cm}^3 \cdot \text{g}^{-1}$) by the bulk density of ACs in $\text{g} \cdot \text{cm}^{-3}$.

The original samples of anthracite in the form of pieces of 90 mm in size were crushed in a jaw crusher with the inoculation of the target fraction of 0.5–2.0 mm. To improve the quality of the prepared ACs, anthracites were de-volatilized in a laboratory rotating electric furnace in an inert atmosphere of carbon dioxide (flow rate 5–7 $\text{L} \cdot \text{min}^{-1}$ at a temperature of 750 °C). The carbonized sample was characterized by the following parameters: bulk density 830–900 $\text{g} \cdot \text{cm}^{-3}$, total pore volume 0.11–0.18 $\text{cm}^3 \cdot \text{g}^{-1}$, strength 85–87 %. The activation of anthracites was carried out in a laboratory rotating electric furnace at a temperature of 850 °C in an environment of carbon dioxide and water vapor in a ratio of 1 : 3; the activating agent was supplied at a flow rate of 5–7 $\text{L} \cdot \text{min}^{-1}$ [17].

Table 2. Reserves and resources of anthracite (million tons) of the main coal basins and deposits of the Russian Federation (RF) as of 01 January 1997

| Coal basin | Total inventory | Reserves accounted for by the State Balance Sheet of the RF | | | Forecast resources | |
|----------------|-----------------|---|----------------|--|--------------------|--------------------------|
| | | A + B + C ₁ | C ₂ | Total (A + B + C ₁ + C ₂) | Total | Including P ₁ |
| Donetsk, RF | 15,942 | 5,716 | 1,604 | 7,320 | 8,358 | 1,093 |
| Gorlovsky | 6,453 | 323 | 425 | 748 | 5,243 | 858 |
| Kuznetsky | 11,384 | 553 | 275 | 828 | 10,247 | 5,448 |
| Pechorsky | 479 | – | – | – | 479 | – |
| Eastern Urals | 88 | – | – | – | 88 | 55 |
| Magadan region | 50 | 28 | 22 | 50 | – | – |
| Total | 34,553 | 6,620 | 2,326 | 8,946 | 24,415 | 7,454 |

Table 3. Characteristics of the initial anthracite of the Gorlovsky deposit of Kuzbass

| The sample No. | Bulk density, $\text{g} \cdot \text{dm}^{-3}$ | Strength, % | Content, % | | Total pore volume, $\text{cm}^3 \cdot \text{g}^{-1}$ |
|----------------|---|-------------|------------|------|--|
| | | | ash | bats | |
| 1 | 1,020 | 88.6 | 3.05 | 4.5 | 0.10 |
| 2 | 1,100 | 87.5 | 3.26 | 4.8 | |

The adsorption isotherms of the prepared AC CAS (Crushed Anthracite Sorbent) measured on an ASAP 2020 specific surface area and porosity analyzer (Micromeritics, USA) with the development of a micropore volume of $0.21\text{--}0.23\text{ cm}^3\cdot\text{g}^{-1}$ made it possible to calculate the micropore width, which was 1.58 nm. This micropore width is most favorable for the absorption of a wide class of organic pollutants from both liquid and gaseous media.

Table 4 shows the quality indicators of the AC CAS from anthracites of various pools.

As follows from the data given in Table 4, the quality indicators of AC obtained from anthracites of various coal basins of Russia are quite close and are characterized by high adsorption properties per unit volume.

Table 5 shows the technical characteristics of the AC CAS prepared from the anthracite from the Gorlovskoye deposit of Kuzbass in comparison with the activated carbon prepared from AG-3 coal (SS grade) for water treatment purposes (JSC “Sorbent”, Perm) in RF and the AC prepared from GCN 830 coconut shells (“Norit” company, Netherlands), which is widely used in the world.

Table 4. Qualitative characteristics of CAS based on anthracite from various deposits

| Quality indicators | CAS Omsuk-chansky | CAS Donbass | CAS Kuzbass |
|---|-------------------|-------------|-------------|
| Bulk density, $\text{g}\cdot\text{dm}^{-3}$ | 720 | 780 | 798 |
| Abrasion resistance, % | 80.0 | 75.2 | 75.8 |
| Ash content, % by weight | 3.1 | 2.2 | 3.8 |
| The micropore volume: | | | |
| – $\text{cm}^3\cdot\text{g}^{-1}$ | 0.23 | 0.22 | 0.21 |
| – $\text{cm}^3\cdot\text{cm}^{-3}$ | 0.16 | 0.17 | 0.17 |
| Dynamic activity for benzene, min | 54 | 53 | 51 |
| Iodine adsorption activity: | | | |
| – $\text{mg}\cdot\text{g}^{-1}$ | 600 | 600 | 570 |
| – $\text{mg}\cdot\text{cm}^{-3}$ | 432 | 468 | 455 |

Table 5. Technical characteristics of active coals

| Quality indicators | AG-3 | Anthracite-based CAS | GCN 830 Norit |
|---|---------|----------------------|---------------|
| Bulk density, $\text{g}\cdot\text{dm}^{-3}$ | 400–500 | 780 | 450 |
| Abrasion resistance, % | 70–75 | 85 | 92 |
| Ash content, % by weight | 12–15 | 4.5 | 2.4 |
| The micropore volume: | | | |
| – $\text{cm}^3\cdot\text{g}^{-1}$ | 0.20 | 0.18 | 0.50 |
| – $\text{cm}^3\cdot\text{cm}^{-3}$ | 0.09 | 0.14 | 0.22 |
| Dynamic activity for benzene, min | 40–42 | 53 | 62 |
| Iodine adsorption activity: | | | |
| – $\text{mg}\cdot\text{g}^{-1}$ | 650 | 600 | 1,000 |
| – $\text{mg}\cdot\text{cm}^{-3}$ | 297 | 468 | 450 |
| methylene blue: | | | |
| – $\text{mg}\cdot\text{g}^{-1}$ | 120 | 89 | 110 |
| – $\text{mg}\cdot\text{cm}^{-3}$ | 56 | 69 | 60 |

As follows from the data in Table 5, CAS activated carbon in terms of the development of a microporous structure and adsorption properties for iodine and methylene blue is 1.5 times higher than that of domestic AG-3. But it is not inferior to the imported GCN 830, while maintaining a sufficiently high abrasion strength according to Russian Standard 16188-70. The purity of the obtained DAS activated carbon (which is especially important for water purification) is indicated by the low ash content (4.5 %), which is at the level of activated carbon from coconut shells and 3 times less than in AG-3. The patent for active carbon made of anthracite grade DAS belongs to JSC ENPO Inorganica (RF) [18].

3. Results and Discussion

It was expedient to consider the possibility of using this type of active carbons for water purification from organic substances dissolved in water.

3.1. Extraction of organic pollutants from water

Table 6 shows the test results of activated anthracite brand DAS, domestic AG-3 (JSC “Sorbent”, Perm, RF) and Belgian TL-830 (“Filtrosorb”, Belgium) on the efficiency of formaldehyde removal. Studies have shown that activated anthracite can compete with AG-3 and TL-830 for the extraction of formaldehyde from water. Moreover, testing was carried out by the carbonization method, when activated carbon was introduced into a flask with water at a contact time of 0.5 hours.

Studies have also been conducted on the effectiveness of removing phenol from water. The results given in Table 7 showed that DAS is not inferior to industrial active coals of domestic and foreign production.

Similar studies on the efficiency of extraction of difficultly sorbed phenol as the most common anthropogenic pollutant in both waste and natural waters were carried out for the DAS sorbent and industrial active carbon KAD-I (Sorbent JSC, Perm). The results of these tests are shown in Table 8.

Table 6. The coals efficiency to formaldehyde

| The coals | Initial formaldehyde concentration, mg·L ⁻¹ | | |
|-----------|--|-------|-------|
| | 0.110 | 0.100 | 0.060 |
| AG-3 | 0.032 | 0.040 | 0.016 |
| TL-830 | 0.042 | 0.040 | 0.022 |
| CAS | 0.033 | 0.038 | 0.019 |

Table 7. The coals efficiency to phenol, mg·L⁻¹

| Indicators | The coals | | |
|------------------------------|-----------|--------|--------|
| | AG-3 | TL-830 | DAS |
| Phenol initial concentration | 0.0100 | 0.0100 | 0.0100 |
| Equilibrium concentration | 0.0083 | 0.0077 | 0.0091 |
| Phenol initial concentration | 0.0200 | 0.0200 | 0.0200 |
| Equilibrium concentration | 0.0170 | 0.0140 | 0.0182 |
| Phenol initial concentration | 0.0600 | 0.0600 | 0.0600 |
| Equilibrium concentration | 0.0510 | 0.0430 | 0.0530 |

Note: Test conditions: 1 g of coal per 1 liter of water, contact time 0.5 h.

Table 8. Efficiency of drinking water purification from phenol by active carbons

| Indicators | The coals | | Excess, times |
|---|-----------|-------|---------------|
| | CAS | KAD-I | |
| Sorption capacity to slip, mL·g ⁻¹ : | | | |
| – at a layer height of 120 mm | 9.40 | 2.15 | 3.8 |
| – at a layer height of 520 mm | 3.98 | 8.84 | – |
| Sorption capacity to saturation, mL·g ⁻¹ | | | |
| – at a layer height of 120 mm | 72.20 | 29.85 | 2.5 |
| – at a layer height of 520 mm | 94.00 | 38.16 | – |

Note: Test conditions: sorbate concentration 50 mg·dm⁻³, filtration rate 4 m·h⁻¹.

In this experiment, drinking water was filtered through columns with active carbon and the CAS advantage in terms of a high volume of micropores per unit volume (V_{mi} , $\text{cm}^3 \cdot \text{cm}^{-3}$) was fully manifested.

Thus, it can be stated that the sorption capacity for phenol of the CAS sorbent exceeds the sorption capacity of the industrially manufactured semicoke-based KAD-I sorbent by $\sim 2.5\text{--}3.5$ times. CAS sorbent can be effectively used for the purification of phenol-containing wastewater as a load into sorption filters.

Studies on the effectiveness of reducing highly toxic contaminants such as acid fluorides by the CAS sorbent have shown that its dispersed composition is of significant importance when used in filters with a load not exceeding 1.0 m. The research results are presented in Table 9.

The studies were carried out under the same dynamic conditions for three fractions of the CAS sorbent:

- layer height 180 mm;
- filtration rate of sorbate solutions 10 m per h;
- sorbate concentration in working solutions $\sim 1.0 \text{ mg} \cdot \text{dm}^{-3}$.

Based on the results of the studies carried out, the following conclusions can be drawn:

- the dispersed composition of the sorbent for water purification is of great importance in filters of

water purification means with a charge layer height of no more than a meter;

- the dispersion of the CAS sorbent for filters of water treatment means should not exceed 0.3 mm.

3.2. CAS application in mobile water treatment facilities

AC CAS was used in mobile water treatment facilities to compare it with the BAU-MF sorbent widely used for these purposes (UralKhimSorb, Perm, RF). It should be noted that the bulk density of these sorbents is significantly different; therefore, the studies were carried out by comparing them both in terms of the height of the filtering layer and in terms of the sorbent mass. The research results are presented in Table 10.

The analysis of the research results showed that the dynamic capacity of the CAS sorbent was approximately at the same level as BAU-MF. At the same time, the application of the CAS sorbent in filters of mobile water treatment facilities will increase their resource by two times while maintaining the hydrodynamic parameters of the filter. It should be noted that the mass of the filter will increase 2.6 times. In addition, if there is no need to increase the resource for the water treatment agent, the application of the CAS sorbent will reduce the dimensions of the filter.

Table 9. The decrease in the concentration fluoro-anhydrides in the purified water by passing it through the filter elements with CAS

| The CAS dispersion, mm | The fluoro-anhydrides concentration, ... $\text{mg} \cdot \text{L}^{-1}$, after ... min | | |
|------------------------|--|----------|--------|
| | 30 | 60 | 90 |
| 1.0 | 0.09 | 0.12 | 0.60 |
| 0.6 | 0.006 | 0.02 | 0.08 |
| 0.3 | < 0.0001 | < 0.0001 | 0.0001 |

Table 10. Efficiency of BAU-MF and CAS sorbents for water purification from fluoro-anhydrides

| The sorbent type | The sorbent layer height, cm (weight, g) | The fluoro-anhydrides concentration, ... $\text{mg} \cdot \text{L}^{-1}$, after... min | | |
|------------------|--|---|--------|--------|
| | | 20 | 60 | 180 |
| BAU-MF | 18 (13.5) | 0.0005 | 0.0008 | 0.0300 |
| CAS | 18 (35.3) | 0.0001 | 0.0001 | 0.0001 |
| CAS | 6 (13.5) | 0.0002 | 0.0060 | 0.0800 |

3.3. CAS application in household filters

Household filters for the purification of drinking water are an important tool for preserving health due to the lack in most settlements of the final purification of drinking water at waterworks with the help of granulated active carbon. Therefore, the CAS in efficiency for household filters was measured using the water filter “Mechta” produced by JSC “ENPO” Inorganic” (Elektrostal, RF), which has an adsorption system in the form of a porous block.

Table 11 shows the comparative characteristics of the sorption blocks of the “Mechta” filter made from the CAS prepared from anthracite activated carbon and also industrial AC prepared from AG-3 coal, previously used in these blocks.

As follows from the data given in Table 11, the use of active carbon DAS in the sorption units of filters for additional purification of drinking water provides a higher purification efficiency from both organic and inorganic pollutants.

The tests of another filter for the additional purification of drinking water “Barrier”, operated with grained AC, were carried out in the company JSC “BVT Barrier RUS” (Moscow, RF). It was shown that CAS coal with a grain size of 1–3 mm fully meets the

technical requirements that apply to AC based on coconut shells used in these filters.

The efficiency of wastewater purification from heavy metals was measured at the wastewater treatment facility of the gold recovery plant of “Polymetal” company in the Magadan region (RF) through a layer of coal of class (–3.0 + 0.2) mm at a filtration rate of 0.5 m per h. The findings of the filtration efficiency evaluation through the CAS sorbent layer with a height of 150 mm at a filtration rate are shown in Table 12.

As can be seen from the data presented in Table 12, the CAS sorbent has a very high efficiency in the extraction of heavy metals from water. Moreover, for all metals, except for iron, it was lower than the MPC, and for such metals as manganese, zinc, copper, cadmium, nickel, the concentration in the treated waste water decreased tens and even hundreds of times.

Based on the above studies, it can be concluded that a simple replacement of the sorption load in the existing water supply systems for the CAS sorbent at water treatment plants will increase their resource at least twice. In addition, the bulk density of the CAS sorbent is comparable to the bulk density of quartz sand, so it will not be washed out during

Table 11. Comparative characteristics of sorption blocks

| Block Type | The water purification efficiency | |
|-------------------|-----------------------------------|--|
| | From organic pollutants, % | The content of Fe ³⁺ in the filtered water, mg·dm ⁻³ |
| Based on the AG-3 | 85 | 0.5 |
| Based on CAS | 94 | 0.4 |

Table 12. The efficiency of waste water purification from metal

| Recoverable metal | Unit of measurement | MPC | Source water | Purified water |
|-------------------|---------------------|------|--------------|----------------|
| General iron | mg·dm ⁻³ | 0.10 | 5.6 | 4.8 |
| Common manganese | | 0.01 | 2.3 | < 0.1 |
| Common zinc | | 0.01 | 51 | < 0.04 |
| Common lead | | 0.01 | < 0.2 | < 0.2 |
| Common copper | | 0.00 | 48 | < 0.1 |
| Common cadmium | | 0.01 | 0.12 | < 0.05 |
| Common magnesium | | 40.0 | 51 | 40 |
| Common nickel | | 0.01 | 0.32 | < 0.2 |

backwashing of the filtration unit. Consequently, it can be assumed that a simple replacement of quartz sand at the final filtration stage with CAS will allow simultaneous filtration of mechanical impurities and sorption of molecular toxicants. This will provide high quality, clean and healthy water to the population without significant capital expenditures, without building an additional coal cleaning section. Calculations show that for an average city with a population of 100 thousand people, this will save 100 million rubles.

Thus, the high adsorption activity of CAS activated carbon with respect to both organic and inorganic pollutants during water treatment makes it possible to predict its effectiveness in both mobile and stationary water supply systems. CAS activated carbon has a certificate for its use for the purification of drinking water and circulating and waste water [19].

3.4. Ambient air quality monitoring

In the Presidential Decree (May 2018), great importance is attached to a radical reduction in the level of air pollution in large industrial centers, including a reduction by at least 20 % of the total volume of emissions of pollutants into the air in the most polluted cities [12].

Benzene is a test substance for assessing the quality of AC when extracting organic vapors from air. Therefore, in accordance with Russian Standard 17218-71 [20], an assessment of CAS activated carbon for the time of protective effect (TPE) was carried out for benzene vapors with a vapor concentration in the air of 5 mg·L⁻¹ in comparison with industrial activated carbon AG-3 (Sorbent JSC, RF). The test results showed that the TPE for benzene vapors for CAS activated carbon was 51–54 minutes, and for AG-3 – 40–42 min, i.e. the TPE for benzene vapors for CAS is 20–35 % higher than for industrial activated coal AG-3.

Purification of gas emissions from nuclear power plants is perhaps the most important aspect of using AC to protect the atmosphere, because the half-life of some isotopes of radioactive iodine is 1.5 million years.

In the laboratory of activated coals of ENPO Inorganika JSC in February 2021 on the basis of CAS activated carbon prepared from anthracite from the Gorlovskoye deposit of Kuzbass, in accordance with the technological regulations VTR 2568-379-04838763-2010 (however, the amount of impregnants was halved: potassium iodide was reduced to 0.75 % from 1.5 %, and triethylenediamine was reduced to 1 from 2 %), a sample of the CAS-IK sorbent

Table 13. The sorption properties of sorbents for radionuclides

| Sample | Cleaning efficiency (sorption activity), % | |
|----------------|--|----------------------------------|
| | I ¹³¹ | CH ₃ I ¹³¹ |
| VSK-5IK | 99.992 | 99.91 |
| TC for VSK-5IK | 99.900 | 99.00 |
| CAS-IK | 99.998 | 99.97 |

(VSK-5IK type) was prepared to absorb gaseous iodine radionuclides: I¹³¹ and CH₃I¹³¹ (methyl iodide).

Table 13 shows the results of the study of the adsorption activity for iodine radionuclides of the obtained prototype and the commercial VSK-5IK sorbent, as well as the requirements of TC 2568-379-04838763-2010 for the VSK-5IK sorbent currently produced by ENPO Inorganic.

As follows from the data given in Table 13, the sorbent CAS-IK in sorption of iodine radionuclides is not inferior to the industrial sorbent VSK-5IK, obtained on the basis of AC from coconut shells and exceeds the requirements of the technical conditions for the industrial sorbent VSK-5IK by two orders of magnitude. Thus, the developed new sorbent CAS-IK can be successfully used in gas cleaning systems at Russian NPPs and NPPs built abroad using Russian technologies.

The high volume of micropores and high adsorption properties of CAS per unit volume can significantly increase the resource of sorption air purification systems at nuclear power plants or dramatically reduce the size of treatment plants, which is important from an economic point of view.

3.5. Monitoring of the lithosphere quality

A particularly significant threat to the biosphere is the decline in soil fertility and even the complete depletion of farmland as a result of man-made activities. But the soils of farmland on the planet are only 6% of the total land area, and almost 30 % of the most fertile soils – chernozems – belong to Russia. Considering that by the end of the 21st century more than 10 billion people will be living on the planet, the protection and rehabilitation of soils should be given top priority.

In the Russian Federation alone, there are almost 50 million hectares of soils contaminated with pesticides in excess of the established standards [21]. That is why the Federal Law of 03.08.2018 No. 280-FZ “On organic products and on amendments to certain legislative acts of the Russian Federation” was adopted, which explicitly states that when implementing organic farming, methods, methods and technologies are used to ensure favorable the state of the environment, strengthening of human health, preservation and restoration of soil fertility.

The essence of carbon-adsorptive detoxification of soils contaminated with pesticides consists in introducing AC into the contaminated soil in the form of grains or powder with a micropore volume of $0.20\text{--}0.30\text{ cm}^3\cdot\text{g}^{-1}$ and then embedding it to a depth of 10–15 cm; then a given crop is sown into the charcoal-treated soil.

When solving environmental problems of the agro-industrial complex (AIC), ACs are characterized by such advantages as selectivity of sorption of organic toxicants, universality of sorption properties, high absorption capacity, hydrophobicity, convenient preparative form (grain, powder) and low cost.

It has been established that agrosorbents should have a micropore volume of at least $0.2\text{--}0.3\text{ cm}^3\cdot\text{g}^{-1}$ with a significant development of thin pores (0.8–1.2 nm), which allows to firmly retain both the molecules of the pesticides themselves and the products of their destruction, while the transport porosity (volume of macro- and mesopores) must also be well developed to ensure good kinetics of absorption of these substances. On the basis of numerous theoretical and experimental studies, we proposed DAS active carbon for detoxification of farmland soils from herbicide residues using the Agrosorb technology.

Table 14. Results of soil detoxification from phytotoxicants using active carbons

| The activated carbon trade mark | The level of soils detoxification from phytotoxicants, % decrease from the initial concentration* | Protected yield, % to control |
|---------------------------------|---|-------------------------------|
| CAS | 89–90 | 15–16 |
| SKT-3 | 75–76 | 6–8 |
| AG-3 | 73–74 | 5–6 |

* Residual amounts of phytotoxicants in the soil were determined by the HPLC method.

In 2001, the Herbolgy Department of All-Russian Research Institute of Phytopatology carried out research on the restoration of soil fertility of agricultural lands using the method of carbon adsorption detoxification (Agrosorb technology) of residual amounts of pesticides and endogenous phytotoxins accumulated in soils during natural soil fatigue. As adsorbents-detoxifying agents, we used new anthracite-based AC CAS, as well as industrial active carbons SKT-3 (JSC EKHMZ, Elektrostal) from peat and AG-3 coal at doses of 100 kg per ha. Cucumbers, tomatoes, beets, and radishes were chosen as the main test plants, which exhibit the most pronounced sensitivity to various phytotoxicants (sulfonylureas, imidazolinones) present in soils. The findings of the small-plot experiments are summarized in Table 14, where, for comparison, similar dependences are shown for standard industrial adsorbents such as SKT-3 and AG-3.

As follows from the data in Table 14, the application of the new ACs CAS gives an 89–92 % decrease in the concentration of phytotoxicants in the soil and an increase in the yield of test plants in contaminated areas up to 15–19 % versus, respectively, 73–76 % and 5–8 % for well-known coals SKT-Z and AG-3. Similar patterns were established for other crops (corn, rapeseed).

The performed studies allowed us to make the following conclusion that the new ACs trade mark DAS based on anthracite provides a higher level of detoxification of phytotoxicants in the soil compared to the previously known brands of AC. Thus, AC DAS is an effective adsorbent, promising for use in crop production in order to improve the ecological state of agricultural land.

The expected economic effect from the restoration of soil fertility using the CAS carbon adsorbent will be up to \$ 500 per hectare.

3.6. ACs production volumes and production organization prospects

To implement the above-described most important coal adsorption technologies that ensure the environmental safety of Russia, attention should be paid to the development of the production of active coal in our country.

The total volume of ACs production in the world today is 1 million 250 thousand tons per year and is characterized by a steady growth of 5 % per annum. The maximum productivity for active coals of the 4 main enterprises of the USSR reached 40 thousand tons per year (1989). Currently, the Russian Federation produces only 3 thousand tons per year at

the only remaining plant. About 25-30 thousand tons per year are purchased imported ACs (USA, Holland, France, China, etc.) [22].

Speaking about the environment and economy of the country, one should pay attention to the specific production of ACs, which in the USA, Japan, and Western Europe is at the level of 0.5 kg per capita annually, in Russia, this figure is currently 0.02 kg per capita a year. Thus our ecology, especially drinking water supply, is 25 times lower than that of the world level. Based on the foregoing, our country needs to produce at least 70 thousand tons of AC per year for sustainable economic development and creating a high quality of life for the population. The same approach will make it possible to implement the set by the President of Russia V.V. Putin on October 30, 2015 the task of improving individual and collective protective equipment [23].

Thus, the earliest possible organization of new ACs production in the Russian Federation on the basis of domestic (primarily Kuzbass) coal raw materials will certainly give a powerful impetus to the development of productive forces and ensure high quality environmental protection, which fully fits into the concept of sustainable development and creation high quality life of people.

4. Conclusions

Based on the results of this study, it was found that due to its physicochemical properties, ACs can solve a wide range of issues of biosphere protection. In terms of adsorption properties per unit volume, anthracite-based activated carbon corresponds to the world level and significantly exceeds domestically produced ACs.

The study confirmed the high adsorption properties of CAS activated carbon for drinking water purification, wastewater treatment, protection of the atmosphere and detoxification of farmland soils. The necessity of building new active coal plants has been substantiated.

5. Funding

This study did not receive external funding.

6. Conflict of interests

The authors declare no conflict of interest.

References

1. Mukhin VM, Korolev NV. Adsorption is returning (the role and place of active carbons in ensuring environmental safety. *Al'manakh «Bezopasnaya Rossiya»*. 2019:46-49. (In Russ.)

2. Keltsev NV. *Basics of adsorption technology*. Moscow: Chemistry; 1976. 511 p. (In Russ.)

3. Fenelopov VB. *Porous carbon*. Novosibirsk: Boreskov Institute of catalysis Publ.; 1995. 517 p. (In Russ.)

4. Barinov SV, Gerunova LK, Tirkaya JI, Pyanova LG, Baklanova ON, Liholobov VA. *Development of carbon sorbents and prospects of their use in obstetric practice*. Omsk: Maksheyeva YeA publ.; 2015. 130 p. (In Russ.)

5. Mukhin VM, Klushin VN. *Production and use of carbon adsorbents*. LAR LAMBERT Academia Publ.; 2018. 352 p. (In Russ.)

6. Mukhin VM, Kurilkin AA, Voropaeva NL, Leksyukova KV, Uchanov PV. A position of active carbons in the ecology and economy, new technologies of their production. *Sorbtsionnyye i khromatograficheskiye protsessy = Sorption and chromatography processes*. 2016;16(3):346-353. (In Russ.)

7. Mukhin VM, Tarasov AV, Klushin VN. *Active coals of Russia*. Moscow: Metallurgiya; 2000. 352 p. (In Russ.)

8. World health organization. *Water safety and quality*. Available from: https://www.who.int/water_sanitation_health/water-quality/ru/ [Accessed 11 April 2019] (In Russ.)

9. Popular science encyclopedia Water of Russia: *State report "About the condition and use of the Russian Federation water resources in 2018"*. Available from: <https://water-ru.ru/water/gosdoc/612.html> [Accessed 20 September 2019]. (In Russ.)

10. *Worldwide water consumption*. Available from: https://www.yestravel.ru/world/geography/freshwater_withdrawal/ [Accessed 30 July 2019]. (In Russ.)

11. Smirnov AD. *Sorption water treatment*. Leningrad: Khimiya; 1982. 168 p. (In Russ.)

12. Decree of the President of the Russian Federation of 05/07/2018, No. 294 "On national goals and strategic objectives for the development of the Russian Federation until 2024". (In Russ.)

13. Schauz JJ, Parry RH. Industrial production of activated carbons. *Industrial and Engineering Chemistry*. 1962;54(12):24-28.

14. Olontsev VF, Mokrova NV, Sazonova EA. *Modeling the processes of intentional production of activated carbons from fossil coal*. Yekaterinburg: USURT Publ.; 2012. 104 p. (In Russ.)

15. Kizilstein LA, Spitsgluz AL. *Atlas of microcomponents and petrogenetic types of anthracites*. Rostov-na-Donu: SFedU Publ.; 1998. 254 p. (In Russ.)

16. Dubinin MM. *Scientific basis for the development of active carbon production*. Moscow: IPCE RAS Publ.; 1976. 45 p. (In Russ.)

17. Mukhin VM, Uchanov PV, Sotnikova NI. Development of technology for active carbon-based coal and study of its properties. *Sorbtsionnyye i*

khromatograficheskiye protsessy = Sorption and chromatography processes. 2013;13(1):83-90. (In Russ.)

18. Mukhin VM, Soloviev SN, Dubovik BA, Pupyrev EI, Limonov NV, Sotnikova NI, Uchanov PV. *A method for producing active carbon based on anthracite*. Russian Federation Patent No. 2518964. 10 June 2014. (In Russ.)

19. Expert opinion No. 1210 FBUZ “Center for Hygiene and Epidemiology of the Vladimir Region”. 04 September 2014. (In Russ.)

20. Russian Standard 17218-71. *Active carbons. Method for determination of protective action time by benzene*. 15 July 1986. (In Russ.)

21. Mukhin VM, Spiridonov YuY. Improvement of soil contaminated with pesticides using carbon adsorption technologies. *Agrarnaya nauka*. 2019;(2):156-159. DOI:10.32634/0869-8155-2019-326-2-156-159 (In Russ.)

22. Mukhin VM, Korolev NV. Ecological aspects in using active charcoal in oil and gas industry. *Neft. Gas. Novacii*. 2019;(4):60-62. (In Russ.)

23. Mukhin VM, Korolev NV. Synthesis of active coal on the basis of the coal tar pitch composition. *Khimiya v interesakh ustoychivogo razvitiya = Chemistry for Sustainable Development*. 2018;(26):577-582. DOI:10.15372/KhUR20180602 (In Russ.)

Информация об авторах / Information about the authors

Мухин Виктор Михайлович, доктор технических наук, профессор, начальник лаборатории активных углей, эластичных сорбентов и катализаторов, АО «ЭНПО «Неорганика», Электросталь, Московская область, Российская Федерация; Author ID (Scopus) 7103124020; e-mail: victormukhin@yandex.ru

Victor M. Mukhin, D. Sc. (Engineering), Professor, Head of the Laboratory of Active Carbons, Elastic Sorbents and Catalysts of the JSC “Elektrostal Scientific and Production Association “Neorganika”, Elektrostal, Moscow region, Russian Federation, AuthorID (Scopus) 7103124020; e-mail: victormukhin@yandex.ru

Received 01 December 2020; Accepted 10 February 2021; Published 21 April 2021



Copyright: © Mukhin VM, 2021. This article is an open access article distributed under the terms and conditions of the Creative Commons Attribution (CC BY) license (<https://creativecommons.org/licenses/by/4.0/>).

Studies of the pore space of the UPM-K, UAM-50, UAM-100 composite ultrafiltration membrane

Sergey I. Lazarev^a, Olga A. Kovaleva^{a,b}, Irina V. Khorokhorina^a,
Tatyana A. Khromova^a✉, Sergey V. Kovalev^{a,b}

^a Tambov State Technical University, 106, Sovetskaya St., Tambov, 392000, Russian Federation,

^b Derzhavin Tambov State University, 33, Internatsionalnaya St., Tambov, 392000, Russian Federation

✉ tatyanka.xromova96@mail.ru

Abstract: The development of methods for assessing the distribution of pores by radii (or diameters) and studying the microstructure of the surface of a membrane partition is an urgent task. The authors of the paper carried out experimental studies of the pore diameter distribution for the UPM-K ultrafiltration membrane, determined the porosity and hydrodynamic permeability of the UAM-50, UAM-100 membranes. The analysis of the experimental results showed that the UPM-K ultrafiltration membrane had an average pore diameter of 54 nm. The UAM-50 and UAM-100 membranes were characterized by an asymmetric structure (an active layer (dense) and a porous substrate), while the pores were 2.5–40 and 10–40 nm in size, respectively. The experiments on the study of the hydrodynamic permeability of UAM-50, UAM-100 ultrafiltration membranes when separating a solution of sodium lauryl sulfate showed that the kinetic response curves of the “membrane-solution” system were conventionally divided into two stages. The first stage of the process was faster and lasted only a few minutes. After 7.8 and 13.05 min, the hydrodynamic permeability decreased by ~ 27 %, 7 %, which was due to structural changes in the cellulose acetate layer under the action of mechanical load (transmembrane pressure). The second stage was slower – with a duration of ~ 33 and 60 min and a decrease in hydrodynamic permeability by 41 % and 11 %. Based on the analysis of the approximating function, the rate constants of the membrane separation of solutions and the empirical coefficients of the equation are found.

Keywords: membrane pore space; pore diameter; normal distribution function; electron microscopic studies.

For citation: Lazarev SI, Kovaleva OA, Khorokhorina IV, Khromova TA, Kovalev SV. Studies of the pore space of the UPM-K, UAM-50, UAM-100 composite ultrafiltration membrane. *Journal of Advanced Materials and Technologies*. 2021;6(1):42-53. DOI: 10.17277/jamt.2021.01.pp.042-053

Исследования порового пространства композиционной ультрафильтрационной мембраны УПМ-К, УАМ-50, УАМ-100

С. И. Лазарев^a, О. А. Ковалева^{a,b}, И. В. Хорохорина^a, Т. А. Хромова^a✉, С. В. Ковалев^{a,b}

^a Тамбовский государственный технический университет,
ул. Советская, 106, Тамбов 392000, Российская Федерация,

^b Тамбовский государственный университет им. Г. Р. Державина,
ул. Интернациональная, 33, Тамбов 392000, Российская Федерация

✉ tatyanka.xromova96@mail.ru

Аннотация: Разработка методик оценки распределения пор по радиусам (или диаметрам) и исследования микроструктуры поверхности мембранной перегородки является актуальной задачей. Авторами работы проведены экспериментальные исследования распределения пор по диаметрам для ультрафильтрационной мембраны УПМ-К, определены пористость и гидродинамическая проницаемость мембран УАМ-50, УАМ-100. Анализ результатов эксперимента показывает, что ультрафильтрационная мембрана УПМ-К имеет среднее значение диаметров пор – 54 нм. Для мембран УАМ-50, УАМ-100 характерна ассиметричная структура (активный слой (плотный) и пористая подложка), при этом поры имеют размеры 2,5...40,0 нм и 10...40 нм, соответственно. Эксперименты по исследованию гидродинамической проницаемости ультрафильтрационных мембран УАМ-50, УАМ-100 при разделении раствора лаурилсульфата натрия показали, что кинетические кривые отклика системы

«мембрана-раствор» условно разделяются на две стадии. Первая стадия процесса протекает быстрее и длится всего несколько минут. Через 7,80 и 13,05 мин гидродинамическая проницаемость уменьшается соответственно на ~27 и 7%, что обусловлено структурными изменениями в ацетатцеллюлозном слое под действием механической нагрузки (трансмембранного давления). Вторая стадия более медленная – продолжительностью ~33 и 60 мин с уменьшением гидродинамической проницаемости соответственно на 41 и 11%. На основе анализа аппроксимирующей функции найдены константы скорости мембранного разделения растворов и эмпирические коэффициенты уравнения.

Ключевые слова: поровое пространство мембраны; диаметр пор; функция нормального распределения; электронно-микроскопические исследования.

Для цитирования: Lazarev SI, Kovaleva OA, Khorokhorina IV, Khromova TA, Kovalev SV. Studies of the pore space of the UPM-K, UAM-50, UAM-100 composite ultrafiltration membrane. *Journal of Advanced Materials and Technologies*. 2021;6(1):42-53. DOI: 10.17277/jamt.2021.01.pp.042-053

1. Introduction

At industrial enterprises of the Russian Federation, CIS countries and foreign countries in various industries (petrochemistry, chemical engineering), baromembrane separation processes are used to regenerate different solutions. At the same time, there is a problem of ensuring high quality indicators for the purification of various aqueous media containing both organic and inorganic compounds. The processes of membrane purification of various technological solutions, especially food and biological ones, are accompanied by sedimentation and fouling of the membrane surface. The study of various characteristics of membranes depends on many factors (differential transmembrane pressure, electric potential on the membrane, etc.). In a particular case, similar characteristics are associated with the hydrodynamic permeability of the solution through the membrane, and this also depends on the distribution of pores along the radii for a particular type of membrane. The development of methods for assessing the distribution of pores by radii (or diameters) and the study of the surface microstructure for a particular membrane partition is still relevant today [1–11].

In [12], the information was presented on the development of a digital image processing software package for calculating porosity, pore diameter distribution, pore area distribution and pore shape distribution on the membrane surface by processing images of the membrane surface and cross section obtained using SEM. Comparison with the results of the analysis using the IBAS I/II image analysis instrument (made in Germany), the porosity analyzed by the developed software package is larger, while the distribution variance is wider.

The problems and prospects of using the ultrafiltration method in the separation of solutions and water purification were described in [13].

The pore size for ultrafiltration membranes ranged from 5 nm to (0.05–0.1) μm . The authors showed micrographs made using an electron microscope when studying polymer membranes made of various materials, for example, cellulose acetate, polyethersulfone, etc.

The authors of [14] proposed a new, simple and effective test for pore size based on the synthesis and transfer of hard nanoparticles across the membrane. Monodispersions of gold and silver 3–50 nm provided a complete pore size distribution, including d100, the pore diameter at which the membrane had 100% retention capacity. The maximum pore size in the UV membrane structure was difficult to determine by other methods, although it was necessary for accurate separation analysis. The d100 values in the tested UV membranes ranged from 40 nm to 50 nm depending on the membrane material. Polymer membranes were more flexible than ceramic membranes and their d100 are usually much higher than MWCO.

Application of ultrafiltration solutions for purification processes is one of the most important stages in the production of high-purity water, liquid chemicals and biopharmaceutical products.

For example, in [15], the findings of the study of PA-100 ultrafiltration membranes based on aromatic polyamide performed on a SmartSPM-1000 atomic force microscope were described. The images obtained in this way passed the procedure for identifying pore sizes based on the Gwyddion program by two different methods (threshold and watershed). A statistical analysis procedure was carried out to study the pores. The authors noted that the watershed method allowed obtaining more detailed and reliable information on the distribution of the pores of the studied membrane over its surface.

Based on the analysis of the literature data and the demand for research on the identification of membrane pore sizes on the surfaces of ultrafiltration

membranes, we selected the objects for the research and the experimental procedure.

In the processes of membrane separation of solutions, the kinetics of the process is determined by the efficiency and productivity of purification and concentration of technological and industrial solutions. An important role in the study of the mechanism is given to the structural characteristics of membranes, which affect the kinetics of the membrane process. The authors in [16] analyzed the data on specific output flux and retention capacity for several commercial membranes, including the ESPA membrane, which shows good results in the separation of solutions containing NaCl, $(\text{NH}_4)_2\text{CO}_3$. It was found that the degree of separation is influenced by such factors as the molecular weight and molecular structure of the solute.

In [17], the authors investigated a low-pressure membrane process for removing cerium and neodymium from industrial solutions, where the permeability was analyzed by the concentration of the solute using inductively coupled plasma atomic emission spectroscopy.

The authors of [18] presented a classification of membranes and membrane water treatment methods according to various criteria, analyzed membrane separation methods and the possibility of their application for wastewater treatment of chemical and oil refineries. It was noted that hybrid technologies based on the use of membrane catalytic reactors with ultrafiltration ceramic or metal-ceramic membranes in the presence of ozone are the most preferable for the treatment of wastewater from chemical and petrochemical enterprises.

The authors of [19] calculated the hydrodynamic permeability of a membrane consisting of a set of porous spherical particles with a rigid impermeable core. The calculations used the cell method proposed by Happel and Brenner.

In [20], the authors investigated the ultrafiltration process using a polysulfone membrane. Membranes were prepared by phase inversion using a polysulfone (PSf) polymer base, polyvinylpyrrolidone (PVP), and N-methyl-2-pyrrolidone (NMP). The characteristics of the morphology of the surface layer were determined using SEM and atomic force microscopy (AFM).

In [21], the authors studied the mechanism of fouling of various types of UV membranes with different pore sizes by cross-flow filtration of biological suspensions. The experiments were carried out using two types of membranes (cellulose-ox-

and polyethersulfone) and three substances with different molecular weights.

In [22], the possibility of using electrosynthesized ultrafiltration membranes for concentration and purification from phenolic impurities of aqueous extracts of arabinogalactan was shown. It was found that the modification of the surface of ion-exchange membranes with ionic surfactants of various natures makes it possible to increase the separation of mono- and divalent ions by a factor of 2–3 in comparison with industrial ion-exchange membranes.

The issues of evaluating the resources of membrane performance are considered in the article [23], where the authors carry out a theoretical analysis of the operation of low-pressure membranes in the process of separation of solutions. In [24], the authors noted that the pore size of the membrane and surface porosity mainly regulate the morphology of the PSU membrane, which increases the efficiency of the membranes and reduces membrane fouling. In [25], the structure and permeable properties of the surface of the initial UV membranes made of polysulfone (PS-100), polyacrylonitrile (PAN-100) and modified by applying thin films of polyvinylpyridine by the Langmuir-Blodgett method were studied by atomic force microscopy. It has been established that the deposition of thin films on the PS-100 membrane leads to a twofold decrease in the specific output flow for water, but a significant increase in the retention coefficient is observed.

The analysis of the studies [1–25] made it possible to evaluate the significance of kinetic and structural characteristics in the processes of ultrafiltration separation of solutions containing surfactants.

Therefore, the aim of the paper is to conduct experimental studies of the pore diameter distribution for the UPM-K UV membrane and to determine the porosity and hydrodynamic permeability of the UAM-50, UAM-100 membranes.

2. Materials and methods

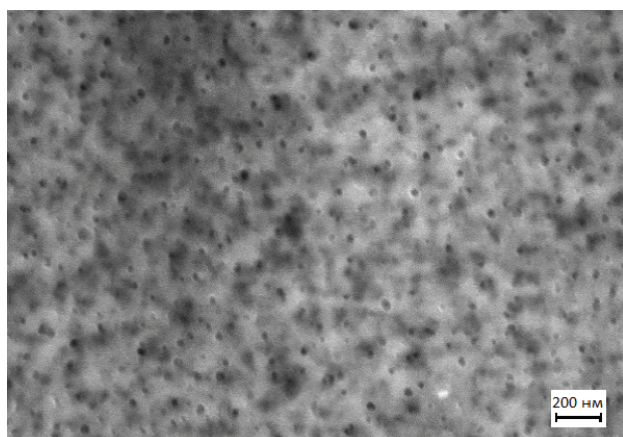
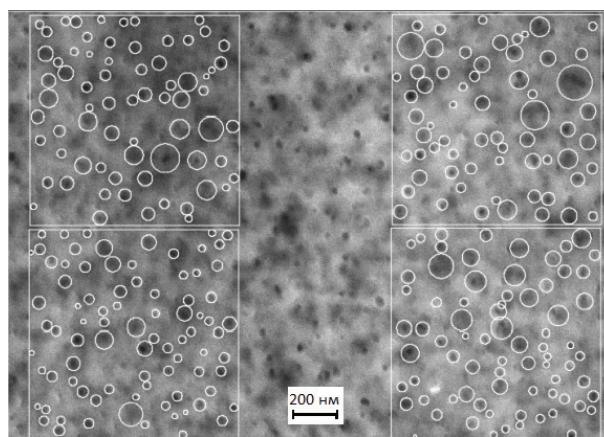
2.1. Materials

The object of the study was the UPM-K, UAM-50, UAM-100 UV membranes (ZAO STC Vladipor, Vladimir), the characteristics of which are presented in Table 1 [26].

The choice of porous ultrafiltration membranes as the object of the study is due to high retention capacity, good performance and its maximum applicability in industrial practice.

Table 1. Characteristics of the UPM-K, UAM-50, UAM-100 type membranes

| Permeable membrane brand | Permeable membrane type | Active layer material | Specific solvent flow J , $\text{m}^3/\text{m}^2 \text{ s}$, for $P = 0.5 \text{ MPa}$ | Retention rate for 0.15 % NaCl solution |
|--------------------------|-------------------------|-----------------------|---|---|
| UPM-K | | Polyamide | $1.16 \cdot 10^{-5}$ | 0.980 |
| UAM-50 | Composite | Cellulose acetate | $2.00 \cdot 10^{-5}$ | 0.985 |
| UAM-100 | | | $1.00 \cdot 10^{-5}$ | 0.985 |

**Fig. 1.** Electronic image of a sample of the UPM-K ultrafiltration membrane at a magnification of 100 and an accelerating voltage of 5 kV**Fig. 2.** Electronic image of the surface of the UPM-K ultrafiltration membrane with three uniform regions along the perimeter at a magnification of 100 and an accelerating voltage of 5 kV

2.2. Methods

The surface of dry samples of UPM-K, UAM-50, UAM-100 ultrafiltration membranes was examined using a Merlin scanning electron microscope (CarlZeiss, Germany, Center for Collective Use of Research Equipment of Derzhavin Tambov State University) (Fig. 1). Some of the original images were transferred exactly to scale into the AutoCad 2018 CAD environment, where further image processing took place.

First, in the photographs of the membrane surface (Fig. 2), three uniform regions were visually selected (without significant deviations of the geometric elements of the surface microstructure). The area of the selected square elements was $1 \cdot 10^6 \text{ nm}^2$, the scale of the regions strictly corresponded to the scale of the photographs. Then the pores were visually determined, which were described by a circle using the program. After marking the pores, the procedure for exporting data to the automated design system AutoCad 2018 was carried out using the console command EXTRACT DATA. Radial dimensions on the surface (active) layer of the membrane in nm were calculated using the AutoCad2018 program intended for computer-aided design.

Using the AutoCad 2018 software function of “data extraction”, the main characteristics (diameter, area of each element) were found for all four square sample areas. Using the data retrieval function made it possible to perform surface analysis on each membrane.

To assess the error in determining the pore size, 5 electronic images were analyzed, obtained for different areas of the surface of the membrane under study. The procedure for processing each electronic image was repeated 10 times. The statistical processing of the results confirmed that the relative standard deviation did not exceed 0.1.

To calculate the area of the clean surface of the square sample areas, the sample areas were added, and then they were subtracted from the total sample area. Then the coefficient of contamination was determined according to the following calculation formula (1):

$$K = \frac{S_c}{S_d}, \quad (1)$$

where S_c , S_d are the area of the clean and darkened surface on the membrane, nm^2 .

The obtained characteristics are presented in Table 2.

Table 2. Estimated area of the UPM-K membrane

| Membrane type | Darkened surface area, S_d, m^2 | Clean surface area, S_c, nm^2 | Clogging coefficient, K |
|---------------|-----------------------------------|---------------------------------|-------------------------|
| UPM-K | $793.1 \cdot 10^3$ | $3.20 \cdot 10^6$ | 0.25 |

For analytical processing of the data obtained as a result of the research, Microsoft Excel 2010 was used. Using the descriptive statistics function, the program determined such parameters as the standard deviation and the average pore diameter.

For further calculations, it is necessary to verify the correctness of the analysis of the data obtained. This can be solved by constructing histograms. The construction of histograms is performed using the standard settings of Microsoft Excel 2010. The program performs an automated selection of the range obtained during the calculation of the data and builds histograms for the UPM-K membrane.

In the automated calculation of the computer, the range is independently selected, which is determined by the calculation formula (2):

$$R = X_{\max} - X_{\min}, \quad (2)$$

where X_{\max} is maximum sample value; X_{\min} is minimum sample value.

This parameter (range) shows what the width of the histogram will be and determines the spread of the obtained values. Then the computer divides the resulting range into several intervals, the number of which is calculated by the formula (3):

$$k = \sqrt{n \pm 2}, \quad (3)$$

where n is coefficient that takes into account the number of found sample diameters.

Then, by means of the computer, the width of the interval (h) was calculated by the formula (4):

$$h = \frac{R}{k}. \quad (4)$$

Then, the function of the normal distribution of the diameters of the pores of the membranes was constructed.

3. Results and discussion

3.1 Pore diameter distribution for UPM-K UV membrane

The standard deviation and the average pore diameter of the UPM-K ultrafiltration membrane determined on the basis of the study and the data

obtained according to the previously presented method are presented in Table 3.

Fig. 3 shows a histogram of distribution of pore diameter sizes per intervals of pore diameter sizes for the UPM-K membrane.

The resulting histogram shown in Fig. 3 represent combs (multimodal type). Among the various laws, the most used is the normal distribution law (Gauss's law). According to Gauss's law, to which random variables obey, and they are significantly influenced by numerous, approximately equal in strength, factors. The results of multiple measurements obey this law, which is observed in our case [17]. Table 4 shows the values of the studied parameters.

Table 3. Average pore diameter and average deviation

| Membrane type | Average pore diameter of d_{av}, nm | Standard deviation σ |
|---------------|---------------------------------------|-----------------------------|
| UPM-K | 54 | 1.21 |

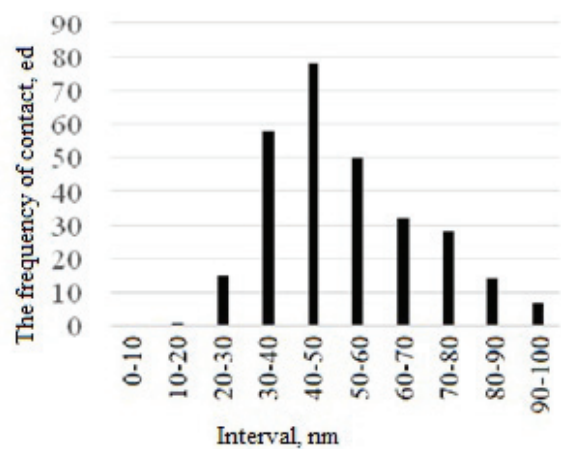


Fig. 3. Distribution of pore diameter sizes by pore diameter size intervals for the UPM-K membrane

Table 4. The main parameters

| Membrane type | UPM-K |
|--------------------|-------|
| Standard deviation | 20.6 |
| Sample variance | 423.6 |
| Excess | 1.5 |
| Asymmetry | 14.3 |
| Interval | 165.6 |

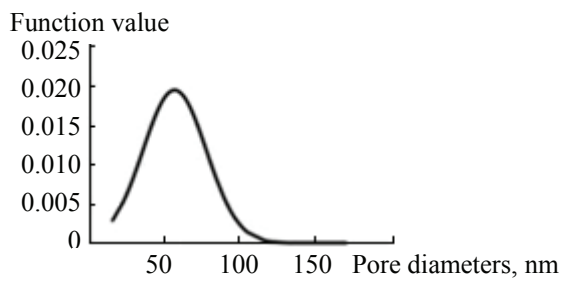


Fig. 4. Sample variance function of the UPM-K membrane from the distribution of the membrane pore diameters

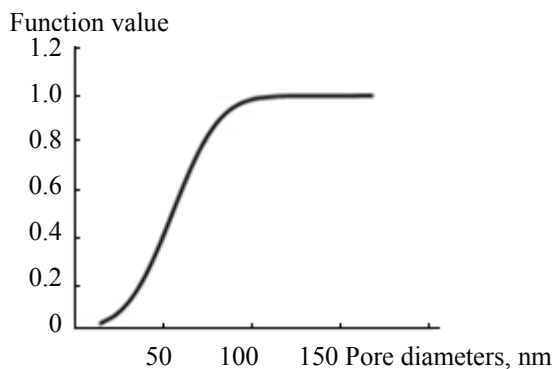


Fig. 5. The function of the normal (integral) distribution of the UPM-K membrane from the distribution of the membrane pore diameters

For the UPM-K membrane (Fig. 4, 5), the graph of the normal distribution function of pore diameters on the membrane is as follows.

According to the hypothesis about the correspondence of the empirical distribution to the normal law, it is necessary to study the reproducibility of the procedure, i.e. the possibility of studying the primary parameters of the process is determined: the arithmetic mean value and the standard deviation.

In analytical form, the normal distribution function for the UPM-K membrane, the following formula is proposed:

$$y = \frac{1}{54.54\sqrt{2\pi}} e^{-\frac{(x-20)^2}{2 \cdot 54.54^2}} \quad (5)$$

Thus, we can claim that the UPM-K UV membrane has different pore diameters – the average hit range is 40–60 nm. It can be concluded that the size of the pores and their frequency of penetration per 1 mm² affects the permeable properties of the studied semi-permeable membranes and, most likely, affects the effect of their overgrowing.

3.2. Experimental studies of porosity of UAM-50, UAM-100 membranes

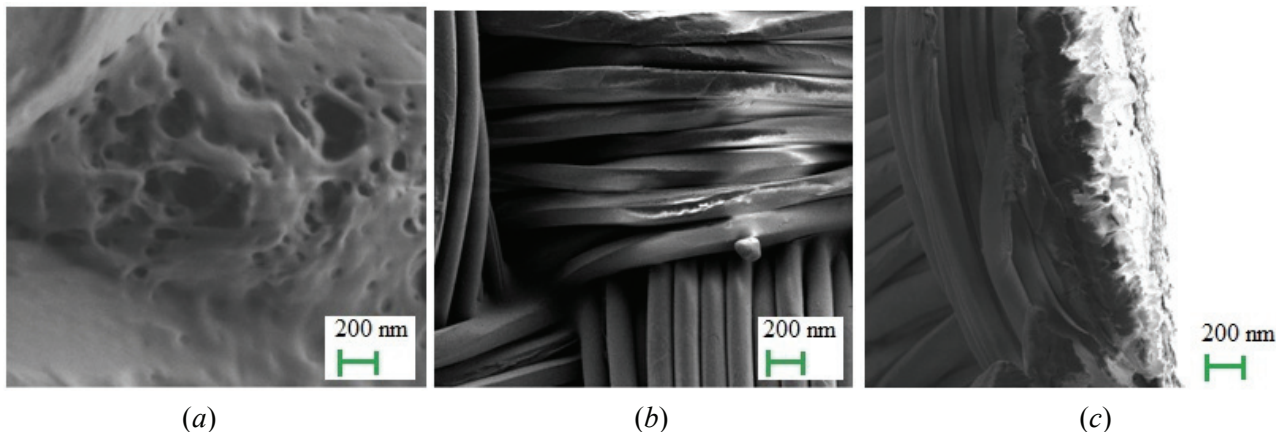
Membranes used in chemical technology for the separation of solutions and industrial effluents, carried out under the influence of transmembrane pressure (microfiltration, ultrafiltration, nanofiltration and reverse osmosis) or electric potential, are composite materials consisting of two (or even three) layers of different materials [28–30]. Resistance is usually an intrinsic property of the membrane, reflecting the pore structure. Due to the compositional structure of membranes, geometric or structural parameters cannot be determined by standard measurements, so other types of experiments are conducted to evaluate the thickness and / or porosity of each layer. Structural parameters are very important to predict the behavior of the membrane, since the permeable and selective properties of the membrane strongly depend on the structure of the pores and their distribution [28], which is also noted by the authors of [28–31]. In particular, ultrafiltration membranes are usually made as two series-connected homogeneous elements with different structural and transport properties [28–31]: a thin and dense active layer, a thick and porous substrate (Figs. 6, 7). Characterization of both layers provides the necessary information about the selectivity and performance of composite membranes.

The analysis of Figs. 6, 7 (c) electron images of UAM-50 and UAM-100 ultrafiltration membranes showed that the membrane actually consists of an active layer and a porous substrate. It is noted that the active layer of the UAM-50 membrane has a min thickness of up to 27 nm, and that of for UAM-100 has a min thickness of up to 15 nm.

On the surface of the UAM-50 and UAM-100 membranes, pores are visible, the average size of the diameter of which for several samples is 2.5÷40 nm and 10÷40 nm, respectively. Selected areas of the image are given for comparison and assessment, since along with small, medium pores, there are also wider ones, the size of which reaches 100 nm.

Analyzing the surface of the cross-section of membrane samples, two layers are observed: dense and more porous. The pore space is formed by through and dead-end bottle-shaped pores with diameters up to 40 nm, which are inhomogeneous along the entire pore length.

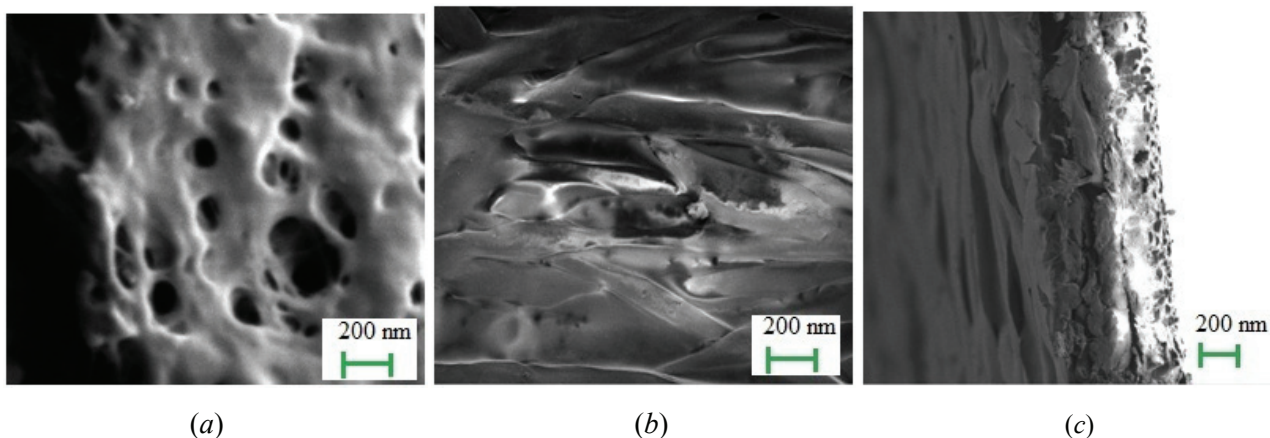
Also, when analyzing images, it can be concluded that the active layer of ultrafiltration membranes has an asymmetric pore structure. The active layer of the membrane can be divided into two components: a selective layer with a small pore size, and a pore substrate, in which the pores increase



(a) (b) (c)

Fig. 6. Electronic images of the UAM-50 ultrafiltration membrane:

a – image of the membrane surface – its active layer; *b* – the substrate surface, for this membrane – fabric-type nylon; *c* – image of an active cellulose acetate layer section of a substrate membrane



(a) (b) (c)

Fig. 7. Electronic images of the UAM-100 ultrafiltration membrane:

a – image of the membrane surface – its active layer; *b* – substrate surface, for this membrane – felted nylon; *c* – image of the active cellulose acetate layer section of the membrane

in diameter as they approach the substrate [28]. It should be noted that the studied type of membranes is chemically and structurally heterogeneous. They consist of a highly porous substrate coated with a thin, dense film of another polymer.

A schematic representation of the ultrafiltration membrane is shown in Fig. 8.

Studies of the surface and drainage layers of ultrafiltration membranes by electron microscopy have shown that all membranes have an anisotropic structure – their structural parameters change along the membrane thickness. Therefore, for them, the pore space as a whole can be characterized only by the values of the total volumetric porosity and average pore radius (Fig. 9). To study these parameters, we used the method of nitrogen adsorption on an AUTOSORB-iQ-C sorbtometer (Quantachrome, USA).

Table 5 shows the results of studying the specific surface area and porous structure of the studied membranes.

The analysis of images obtained using scanning electron microscopy showed that the pores of UAM-50 and UAM-100 composite ultrafiltration membranes are within the range of up to 100 nm, while the average pore diameter of the membranes is 2.5÷40 nm. It is noted that the analysis of the obtained images of membranes and the parameters of their porous structure are practically comparable with the results obtained by other methods, for example, nitrogen adsorption.

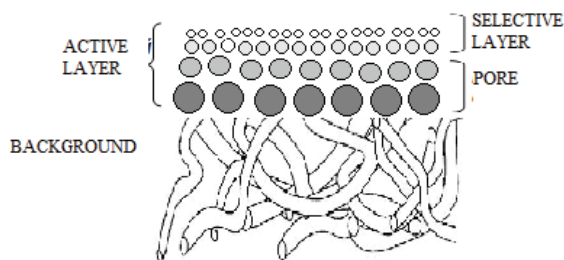


Fig. 8. Schematic representation of the ultrafiltration membrane [28]

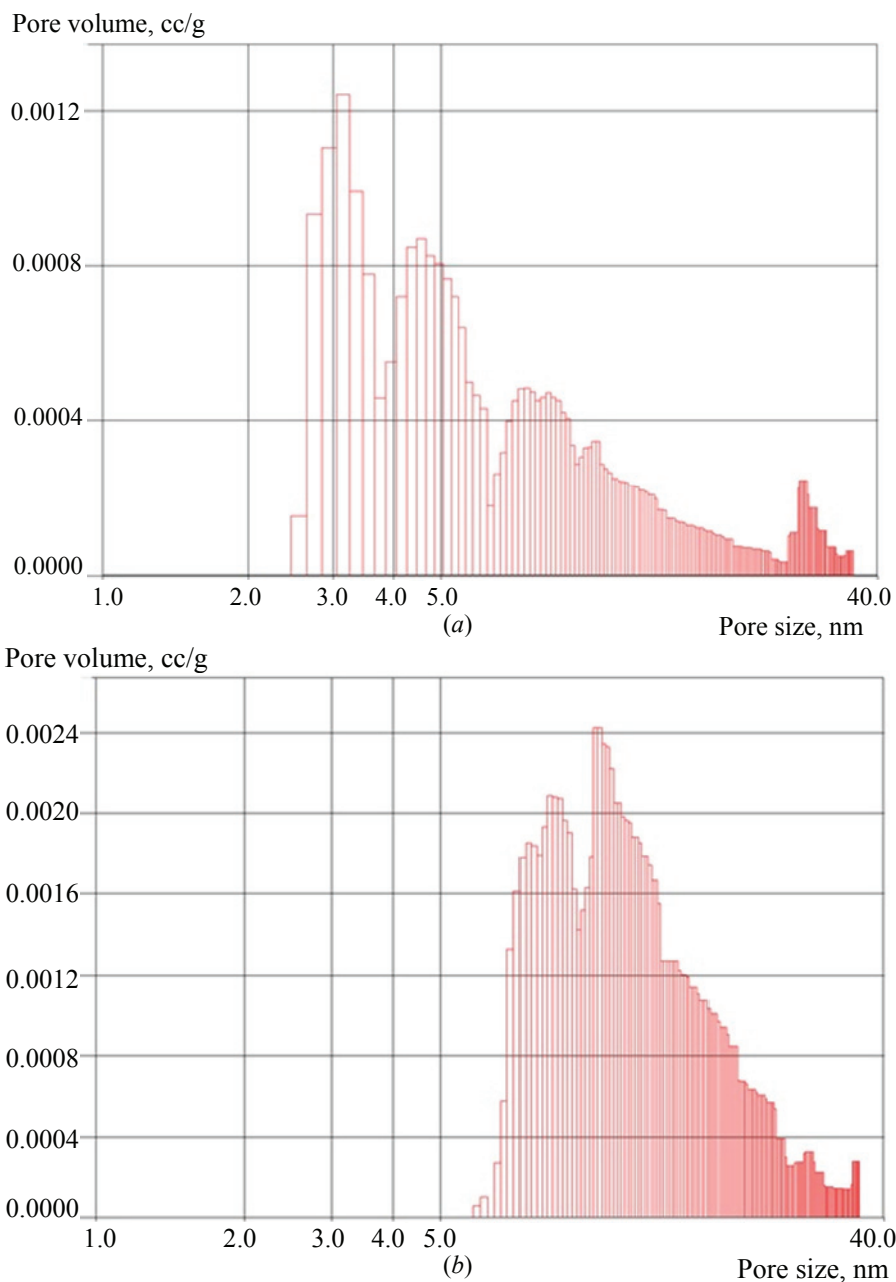


Fig. 9. Pore distribution histogram for UAM-50 (a) and UAM-100 (b) ultrafiltration membrane

Table 5. Characteristics of the UAM-50 and UAM-100 membranes

| Investigated parameters | Membranes | |
|---|-----------|---------|
| | UAM-50 | UAM-100 |
| Pore volume, $\text{cm}^3 \cdot \text{g}^{-1}$ (cc/g) | 0.037 | 0.128 |
| Surface area, $\text{mL} \cdot \text{g}^{-1}$ | 10.394 | 19.327 |
| Lower confidence limit, nm | 0.984 | 0.899 |
| Installation error, % | 6.829 | 3.103 |
| Pore size, nm | 3.169 | 10.681 |

3.3 Experimental studies of the hydrodynamic permeability of UAM-50, UAM-100 membranes

In experimental studies, the UAM-50 and UAM-100 industrial semi-permeable composite membranes were used, the main characteristics of which are given in Table 1 [32].

Before starting experimental studies, the membrane samples were visually checked for defects. Then they were immersed in the test solutions. Afterwards, a flat-chamber type separating ultrafiltration module was assembled. The membrane was fixed on a substrate (Whatman paper) so that the membrane did not have contact with metal surfaces,

the active layer to the solution to be separated. The shared module was attached to the laboratory setup described in [33]. The amount of collected permeate was determined every 30 minutes. At the end of the experiment, the pressure was released, the installation was turned off. The time was recorded with a stopwatch.

The experimental dependences of the hydrodynamic permeability for ultrafiltration membranes on the time of the separation process of a solution containing sodium lauryl sulfate was calculated by the formula (6):

$$\alpha = \frac{V}{F_m \tau P}, \quad (6)$$

where V is the volume of the collected permeate, m^3 ; F_m is the flat membrane working surface area, m^2 ; τ is the duration of experiment, s; P is the transmembrane pressure, MPa.

Fig. 10 shows the kinetic dependences of the hydrodynamic permeability on the time of the experiment.

As seen from Fig. 10, the hydrodynamic permeability during separation on an asymmetric membrane of cellulose acetate (UAM-50 (curve 1), UAM-100 (curve 2)) is variable over time.

When analyzing the dependences of the change in hydrodynamic permeability on time (τ), it was found that such dependences are well approximated by the sum of two exponential functions (Fig. 10) at ($R^2 = 0.976$)

$$J = y_0 + A_1 e^{-\tau k_1} + A_2 e^{-\tau k_2}, \quad (7)$$

where the values of the process rate constants – $k_1 = 1/\tau_1$, $k_2 = 1/\tau_2$ and the equation coefficients are given in Table 6.

α , mL/(cm²·min·MPa)

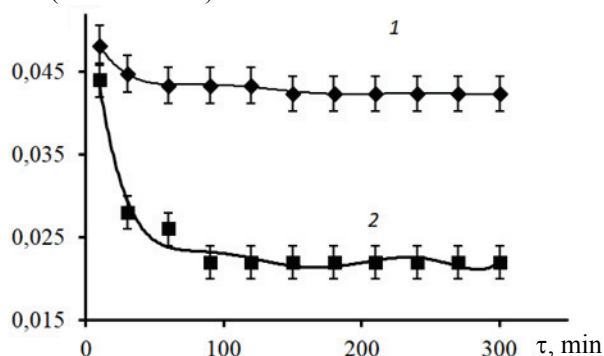


Fig. 10. The dependence of the hydrodynamic permeability on the time of the experiment for ultrafiltration membranes at a constant transmembrane pressure $P = 1.0$ MPa:
1 – UAM-50 series membrane;
2 – UAM-100 series membrane

Table 6. Design values of the process rate constants for UAM-50 and UAM-100 ultrafiltration composite membranes

| Membrane parameters | y_0 | A_1 | A_2 | τ_1 | τ_2 | R^2 |
|---------------------|-------|--------|--------|----------|----------|-------|
| UAM-50 | 0.042 | 0.0057 | 0.0035 | 13.05 | 60.85 | 0.975 |
| UAM-100 | 0.022 | 0.0376 | 0.0151 | 7.87 | 33.11 | 0.977 |

Experimental studies of the hydrodynamic permeability of membranes during the separation of a solution containing sodium lauryl sulfate made it possible to determine that the kinetic curves of the response of the “membrane-solution” system under the action of transmembrane pressure can be conditionally divided into several stages. The first stage of the process was faster and lasted only a few minutes – 7.8 and 13.05 min, respectively. The hydrodynamic permeability decreased by ~ 27 % and 7 %, respectively. The observed effect was due to structural changes in the cellulose acetate layer under the action of mechanical stress (transmembrane pressure). The second stage was slower, lasting ~ 33 and 60 min, with a decrease in hydrodynamic permeability by 41 % and 11 %, respectively. Apparently, the decrease in permeability is associated with the process of structural rearrangement in the polymer substrate of the UAM-100 and UAM-50 membranes, respectively. At the same time, the dependence of the change in hydrodynamic permeability on the macroscopic parameters of the membranes, for example, such as pores, which undergo deformation and partial compression as a result of pressure, is noted. Earlier it was shown that the drainage layer of UV membranes UAM-50, UAM-100 is made of fabric-type and felted-type, respectively.

It is known that in the process of transmembrane separation, the process solution interacts with the active layer of the membrane, changes its structural properties, and the pressure compresses the active layer. As noted earlier in [34], the supramolecular structure of the cellulose acetate active layer of membranes is due to two types of hydrogen bonds – (OH...O), (CH...O=C) and the dipole-dipole interaction of carbonyl groups. Sorbed water breaks weak intermolecular bonds (CH...O) in the structure of cellulose acetate, which increases the polarity of carboxyl groups due to the induction effect. Therefore, strong hydrogen bonds with water molecules arise between the oxygen atoms of the polar groups of cellulose acetate, forming a

polymolecular layer of bound water. As a result, the pore size decreases and, accordingly, the hydrodynamic permeability of the permeate decreases.

4. Conclusions

Using the data on the study of the pore diameter and their distribution over the sample surface, an electron microscopy procedure was developed in conjunction with the use of the AutoCad 2018 computer-aided design system and Microsoft Excel 2010 tools, which made it possible to study the pore diameter distribution of UPM-K ultrafiltration membranes. As a result of the studies carried out, it was found that the size range of pore diameters on the surface of UPM-K membranes corresponds to the law of normal distribution, for which mathematical expressions have been obtained showing that for the UPM-K membrane sample the largest pore diameter is 70 nm, and the average pore diameter is 54 nm. For the UAM-50 and UAM-100 ultrafiltration membranes, it is noteworthy that their structure was asymmetric (active layer (dense) and porous substrate), and the pores had sizes from 2.5 to 40 nm and from 10 to 40 nm, respectively.

Experimental studies of the membranes hydrodynamic permeability allow to determine that the kinetic curves of the response of the “membrane-resolution” system under the action of transmembrane pressure have several stages. The first stage of the process was 7.8 min and 13.05 min, and the hydrodynamic permeability decreased by ~ 27 % and 7%, respectively. The second stage was slower, lasting ~ 33 min and 60 min, with a decrease in hydrodynamic permeability by 41 % and 11 %, respectively. This was due to the process of structural rearrangement in the polymer substrate for the membranes.

5. Funding

This study did not receive external funding.

6. Conflict of interests

The authors declare no conflict of interest.

References

1. Ulbricht M. Advanced functional polymer membranes. *Polymer*. 2006;47(7):2217-2262. DOI:10.1016/j.polymer.2006.01.084
2. She Q, Wang R, Fane AG, Tang CY. Membrane fouling in osmotically driven membrane processes: A review. *Journal of Membrane Science*. 2016;(499):201-233. DOI:10.1016/j.memsci.2015.10.040
3. Jhaveri JH, Murthy ZVP. A comprehensive review on anti-fouling nanocomposite membranes for pressure driven membrane separation processes. *Desalination*. 2016;(379):137-154. DOI:10.1016/j.desal.2015.11.009
4. Kotra-Konicka K, Kalbarczyk J, Gac JM. Modification of polypropylene membranes by ion implantation. *Chemical and Process Engineering*. 2016;37(3):331-339. DOI:10.1515/cpe-2016-0027
5. Ge Zh, He Zh. Effects of draw solutions and membrane conditions on electricity generation and water flux in osmotic microbial fuel cells. *Bioresource Technology*. 2012;(109):70-76. DOI:10.1016/j.biortech.2012.01.044
6. Lazarev SI, Kovalev SV, Konovalov DN, Kovaleva OA. Analysis of kinetic characteristics of baromembrane and electrobaromembrane separation of ammonium nitrate solution. *Izvestiya vysshih uchebnyh zavedenij. Seriya: Himiya i himicheskaya tekhnologiya = ChemChemTech*. 2020;63(9):28-36. (In Russ.)
7. Kovalev SV, Lazarev SI, Kovaleva OA. A Study of the surface morphology of microfiltration membranes of the MFFK and MPS brands by atomic-force-and scanning-electron microscopy. *Journal of Surface Investigation: X-ray, Synchrotron and Neutron Techniques*. 2020;14(4):696-705. DOI:10.1134/S1027451020040126
8. Lazarev SI, Golovin YM, Kovalev SV, Levin AA. Characteristics of thermal action on porous cellulose acetate composite material. *Journal of Engineering Physics and Thermophysics*. 2019;92(4):1050-1054. DOI:10.1007/s10891-019-02019-0.
9. Uglyanskaya VA, Chikin GA, Selemenev VF, Zavyalova TA. *Infrared spectroscopy of ion-exchange materials*. Voronezh: VSU; 1989. 208 p. (In Russ.)
10. Lazarev SI, Kovaleva OA, Popov R, Kovalev SV. Investigation of the process of ultrafiltration separation of technological solutions in the production of alcohol from molasses. *BestPrint: ion transport in organic and inorganic membranes: International conference: Conference Proceedings. Russian academy of sciences; section “membranes and membrane technologies” of D.I. Mendeleev; 2017, BESTPRINT, 23-27 May 2017, Russia*, Krasnodar: BestPrint; 2017. p. 212-214. (In Russ.)
11. Ryzhkin VYu, Lazarev SI, Kovalev SV, Konovalov DN, Mamontov AS, Lua P. Application of microfiltration, nanofiltration, and electronanofiltration processes to improve the efficiency of the solution separation scheme in biochemical production. *Publisher entrepreneur V. A. Chesnokov: topical issues of electrochemistry, environmental protection and*

corrosion: *Materials of international conference dedicated to the memory of Professor, honored scientist of the Russian Federation V. I. Vigdorovich, 23-25 October 2019, Russia*, Tambov: Publishing House V.A. Chesnokov; 2019. p. 447-450. (In Russ.)

12. Akram A, Stuckey D. Flux and performance improvement in a submerged anaerobic membrane bioreactor (SAMBR) using powdered activated carbon (PAC). *Process Biochemistry*. 2008;43(1):93-102. DOI:10.1016/j.procbio.2007.10.020

13. Pervov AG, Andrianov AP, Kondratiev VV, Spirov DV. Development of a computer program for the use of CSM (SAEHAN) nanofiltration membranes for the production of drinking and industrial water. *Membrany*. 2008;(1):9-18. (In Russ.)

14. Arkhangelsky E, Duek A, Gitis V. Maximal pore size in UF membranes. *Journal of Membrane Science*. 2012;394-395:89-97. DOI:10.1016/j.memsci.2011.12.031

15. Khanukaeva DYu, Filippov AN, Bilydukevich AV. Investigation of ultrafiltration membranes using AFM: features of pore size distribution. *Membrany i membrannye tekhnologii = Petroleum Chemistry*. 2014;4(1):37-46. (In Russ.)

16. Yoon Y, Lueptow RM. Removal of organic contaminants by RO and NF membranes. *Journal of Membrane Science*. 2005;261(1-2):76-86. DOI: 10.1016/j.memsci.2005.03.038

17. Murthy ZVP, Choudhary A. Separation and estimation of nanofiltration membrane transport parameters for cerium and neodymium. *Rare Metals*. 2012;31(5):500-506. DOI: 10.1007/s12598-012-0547-y

18. Balandina AG, Hangildin RI, Ibragimov IG, Martyasheva VA. Development of membrane technologies and the possibility of their application for wastewater treatment of chemical and petrochemical enterprises. *Elektronnyj nauchnyj zhurnal "Neftegazovoe delo" = Oil and Gas Business*. 2015;(5):336-375. (In Russ.)

19. Vasin SI, Filippov AN. The permeability of complex porous media environments. *Kolloidnyj zhurnal = Colloid Journal*. 2009;71(1):32-46. (In Russ.)

20. Kumar S, Nandi BK, Guria C, Mandal A. Oil removal from produced water by ultrafiltration using polysulfone membrane. *Brazilian Journal of Chemical Engineering*. 2017;34(2):583-596. DOI:10.1590/0104-6632.20170342s20150500.

21. Karagunduz A, Dizge N. Investigation of membrane biofouling in cross-flow ultrafiltration of biological suspension. *Journal of Membrane Science & Technology*. 2013;3(1):1-5. DOI:10.4172/2155-9589.1000120.

22. Kolzunova LG, Greben VP, Karpenko MA, Rodzik IG. Membrane separation methods and new membranes for these processes. *Vestnik Dal'nevostochnogo otdeleniya Rossijskoj akademii nauk = Vestnik of the Far East branch of the Russian academy of sciences*. 2009;2(144):13-17. (In Russ.)

23. Philippova TS, Filippov AN. Theoretical evaluation of the microfiltration membrane lifetime. *Petroleum Chemistry*. 2014;54(8):705-709. DOI:10.1134/S0965544114080064

24. Abdelrasoul A, Doan HD, Lohi A, Cheng Chil-Hung. Morphology control of polysulfone membranes in filtration processes: a critical review. *ChemBioEng Reviews*. 2015;2(1):22-43. DOI:10.1002/cben.201400030

25. Melnikova GB, Zhavnerko GK, Chizhik SA, Bilydukevich AV. Structure and mechanical properties of ultrafiltration membranes modified by Langmuir-Blodgett films. *Membrany i membrannye tekhnologii = Petroleum Chemistry*. 2016;6(2):144-151. (In Russ.)

26. *Membranes, filter elements, membrane technologies: catalog of CJSC STC "Vladipor"*. 2007. 22 p.

27. Solonin IS. *Application of mathematical statistics in mechanical engineering technology*. Sverdlovsk: Central Ural Book Publishing House; 1966. 200 p. (In Russ.)

28. Khorokhorina IV, Lazarev SI, Golovin YuM, Arzamashev AA. Studies of the surface and drainage layers of ultrafiltration membranes by scanning electron microscopy. *Vestnik tekhnologicheskogo universiteta*. 2019;22(2):126-129. (In Russ.)

29. Lazarev SI, Golovin YuM, Shestakov KV, Kovalev SV. Features of X-ray diffractometric studies of the structural characteristics of polymer membranes. *Vestnik tekhnologicheskogo universiteta*. 2018;21(2):22-25. (In Russ.)

30. Kovaleva OA, Lazarev SI, Konovalov DN, Kovalev SV. Comparative study of methods of separation of technological solutions and waste water of electroplating industries. *Vestnik tekhnologicheskogo universiteta*. 2018;21(5):58-63. (In Russ.)

31. Lazarev SI, Golovin YuM, Kovalev SV, Ryzhkin VYu. Method of automated determination of the morphology of the selectively permeable surface of polymer membranes OPMN-P and OFAM-K. *Zavodskaya laboratoriya. Diagnostika materialov = Industrial Laboratory. Diagnostics of Materials*. 2018;84(9):34-40. (In Russ.)

32. *Vladipor: membranes and filter elements*. Available from: <http://www.vladipor.ru> [Accessed 18 March 2019]. (In Russ.)

33. Lazarev SI, Gorbachev AS, Kuznetsov MA. Influence of pressure, temperature, and concentration on the reverse osmotic separation of an aqueous solution of sodium sulfonate. *Izvestiya vysshih uchebnyh zavedenij. Seriya: Himiya i himicheskaya tekhnologiya = ChemChemTech*. 2005;48(4):126-129. (In Russ.)

34. Lazarev SI, Golovin YuM, Kovalev SV. Structural characteristics and state of water in the cellulose acetate membrane. *Theoretical Foundations of Chemical Engineering*. 2016;50(3):294-302. DOI:10.1134/S0040579516030076

Информация об авторах / Information about the authors

Лазарев Сергей Иванович, доктор технических наук, профессор, Тамбовский государственный технический университет (ФГБОУ ВО «ТГТУ»), Тамбов, Российская Федерация; ORCID 0000-0003-0746-5161; e-mail: mig@tstu.ru

Ковалева Ольга Александровна, доктор технических наук, доцент, Тамбовский государственный университет имени Г.Р. Державина, ФГБОУ ВО «ТГТУ», Тамбов, Российская Федерация; ORCID 0000-0003-0735-6205; e-mail: solomina-oa@yandex.ru

Хорохорина Ирина Владимировна, кандидат технических наук, доцент, ФГБОУ ВО «ТГТУ», Тамбов, Российская Федерация; ORCID 0000-0001-8722-3685; e-mail: kotelnikovirina@yandex.ru

Хромова Татьяна Александровна, аспирант, ФГБОУ ВО «ТГТУ», Тамбов, Российская Федерация; ORCID 0000-0002-8743-9918; e-mail: tatyanka.xromova96@mail.ru

Ковалев Сергей Владимирович, доктор технических наук, доцент, ФГБОУ ВО «ТГТУ», Тамбов, Российская Федерация; ORCID 0000-0002-5961-7561; e-mail: sseedd@mail.ru

Sergey I. Lazarev, D. Sc. (Engineering), Professor, Tambov State Technical University (TSTU), Tambov, Russian Federation; ORCID 0000-0003-0746-5161; e-mail: mig@tstu.ru

Olga A. Kovaleva, D. Sc. (Engineering), Associate Professor, Derzhavin Tambov State University, TSTU, Tambov, Russian Federation; ORCID 0000-0003-0735-6205; e-mail: solomina-oa@yandex.ru

Irina V. Khorokhorina, Cand. Sc. (Engineering), Associate Professor, TSTU, Tambov, Russian Federation; ORCID 0000-0001-8722-3685; e-mail: kotelnikovirina@yandex.ru

Tatyana A. Khromova, Postgraduate, TSTU, Tambov, Russian Federation; ORCID 0000-0002-8743-9918; e-mail: tatyanka.xromova96@mail.ru

Sergey V. Kovalev, D. Sc. (Engineering), Associate Professor, TSTU, Tambov, Russian Federation; ORCID 0000-0002-5961-7561; e-mail: sseedd@mail.ru

Received 10 December 2020; Accepted 17 February 2021; Published 21 April 2021



Copyright: © Lazarev SI, Kovaleva OA, Khorokhorina IV, Khromova TA, Kovalev SV, 2021. This article is an open access article distributed under the terms and conditions of the Creative Commons Attribution (CC BY) license (<https://creativecommons.org/licenses/by/4.0/>).

Detonation nanodiamonds: from synthesis theory to application practice

Valerii Yu. Dolmatov^a✉, Alexander I. Shames^b, Eiji Ōsawa^c, Asko Vehanen^d,
Vesa Myllymäki^d, Alexander O. Dorokhov^e, Valerii A. Martchukov^a, Anatoly C. Kozlov^a,
Sergey Yu. Naryzhny^a, Anastasia Z. Smirnova^a

^a Special Design and Technological Bureau “Technologist”, 33-a, Sovetskiy pr., St. Petersburg, 192076, Russian Federation,

^b Ben-Gurion University of the Negev, P.O. Box 653, Be'er Sheva 8410501, Israel,

^c NanoCarbon Research Institute Limited, Shinshu University, 3-15-1 Tokita, Ueda, Nagano, 386-8567 Japan,

^d Carbodeon Ltd. Oy, Vantaa, Pakkalankuja 5, 01510, Finland,

^e JSC “Plant “Plastics”, 12/3, village of Soviets, Kopeysk, Chelyabinsk region, Russian Federation

✉ diamondcentre@mail.ru

Abstract: The review is devoted to the current state of research and advances in the production and study of the properties of detonation nanodiamonds (DND), their application in technology and medicine. New data on the theory and practice of DND synthesis for the last 1–5 years are considered and systematized. It is shown that the zone of chemical reactions (ZCR) during the blast of explosive materials (EM) is decisive for the fractal pre-diamond structure formation, the final region of the nanodiamonds (1/3–3/4 of the diameter of the explosive charge) formation is determined. The possibility of predicting the DND yield and the influence of parameters on the synthesis process of nanodiamonds from individual EMs of binary and ternary compositions is shown, their optimal formulations are determined. The optimal ZCR width and the existence time of chemical reactions have been identified. The dependence of the DND yield on the nitrogen content in the EM was shown. The most effective method of DND purification and the possibility of obtaining graphite-diamond compositions of a given formulation are presented. The most informative indicators of nanodiamonds characterization are given. The magnetic properties of nanodiamonds are considered and the identity of the properties of DNDs from different EMs is shown. The characteristics of new compositions based on DND are indicated: electrochemical coatings (gold and chromium-diamond), thermal pastes, diamond-containing polymer filaments for a 3D printer, fuel compositions, enterosorbents, compatible with biosystems of the nanodiamond-drug composition.

Keywords: detonation nanodiamonds; detonation synthesis; forecasting; DND structure; electronic paramagnetic resonance; electroplated coatings; polymer-diamond composites, fuels; the medicine; 3D printing.

For citation: Dolmatov VYu, Shames AI, Ōsawa E, Vehanen A, Myllymäki V, Dorokhov AO, Martchukov VA, Kozlov AC, Naryzhny SYu, Smirnova AZ. Detonation nanodiamonds: from synthesis theory to application practice. *Journal of Advanced Materials and Technologies*. 2021;6(1):54-80. DOI: 10.17277/jamt.2021.01.pp.054-080

Детонационные наноалмазы: от теории синтеза до практики применения

В. Ю. Долматов^a✉, А. И. Шамес^b, Э. Осава^c, А. Веханен^d,
В. Мюлльмяки^d, А. О. Дорохов^e, В. А. Марчуков^a, А. С. Козлов^a,
С. Ю. Нарыжный^a, А. З. Смирнова^a

^a ФГУП «Специальное конструкторско-технологическое бюро «Технолог»,
Советский пр., д. 33-а, Санкт-Петербург 192076, Российская Федерация,

^b Университет им. Бен Гуриона в Негеве, Р.О. Вох 653, Беэр-Шева, 8410501, Израиль,

^c NanoCarbon Research Institute Limited, Японский национальный университет в префектуре Нагано,
Токита, 3-15-1, Уэда 386-8567, Япония,

^d Carbodeon Ltd. Oy, Паккаланкуя 5, Вантаа 01510, Финляндия,

^e АО «Завод «Пластмасс», поселок Советов, 12/3, Копейск, Челябинская область, Российская Федерация

✉ diamondcentre@mail.ru

Аннотация: Обзор посвящен современному состоянию исследований и достижений в области получения, изучения свойств детонационных наноалмазов (ДНА), их применения в технике и медицине. Рассмотрены и систематизированы новые данные по теории и практике синтеза ДНА за последние 1 – 5 лет. Показано, что зона

химических реакций (**ЗХР**) при взрыве взрывчатых веществ (**ВВ**) является определяющей для формирования фрактальной праалмазной структуры, определена окончательная область формирования наноалмазов (1/3–3/4 диаметров заряда ВВ). Показана возможность прогнозирования выхода ДНА и влияние параметров на процесс синтеза наноалмазов из индивидуальных взрывчатых веществ, бинарных и тройных композиций, определены их оптимальные составы. Определена оптимальная ширина ЗХР и время существования химических реакций. Определена зависимость выхода ДНА от содержания азота в ВВ. Приведен самый эффективный способ очистки ДНА и возможность получения графит-алмазных композиций заданного состава. Даны наиболее информативные показатели характеристики наноалмазов. Рассмотрены магнитные свойства наноалмазов и показана тождественность свойств ДНА из различных ВВ. Указаны характеристики новых композиций на основе ДНА: электрохимические покрытия (золото- и хром-алмазные), термопасты, алмазосодержащие полимерные нити для 3D-принтера, топливные композиции, энтеросорбенты, совместимые с биосистемами композиции наноалмаз-лекарство.

Ключевые слова: детонационные наноалмазы; детонационный синтез; прогнозирование; строение ДНА; электронный парамагнитный резонанс; гальванические покрытия; полимер-алмазные композиты, топлива; медицина; 3D-печать.

Для цитирования: Dolmatov VYu, Shames AI, Ōsawa E, Vehanen A, Myllymäki V, Dorokhov AO, Martchukov VA, Kozlov AC, Naryzhny SYu, Smirnova AZ. Detonation nanodiamonds: from synthesis theory to application practice. *Journal of Advanced Materials and Technologies*. 2021;6(1):54-80. DOI:10.17277/jamt.2021.01.pp.054-080

1. Introduction

The originality of the method for the synthesis of detonation nanodiamonds (DND) lies in the fact that carbon-containing explosive materials (EM) with a negative oxygen balance (OB) are used, in which there is too little oxygen to oxidize the combustible components of the EM.

The properties description of the carbon products of detonation synthesis in traditional terms applied to crystals and diamond powders encounters many limitations and contradictions. With the deepening of DND studies, the dual nature of this material is increasingly manifested: as a nanocrystal of short length on the one hand, and as a self-ordered fractal cluster structure, on the other.

Having undergone the whole complex of shock-thermal effects and chemical aggression from the gas medium, detonation carbon appears to us as a substance of the most complex structural organization, including pronounced crystal-like formations, continuously transforming into looser and less ordered spatial formations with a wide range of energy states and types of interatomic and intermolecular bonds. The use of DNDs in various branches of industry and science is stimulated by the need to radically improve the performance properties of composites.

To obtain DND, mixed charges are used, as a rule, of TNT with RDX, in which the optimal parameters for specific power, oxygen balance, charge density and type of shell are selected [1]. However, from a technological and economic point of view, the use of an individual EM would be optimal: there is no need for dangerous and time-

consuming stages of crushing and mixing of various explosives, the use of expensive and scarce RDX is excluded. In addition, it is desirable to use a disposable EM having a sufficiently high power and sensitivity to the initiating pulse and giving a significant yield of DND, for example, tetryl (2,4,6-trinitro-N-methyl-N-nitroaniline). Thus, the production of DNDs currently planned for creation at Plastmass Plant JSC (Kopeysk, Chelyabinsk Region) is entirely based on the use of tetryl [2].

The DND price is not high, its industrial production has been established and the sales market expansion is forecasted. Nevertheless, DND cannot be classified as a well-studied diamond material, which is explained by the variability of the chemical composition, structure, and, consequently, properties determined by the peculiarities of the synthesis and purification technology from different manufacturers [1, 3–5].

The aim of this work is to systematize new empirical and theoretical data obtained in the study of the process of detonation synthesis of nanodiamonds, new studies of the properties of DND and DS, the possibility of their application in industrial technologies and medicine.

2. Detonation synthesis of nanodiamonds

2.1. Theory of DND synthesis

The decay of EM is a complex multistage set of sequentially and parallel reactions. During detonation, the chemical equilibrium in the detonation products (DP) does not have time to be established, because the reactions do not go to the

end; the DP contains more or less intermediate compounds. Experimental determination of the composition of cold DPs does not provide information on the composition of DPs in the Chapman-Jouguet plane (Ch-J), since the composition of DPs changes in the course of expansion and cooling. It was found in [6] that at temperatures above 800 K the decomposition of all aromatic nitro compounds proceeds predominantly by a radical mechanism.

In the detonation process, mainly diamond nanoparticles with an average size of 4–6 nm have time to form. A defect structure of the diamond phase is formed, in which, along with vacancies in the crystal lattice and broken bonds, there are oxygen, hydrogen and nitrogen atoms included in the form of structural and non-structural impurities, which are predominantly chemically bonded to the surface of particles or are physically retained on it. DND, purified from non-diamond carbon and from the main part of non-carbon impurities, is a powder consisting of aggregates of primary particles of various sizes and different strengths [3, 7–9].

The detonation wave is a single complex of the shock wave, in the front of which the EM decomposition begins, the zone of chemical reactions (ZCR), which follows the shock wave and ends in the Chapman-Jouguet plane, and, finally, the Taylor unloading wave (isentrope). The maximum pressure and temperature are reached inside the ZCR. It was shown in many works [10–14] that the process of nanodiamond formation proceeds in the ZCR and ends at the beginning of the Taylor expansion of detonation products (DP).

The substance inside the ZCR has a velocity approximately equal to the detonation velocity (shock wave velocity (6–8 km·s⁻¹)), and behind the Ch-J plane the mass velocity of gaseous products is much lower and for the studied individual and mixed EMs ~ 2 km·s⁻¹ [9, 15, 16]. The flow of matter inside the ZCR is plasma ($T \sim 3000\text{--}4500$ K and $P \sim 20\text{--}35$ GPa). After cooling down, DPs consist of N₂, H₂O, C, CO, CO₂, NO, NO₂, CH₄, O₂, N₂O, HCN. In the case of detonation of condensed powerful EM, the density of DP in the ZCR significantly exceeds the density of the original explosive (~ 1.6–1.7 g·cm⁻³) and is in the range of 2.2–2.5 g·cm⁻³. The release of the energy of the decay process of EM molecules continues beyond the Ch-J plane (~ 20 % of the total explosion energy) [9].

The existence of the DND infrastructure in the ZCR is still controversial. As already noted in [17], the energy for the destruction of all interatomic bonds

in EM molecules is not enough, and 4–5 times less than necessary. It is possible that a sufficiently stable formation in the plasma of ZCR is a multiple radical-dimer of carbon with a covalent bond —C—C—. Moreover, most likely, we can talk not about the crystallization of nanosized diamond in the ZCR (due to the practically absence of heat removal from the formed nanoparticle and the short lifetime of the necessary P , T -conditions), but about the process of self-organization of carbon into the condensed phase in accordance with the basic chemical properties carbon atoms, namely, the formation of various types of C—C bonds. Consequently, there is a possibility of the occurrence of a fractal carbon network with simultaneous fluctuations of the carbon density in the ZCR. In the “nodes” of this network with the highest density, the carbon condensate has time to more or less form a three-dimensional ordered core, and the regions with a low carbon density are repeatedly destroyed and recombined in the process of AP expansion. Thus, the DND infrastructure can be either a densified plasma-like carbon core, which becomes liquid carbon behind the Ch-J plane, or the formed energetically favorable carbon framework of cyclohexane, which, outside the Ch-J plane, interacting with each other with an even greater decrease in energy, is rearranged into radical-molecule of adamantane, attacked by radicals —C—C— (diffusion mechanism of nanodiamond formation). It is possible that these two mechanisms of DND formation take place. This is followed by crystallization (amorphization) of liquid carbon or cooling of DND crystallites obtained by the diffusion method from the adamantane infrastructure [17].

Figure 1 shows the nucleation and growth of particles of the condensed carbon phase in the ZCR during the expansion of DPs [18, 19].

The density, fixed by SAXS, of condensed carbon should be higher than 2.5 g·cm⁻³, i.e. higher than the ZCR plasma density. The SAXS signal fixes condensed carbon (without making a distinction between the diamond and non-diamond phases) already in the zone of chemical reactions (ZCR) for TNT, RDX, and TNT-RDX mixtures (70/30; 50/50; 60/40). The response time of the given EM is within 0.1–0.3 μs, ZCR width – from 0.4 to 1.4 mm. The results of works [18, 19] show (see Fig. 1) that the condensed phase of carbon, which has an increased density, appears immediately behind the front of the detonation wave for TNT and TNT-RDX charges. Moreover, the rapid rise of the SAXS signal continues up to ~ 1.8 μs. Then there is a kind of plateau – up to 4.4 μs, and then a slow decline to 15 μs and beyond.

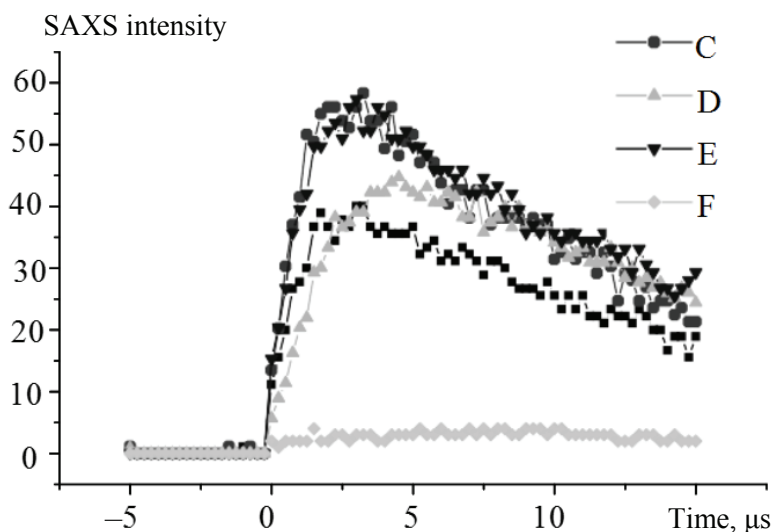


Fig. 1. Small-angle X-ray scattering (SAXS) of the detonation process of condensed carbon-containing EM: B – TF 70/30 (■); C – TNT-RDX 50/50 (●); D – TNT (▲); E – TNT-RDX 60/40 (▼); F – RDX (◆) [18,19]

The formation of the DND infrastructure clearly begins in the ZCR, but takes the form of a closely bound diamond-non-diamond carbon structure (DCS) far beyond the ZCR. Calculations show that in $1.8 \mu\text{s}$ the substance traveled a distance of $\sim 4.4 \text{ mm}$, which is $\sim 35\%$ of the charge diameter, and in $4.4 \mu\text{s}$ $\sim 9.5 \text{ mm}$ (77% of the charge diameter). In fact, this is the zone of DND formation in the form we already know; the process of completion of the formation of DND crystallites occurs at a distance in the range of $1/3$ – $3/4$ of the charge diameter. Further, there is a sharp drop in pressure and temperature with an attack on the formed nanocarbon, including DND crystallites, corrosive gases (CO_2 and H_2O), which contributes not only to a decrease in the size of DCS particles, but also to graphitization of DND crystallites.

It is clear that the state of matter in ZCR plasma cannot be described as solid, liquid or gaseous. If we pay attention to the classical diagram of P , T -carbon [20], then free carbon from TNT ($P \sim 18 \text{ GPa}$, $T \sim 3600 \text{ K}$, DND yield $\sim 1 \text{ wt.}\%$) is clearly not in the state of liquid carbon, but free carbon from BTF (benzotrifuroxane) ($P \sim 36 \text{ GPa}$, $T \sim 4300 \text{ K}$, DND yield $\sim 1 \text{ wt.}\%$), on the contrary, falls into the zone of carbon liquid state.

Thus, immediately behind the front of the detonation wave, primary carbon plasmoids are formed in 10^{-8} – 10^{-9} seconds, which are recorded by the SAXS method. Upon reaching the plateau, i.e. at a distance of $1/3$ – $3/4$ of the charge diameter, the final formation of a complex DCS structure occurs – inside the DND crystallite, and outside – amorphous carbon formations. A high DND yield is achieved when the formation of free carbon takes 28 – 35% of the total

carbon in the molecule or mixed EM, or $(20 \pm 2)\%$ of the total carbon for the formation of DND [21]. For the formation of DNDs with a high yield ($\geq 5 \text{ wt.}\%$), a ZCR with dimensions of $\sim 0.6 \text{ mm}$ is required, which is a rather large distance. Thus, the following conclusions can be drawn: 1) for the formation of DND, the time of chemical reactions in the ZCR should be within the range of 0.1 – $0.3 \mu\text{s}$, and the width of the ZCR should be from 0.4 to 1.4 mm ; 2) the lifetime of a relative plateau for TNT-RDX compositions is from ~ 1.8 to $\sim 4.4 \mu\text{s}$, which corresponds to a distance from the detonation wave front of 4.4 – 9.5 mm or $1/3$ – $3/4$ of the charge diameter; 3) a high DND yield (more than $6 \text{ wt.}\%$) is achieved when $(20 \pm 2)\%$ wt.% of EM carbon is spent on its formation.

2.2. DND synthesis practice

To date, studies of the detonation synthesis of nanodiamonds have revealed the dependence of the yield and quality of DND and DC on the following factors [1, 22–25]: charge composition; specific power of EM; OB; charge density; EM charge shell and its composition; explosive charge modifications (CM); charge forms; composition and heat capacity of the gaseous medium in the explosive chamber (EC); places of initiation of the EM charge; the ratio of the mass of the charge and the volume of the EC; the structure and material of the walls of the EC. The optimal combination of these factors leads to a positive effect.

The armor (shell) of the charge makes it possible to delay the expansion of the DP and, thereby, to complete the chemical reactions in the ZCR as much as possible, providing more time for the formation of

future DND crystallites, increasing their number [1, 18, 19, 23]. When choosing the composition of the EM charge, it is important to proceed from economic factors - to use mass-produced EM, which have a low price. The nomenclature of such individual EM is small and, first of all, it is TNT and RDX. If, in the case of using these individual EM, the yield of DNDs is very low (0.7–0.9 and 0.3–1.0 wt.%, respectively), then from a mixture of these EM (~ 50/50) DNDs yield is up to 8.2 wt.% under optimal conditions of fabrication and detonation. Thus, for the industrial production of DND, it is necessary to have a large-scale production of EM or the availability of EM in large quantities at reasonable prices.

2.2.1. Possibility of nitrogen-free DND obtaining

An increase in the number of application areas of DNDs may lead to the need to obtain and use nitrogen-free DNDs [22]. For example, DNDs are almost ideally suited as a reflective substance for slow neutrons (SN) for constructing traps from them [26]. At the same time, it is necessary to first remove some elements – SN absorbers, which include hydrogen, oxygen, chlorine and metal oxides (incombustible impurities). Nitrogen is mainly located inside the DND crystal lattice and its removal is most likely impossible. The ideas presented in [17] about the mechanism of nanodiamond crystallites formation, where the main role is played by multiple C—C and C—N radicals, show that it is impossible to avoid the explosive flow of nitrogen into a nanodiamond growing by a diffusion method, because in all molecules there is and remains during the decomposition of molecules a dimer with a covalent bond C—N (due to lack of energy in the explosion).

In addition, the extremely low yield of DND from RDX (~ 0.9 wt.%) and from trinitrotriaminobenzene (TNAB) (~ 2.0 wt.%) instead of ~ 13 wt.% expected by the authors [28] becomes clear. In both cases, all carbon atoms are covalently bonded to nitrogen, although in TNAB this bond competes with the C—C covalent bond in the aromatic ring. However, a large number of C-N radicals attacking a growing DND particle does not allow the formation of not only nitrogen-free nanodiamonds, but sometimes even nanocrystallite. Here, at least, there are 2 reasons: 1) according to [22], the amount of nitrogen in TNAB is anomalously high (32.6 wt.%), which interferes with the formation and growth of the carbon infrastructure of nanodiamond (the optimal range for nitrogen is 23–28 wt.%); 2) at a TNAB charge density of 1.83 g·cm⁻³, most likely, there is an effect of overcompressed

detonation, where there is practically no ZCR. The absence of a zone of chemical reactions interferes with the normal nucleation of the DND infrastructure, for which ZCR is clearly required. Thus, the production of nitrogen-free DNDs from commercially available powerful EMs is most likely unrealistic.

The nitrogen content (according to elemental analysis) in DNDs from different manufacturers and obtained in different ways falls within the range of 2.1–2.7 wt.% [22]. The synthesis conditions and the EM composition have little effect on the nitrogen content in DND. The existence of carbon-containing nitrogen-free EM with the required oxygen balance (OB) ~ -35 ÷ -55 % [24] and the required specific power of 30 ÷ 60 kJ·kg⁻¹·μs⁻¹ [29] is unknown. Theoretically, you can use nitroesters, for example, PETN (pentaerythritol tetranitrate) – C(CH₂ONO₂)₄, in which there is no covalent C—N bond. The addition of oxygen-free and nitrogen-free organic compounds to PETN up to the recommended OB would possibly make it possible to obtain nitrogen-free or low-nitrogen DND (<0.5 wt.%).

Detonation charges of TNT, RDX, picric acid, tetryl, TNT-RDX 50/50 and TNT-RDX 60/40 is carried out under the same and maximally optimal conditions. The dependence of the DND yield on the content of covalently bound C-N nitrogen in EM molecules has a pronounced peak-like character, and the DND yield of ~ 2 wt.% really corresponds to the nitrogen content in TNAB saturated with it. (descending branch of the curve). Thus, in [22], the possibility of purposeful production of nitrogen-free DNDs was considered and an insignificant probability of their production was shown when using nitro compounds with a covalent C-N bond; the dependence of the DND yield on the content of nitrogen covalently bound to carbon in EM molecules was defined and the optimal range of nitrogen content was determined from 23 to 28 wt.%; the use of nitroesters is recommended to obtain nitrogen-free or low-nitrogen (<0.5% nitrogen) DND.

2.2.2. Predictive estimate of DND release from individual EM

In [29], graphs of the dependence of the experimental output of DND on the specific power EM, pressure in the Ch-J plane, detonation velocity EM, and the dependence of the specific power on detonation velocity are presented.

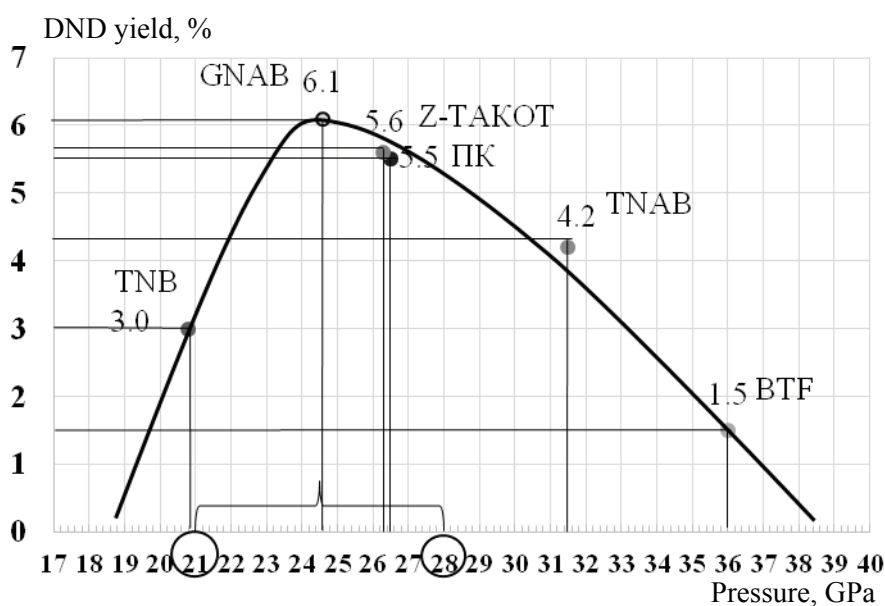
The forecast for the DND yield [21] was carried out according to the EMs given in Table 1 (No. 1–6). These EMs can be of certain interest as possible substitutes for RDX alloys due to the scarcity and high cost of RDX.

Table 1. Predicted DND yield from explosion parameters [21]

| No | EM name* | Q_{sp} , Specific power, $J \cdot kg^{-1} \cdot \mu s^{-1}$ | The obtained DND yield, wt. % | D , detonation speed, $m \cdot s^{-1}$ | P_{Ch-J} , Pressure in the plane Ch-J, GPa | Predicted DND yield, wt. % | | | |
|----|----------|--|-------------------------------------|---|---|----------------------------|---------------|--------|---------|
| | | | | | | by Q_{sp} | by P_{Ch-J} | by D | Range |
| 1 | TNAB | 44,000 | 2.08 | 7,650 | 29.0 | 6.0 | 4.2 | 6.5 | 4.2–6.5 |
| 2 | PA | 37,000 | 1.2** | 7,480 | 26.5 | 5.9 | 5.5 | 5.5 | 5.5–5.9 |
| 3 | GNAB | 32,000 | 6.63 | 7,311 | 24.6 | 5.2 | 6.1 | 4.4 | 4.4–6.1 |
| 4 | BTF | 80,000 | No data | 8,610 | 36.0 | 1.5 | 1.5 | 1.5 | 1.5 |
| 5 | Z-TACOT | 30,000 | 3.34 | 7,250 | 26.3 | 4.9 | 5.6 | 4.0 | 4.0–5.6 |
| 6 | TNB | 32,600 | No data | 7,300 | 20.8 | 5.3 | 3.0 | 43.0 | 4.3–5.3 |

* 1,3,5-triamino-2,4,6-trinitrobenzene (TNAB); 2,4,6-trinitrophenol (picric acid (PA)); bis (2,4,6-trinitrophenyl)-diazine (GNAB); benzotrifuroxan (BTF); 2,4,8,10-tetranitro-5H-benzotriazolo-(2,1-4)-benzotriazoli-6-um (Z-TACOT); 1,3,5- trinitrobenzene (TNB)

** In PA charge 7.7 % water, density $1.49 \text{ g} \cdot \text{cm}^{-3}$.

**Fig. 2.** Dependence of the DND output on the pressure in the Ch-J. plane during EM charge detonation [21]

Since the most known value is the detonation velocity EM (D) (depending on the charge density), it is advisable to use it to determine the approximate specific power (SP) of an EM, and with its help – the DND output.

If for EM the pressure in the Ch-J plane is known, then based on Fig. 2, you can also determine the expected DND output. To check the forecast results, it is necessary to synthesize DND at a EM charge density $\sim 1.6\text{--}1.7 \text{ g} \cdot \text{cm}^{-3}$ in water armor.

Thus, the obtained predictive data on the DND yield can be used for a rough prospects assessment of using EM charges.

2.2.3. Process of DND synthesis from individual, binary and triple EM charges

The use of the water (or water-urotropine) shell of the charge made it possible to increase the time of maintaining the P , T -conditions in the zone of chemical reactions, and effectively reduce the

temperature in post-detonation processes, while preserving the formed DNDs.

In [2], the authors tested the conditions for obtaining DND from tetryl according to [30] (without a shell). However, the yield of nanodiamonds turned out to be negligible (0.37 wt.%) and unsuitable for industrial production. Only the use of an aqueous or water-urotropine shell increased the yield of nanodiamonds by ~ 20 times – up to 6.3–7.05 wt.% with a minimum amount of incombustible impurities in DND – 0.36–0.94 wt.%. This method, taking into account the large reserves of tetryl, makes it possible to recommend the developed method for obtaining DND in industrial production. The oxygen balance of tetryl – 47.4 % is within the recommended range of $-35 \div -55$ % [24], and the charge density, at a sufficiently safe pressing pressure of 1,200–1,400 kgf·cm⁻², is the recommended value of ~ 1.64 g·cm⁻³ [24]. The oxygen balance, which is in the range of $-45 \div -50$ %, and the EM charge density in the range of 1.62 ÷ 1.65 g·cm⁻³ make it possible to provide an economically acceptable DND yield in an amount of 5 wt.% for individual EM.

Thus, a new industrial method for obtaining DND from individual EM tetryl with a high yield (6–7 wt.%) and a high content of DND in the diamond charge (51–63 wt.%) Has been developed, which greatly simplifies the chemical purification of DND.

Double compositions with tetryl, with its content of more than 50 % with TNT, RDX and picric acid,

give DND yield in the range of 5.2–7.34 %. The charge yield is from 10.0 to 16.2 wt.% [2].

Figure 3 shows the dependence of the nanodiamond yield on the tetryl content in binary mixtures, from which it follows that as the tetryl content increases, the DND yield also increases to 7.34 %. The most effective additive to tetryl is TNT, it is slightly inferior to RDX, the lowest yield of DND was obtained when picric acid (PA) was used as an additive.

The use of tetryl, rather than binary compounds, is more expedient, since it excludes:

- the use of RDX, which is very scarce, expensive and dangerous in circulation;
- dangerous operation of mixing tetryl with TNT, RDX or PA;
- the operation of crushing TNT or its recrystallization.

When selling products in the form of DC, the greatest demand will be for the product with the maximum amount of DND in the DC. It was shown in [2] that for this purpose it is advisable to recommend a charge composition containing TNT-RDX 60/40, TNT-RDX 50/50, or pure tetryl.

Thus, it has been shown that tetryl is the only commercially available individual EM suitable for obtaining DND with a high (up to ~ 7.5 %) yield; binary mixtures with tetryl can give a DND yield of up to 7.34 % (in water armor). To obtain DC with the highest (up to 63%) DND content, the use of individual tetryl is optimal.

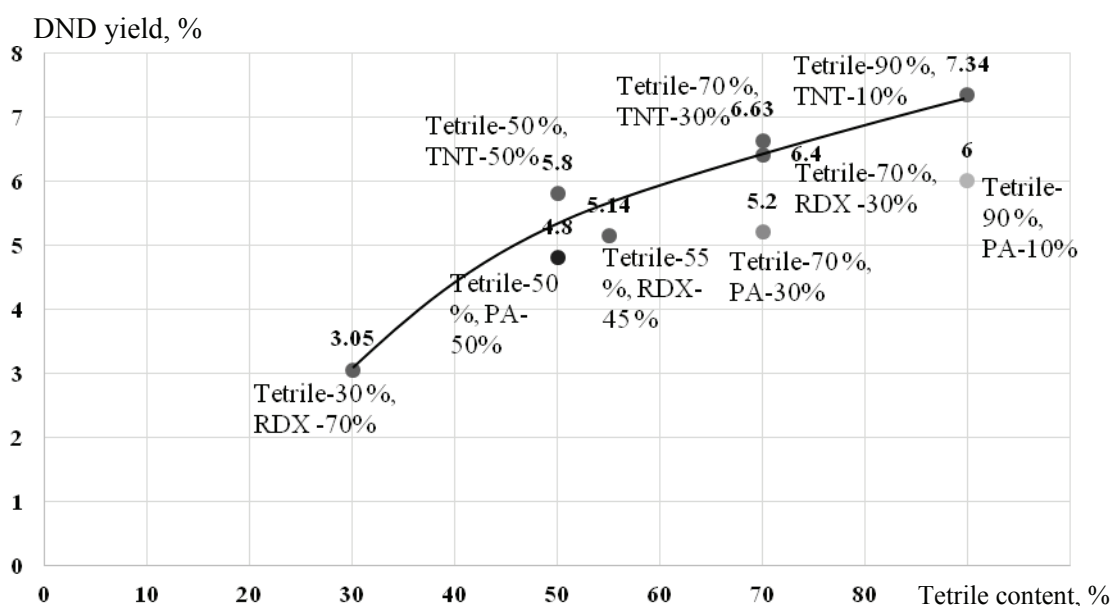


Fig. 3. Dependence of the nanodiamond yield on the tetryl content in binary mixtures [2]

To obtain DND, it is possible to use not only conventional double charges, but also more complex ternary compositions, including those based on tetryl [31]. Such charges make it possible to more accurately control the CB, density, and, ultimately, the DND yield. In addition, the replacement of RDX with conversion tetryl is economically feasible.

It has been shown that the maximum DC yield is also achieved when using 50 wt.% tetryl with TNT-RDX 70/30 (50 %) and TNT-RDX 50/50 (50 %). In these examples, the maximum DND yield is achieved – 7.94 and 8.18 %, respectively.

It was established in [32] that DNDs obtained from tetryl have a size of ~ 5 nm. NMR and EPR data show that the size and structure of tetryl DNDs is similar to nanodiamonds from a classic tetryl-hexogen alloy or a ternary mixture (tetryl + TNT + hexogen). The C^{13} NMR spectra and the behavior of the spin-lattice and spin-spin relaxation rates correlate with those for TNT-hexogen DNDs. The data obtained indicate, most likely, a single mechanism for the formation of nanodiamonds in ZCR, independent of the EM used or their mixtures.

3. Diamond charge and its cleaning

3.1. General properties of DC

DC is a physicochemical system containing diamond-type carbon structures and various graphite-like structures. Most of the non-diamond form of carbon is located on the surface of the diamond core, the fragments of which are connected not only physically, but also by chemical bonds. The isolation of nanodiamonds with reproducible characteristics is impossible without chemical treatment, which provides an energetic effect sufficient to break strong carbon-carbon bonds.

In the technology of obtaining nanodiamonds, chemical purification is the most expensive and difficult stage. Purification technologies determine the operational characteristics of nanodiamonds, and the degree of complexity of their implementation determines the level of DND cost and its availability for various applications. When passing from DC to nanodiamonds, the textural characteristics of the substance change not monotonically, but in a jump-like manner, which distinguishes the charge from other carbon materials [12].

Chemical cleaning of the charge in the liquid phase, combines the processes of oxidation and acid dissolution of metals, and is the most effective. Many methods have been proposed for its implementation. In [33], oxidative treatment is proposed, when the

charge is in the form of a suspension with a solid phase concentration of no more than 5 %, with an aqueous solution of ammonium nitrate in weak nitric acid with $pH < 1$. Ammonium nitrate is taken in a significant excess with respect to DC – 10–15 wt.% NH_4NO_3 per 1 wt. part of the charge. The process is carried out at a temperature of 210–225 °C until the completion of gas evolution, which indicates the completion of the oxidation process and the decay of ammonium nitrate. The decomposition of NH_4NO_3 under oxidation conditions proceeds to nitrogen, and the released oxygen is consumed for the oxidation of non-diamond carbon. The presence of HNO_3 in the reaction mixture ensures the dissolution of metal impurities in the form of soluble metal nitrates.

The advantage of the method is the absence of toxic nitrogen oxides in the gaseous reaction products, which makes it possible to completely abandon expensive systems for the absorption and regeneration of nitric acid. In addition, the low content of nitric acid in the spent reaction mass makes it possible to completely eliminate acid turnover.

3.2. Composites based on partially oxidized charge of detonation synthesis nanodiamonds

Controlled stopping of the DC oxidation process at various stages makes it possible to obtain a product of a given composition, structure, and the required characteristics [34]. From the experimental curves reflecting the kinetics of oxidation, it follows that, depending on the temperature and other initial conditions, there is a transition from a slowly proceeding oxidation reaction of non-diamond carbon to a self-accelerating oxidation process with the completion of the reaction. Carrying out the oxidation process under pressure makes it possible to expand the oxidation temperature range, limited by the boiling of the liquid reaction mass, and significantly reduce the requirements for the permissible concentration of nitric acid and its excess.

Oxidation of non-diamond carbon in DC with nitric acid can proceed to different degrees of reduction and a different set of reaction products (NO , NO_2 , N_2O , N_2). In DC, the following carbon structures can be distinguished by reactivity: 1) Amorphous carbon (residues of short carbon fragments and aromatic rings); 2) Disordered graphite-graphene fragments; 3) Dense “stacks of graphite-graphene structures” with limited access of the oxidizing agent due to steric hindrances. Using

the example of DC oxidation with 5–10 % nitric acid, it was shown that by varying the temperature, the reaction can be inhibited at any desired conversion stage within the range of 0–90 %. Figure 4 shows a diagram of the preparation of graphite-diamond nanocompositions.

Graphite-diamond nanocomposition 1 is a graphite-diamond composition after removal of amorphous carbon and disordered aromatic rings of graphite structures. Contains the maximum amount of carboxyl groups 4–5 wt.%. The content of diamonds is from 55 to 60 wt.%.

Graphite-diamond nanocomposition 2 is a graphite-diamond composition obtained by oxidation of a graphite-graphene shell, with fixation of oxygen-containing groups on carbon sp^2 of aromatic rings, the content of carboxyl groups is 2–3 wt.%. The content of the diamond phase is from 60 to 85 wt.%.

Graphite-diamond nanocomposition 3 is a graphite-diamond composition obtained by oxidation of residual aromatic structures of carbon sp^2 and carbon of sp^3 -transition structures. The content of carboxyl groups varies from 2 to 0.5 wt.%. The content of diamonds is 85–95 wt.%.

Thus, 1) the oxidation of the diamond-containing charge of detonation synthesis with aqueous solutions of nitric acid under pressure in the temperature range of 120–230 °C at various ratios of the reagents was investigated. The range of values of the main parameters has been identified, which allows the selective oxidation of the graphite shell to a given ratio of the diamond and graphite phases; 2) a probable scheme of the reaction as a radical chain process is proposed, which includes the

mechanisms of chain formation and the sources of its development during the oxidative process with the participation of radical-like nitrogen dioxide.

4. DND properties

4.1. DND structure

Primary DND particles have a complex structure [8, 27, 35–37]. According to the assumption of the authors of [8], they are a giant molecule, in which the carbon part is represented by a diamond core, surrounded by a non-diamond carbon shell, with which a layer of surface functional groups is connected (Fig. 5). Purified DND is a gray powder containing aggregates of primary particles of various sizes and different strengths [1, 3, 5, 7]. The content of impurities depends on the conditions of DND synthesis, methods of its purification and subsequent modification [4, 5, 36–42]. On average DND contains oxygen (up to 7 %), hydrogen (0.4–1.8 %), nitrogen (~2.5 %) and an incombustible residue (0.3–7.0 %), consisting of oxides and salts Fe, Cr, Cu, Ca, Si, Zn, etc. Oxygen, nitrogen and hydrogen are partially included in the composition of compounds sorbed on DND (carbon monoxide and dioxide, nitrogen, water, etc.), which can be located on an accessible surface or be Aggregates of nanoparticles are “walled up” in closed pores. But the other part of these atoms is part of the surface functional groups. They are an integral part of the DND supramolecule. Functional groups can be destroyed, exchanged for others, but they are always present on the DND surface, as well as on the surface of macrocrystals and grains of diamond powders of other genetic types.

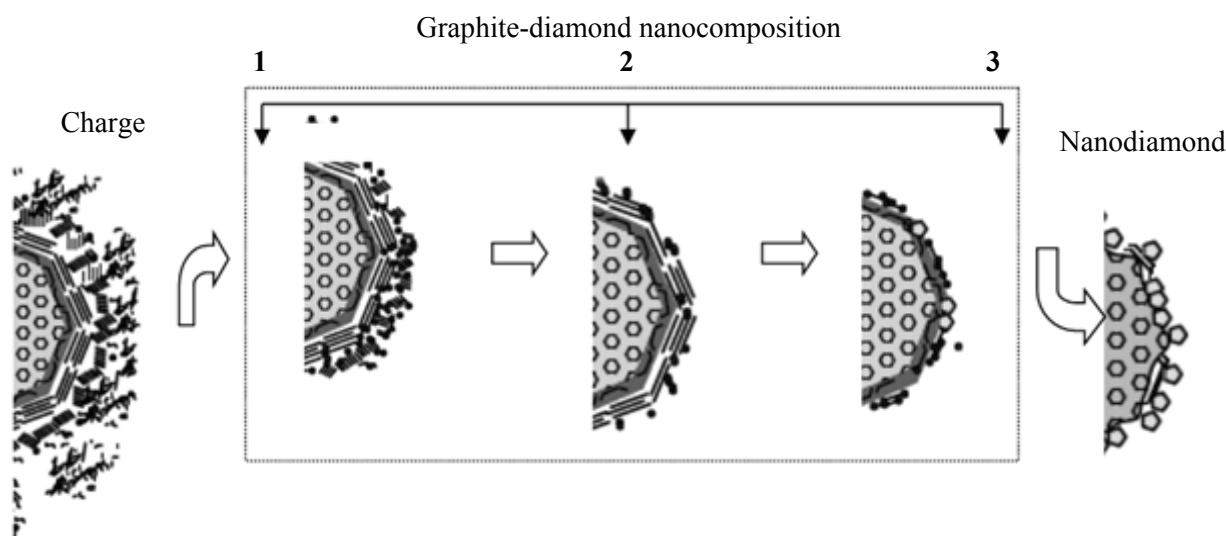


Fig 4. Scheme of obtaining graphite-diamond nanocompositions of various types from DC [34]

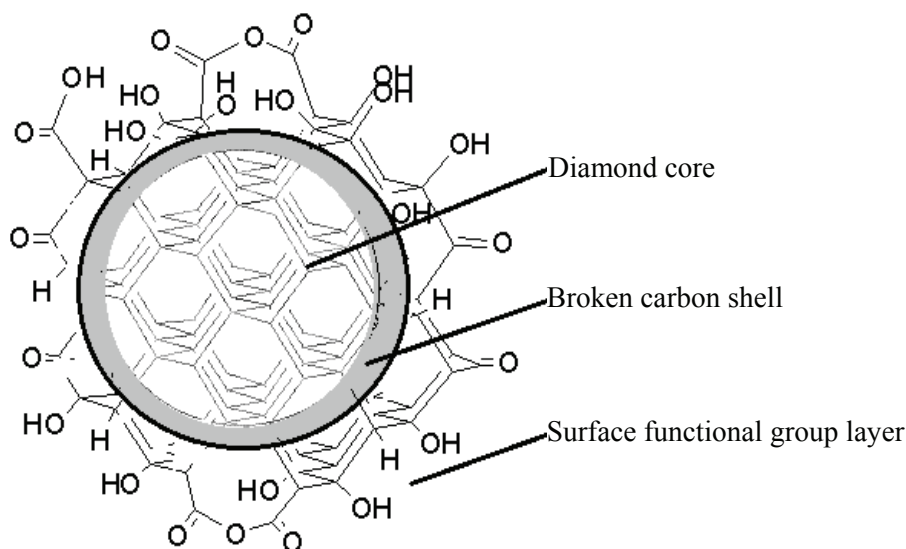


Fig. 5. Possible model of the structure of the primary particle of DND [5, 8]

When studying the diffraction of electrons on DND samples (trade mark UDA-SF FSUE SKTB Technolog, St. Petersburg) and subjected to various chemical treatments, a diffraction pattern typical for diamond is observed [5, 40]. Decomposition of the (111) reflection in a Fourier series made it possible to obtain the crystal potential distribution curve and to confirm that the primary diamond particle has an average size of 5 nm, the diameter of the diamond core being ~ 3 nm, and the thickness of the surface carbon layer ~ 1 nm. The latter has a broken diamond structure, since there is no sharp boundary for the change in the crystal potential.

The symbate dependence of the yield of carbon dioxide and nitrogen during DND oxidation to complete oxidation of the sample indicates that nitrogen is uniformly distributed throughout the volume of the DND particle.

It was shown in [43] that the factor limiting the growth (≤ 8 nm) of the diamond core in DNDs is the violation of long-range order in DNDs, the accumulation of crystal structure defects as the carbon nanoparticle grows in post-detonation processes. Comparison of the distribution of carbon atoms in DND and in defect-free diamond, which differ in lattice parameters, shows that in nanosized diamond there is a change in the coordination number (CN) in the outer coordination spheres (CS). The CS has the absence of atoms (lattice defects), which changes the structure and morphology of the DND surface. Defective structures are more reactive and oxidize more easily during chemical processing.

On the surface of DND particles there is a cover consisting of various functional groups, mainly oxygen-containing, including carboxyl, ester, ether,

lactone, etc., which determines the non-selectivity of the reactions of its modification [5]. The nature of these groups and their ratio are determined by the peculiarities of the technologies for obtaining, isolating and purifying DND [1, 3, 5, 7, 8, 44, 45]. In addition to these functional groups, depending on the processing conditions, halogen- and nitrogen-containing (amine, amide, cyano and nitro groups), sulfone and other groups can be associated with the surface of nanodiamonds [5, 46–51].

O—H stretching vibration bands ($3,500$ – $3,200$ cm^{-1}) are present in all spectra, the shape depends on the type of DND, the maxima of asymmetric and symmetric bands at $3,410$ and $3,230$ cm^{-1} correspond to particles with strong hydrogen bonds and, in some cases, to the $3,290$ cm^{-1} , which is probably an overtone band of liquid adsorbed water [45]. All types of DND differ in the position of the main maximum and in the carbonyl band width of about $1,750$ cm^{-1} . For most varieties, it is located at $1,740$ cm^{-1} , for DND-TAN and DND-STP (manufactured by FGUP SKTB Technolog, St. Petersburg, Russia), it is located at $1,786$ cm^{-1} . The reproducibility of this band is the highest among other bands in the spectrum, and it is usually the same for different brands of the same manufacturer, for example, for DND-TAN and DND-STP. In terms of the characteristics of the DND brand, groups of nanodiamonds can be distinguished by the amount of bound water ($1,630$ cm^{-1}) and the intensity of the OH continuum $3,600$ – $3,000$ cm^{-1} and carboxyl groups C=O and C—O—H bands at $1,760$ – $1,740$ and $1,440$ – $1,340$ cm^{-1} , respectively.

4.2. Electron Paramagnetic Resonance of detonation nanodiamonds

The phenomenon of magnetic resonance is the resonant absorption of electromagnetic radiation by quantum objects with non-zero spin values, subjected to an external static magnetic field. These objects may be unpaired electron spins (the cases of Electron Spin/Paramagnetic Resonance ESR/EPR and its derivatives Electron Nuclear Double Resonance – ENDOR, Optically Detected Magnetic Resonance – ODMR etc.) or non-zero nuclear spins (the cases of Nuclear Magnetic Resonance – NMR and closely related Magnetic Resonance Imaging – MRI). Both a deep theoretical background and application of various magnetic resonance techniques to studies of a large variety of physical objects may be found in Refs. [52–54]. These non-destructive techniques provide researchers and technologists the potential to uniquely identify the electron-nuclear structure of various substances containing magnetic species, from gases to complex biological molecules. They are capable of providing important information on the structure and dynamics of a system, including the chemical and physical processes occurring there.

Plenty of defects and impurities in crystalline diamond samples (including the most intriguing optically active triplet centers like NV⁻) carry non-zero electron spins which makes EPR and related techniques the most adequate ones for providing useful information on the anisotropy of electronic g tensor; zero field couplings in species with $S > 1/2$; hyperfine interaction with principle nuclei of surrounding atoms, etc. [52]. Traditionally, these phenomena are interpreted within the framework of the spin-Hamiltonian (SH) concept, where SH is an energy operator describing all existing interactions (electric, magnetic, exchange) of the electron and nuclei spins with their surrounding and external fields applied [53, 54]. Useful data obtained from EPR spectra are presented as corresponding SH parameters (g -values, hyperfine splitting A , zero-field splittings D , E etc.). Well-developed theoretical tools in combination with state-of-the-art experimental techniques allow one to obtain tiny details of a defect's nature, surroundings and interactions. However, the EPR study of DND samples has its specificity dictated by the form of the diamond sample. In many cases, conventional EPR deals with bulky samples. In contrast to well-ordered single crystal diamonds and crystalline diamond films, bulky DND samples appear as non-oriented powders. Dynamic synthesis techniques (detonation, shock wave, laser ablation) provide diamonds in the form of nanometer-sized powders; a typical sample is an

ensemble of small particles characterized by a distribution of individual sizes and properties of these particles. Thus, EPR spectra of DND samples are spatially averaged, which causes certain decrease in spectral resolution, reduction in sensitivity (due to additional line broadening) and complications in interpretation of the EPR data. Moreover, the specificity of DND synthesis conditions and high surface-to-volume ratio (characteristic feature of all nanoparticles) induce unusual densities of some defects thus confusing the hierarchy of interactions between magnetic centers. The latter brings new complexity in deciphering of EPR spectra.

Real DND samples demonstrate a large variety of magnetic properties which descend mainly from the origin of the samples as well as any subsequent treatments performed on them. For instance, each DND particle inherits, first of all, some magnetic features of its ancestors. Further, the detonation synthesis itself creates new carbon inherited defects within surface layers of nanoparticles and may be considered as a source of synthesis originated magnetic impurities. First, there should be clear discrimination between two types of defects: those that are either inherent or induced in the *diamond core* or on/within the *surface/interface layer of the diamond nanoparticle* as a result of the synthesis (e.g. atoms from initial explosives etc.); and those that are not directly induced on or within the diamond, but are instead unrelated magnetically active impurities which may stem from various post-processing techniques (e.g. impurity contamination the detonation synthesis chamber). In both research and practical applications of DND, the most of uncontrolled impurities are undesirable species that may (and have to) be removed by the proper choice of a purification technique [55]. In this respect just EPR is a powerful analytic tool for assessing the content of initial magnetic impurities and the efficacy of purification procedures. Non-impurity magnetism in DND originates from three main sources: (i) intrinsic paramagnetic defects inherited from source materials, where these defects were created in the process of diamond formation or synthesis (e.g. metallic impurities from catalysts, nitrogen); (ii) defects induced by synthesis (e.g. dangling bonds along cleavage planes); and (iii) intentionally induced defects introduced to modify the properties of the initial diamond material (e.g. NV⁻ centers or other irradiation induced defects). The latter type of defect may be sub-classified into: defects attached to the diamond surface and subsurface interface layers by modification of the surface chemistry (particularly in smaller particles with high specific surface area); and

defects induced by ionizing irradiation/ion implantation of raw diamond materials or resulting small particles.

Detonation technique of diamond synthesis directly provides diamond particles of nanometric sizes. In the most cases size distribution in DND samples is quite narrow with the average particle sizes below of ~4–6 nm. In facts, real DND samples rarely consist of well separated single nanoparticles but are rather quite large (hundreds of nanometers or even micron-sized) polycrystalline aggregates of single ND particles. Various techniques are used for disaggregation of these entities into solitary ND crystallites, but all of them are much “softer” than usual nanonization processes applied to bulk crystalline diamonds. It has been demonstrated that disaggregation did not create additional mechanically induced paramagnetic defects [56, 57]. Thus, all paramagnetic defects in initial (non-modified) DND are intrinsic defects, emerged in DND particles at their generation.

Already early EPR studies of detonation DND revealed well pronounced paramagnetism. DND samples synthesized by different explosion techniques and obtained from different manufacturers exhibited similar EPR characteristics, more specifically: absence of characteristic hyperfine EPR patterns due to substitutional paramagnetic nitrogen in diamond lattice (so called P1 or N0 centers) and presence of a strong singlet Lorentzian-like signal with $g = 2.003$ and line width $\Delta H_{pp} \sim 0.7\text{--}1.0$ mT attributed to paramagnetic $S = 1/2$ defects in the diamond structure (dangling bonds etc.). The results of the measurements done on various detonation DND powders are summarized in Refs. [56, 58] and references therein. Precise measurements of the g -factor for the most intensive signal provide $g = 2.00282 \pm 0.00003$ within the temperature range of 4.2–300 K. The observed shift of this g -factor from the free electron value ($g_e = 2.0023$) may be interpreted in terms of the model of unpaired spins localized at a mesoscopic object (to which DND particles belong as well). This interpretation allows estimating the size of the DND particle as 20–60 Å, which correlates well with the DND dimensions derived from XRD and HRTEM. Careful SQUID and EPR study of well purified detonation DND (sample ND2) revealed the density of $S = 1/2$ spins 6.3×10^{19} spin/g or 1255 ppm, which corresponds to 13–15 $S = 1/2$ defects per each DND particle [59]. The defects' densities in diverse DND samples of different origins vary around the density in ND2 with deviations not exceeding 30%. Thus, DND fabricated from non-conventional explosives (like

Tetryl) show the same EPR characteristics as the aforementioned ND2 sample (i.e. $g = 2.0028 \pm \pm 0.0002$, $\Delta H_{pp} = 0.72$ mT and 0.80 mT for the DNT1 and DNT7 samples, correspondingly), but enhanced defects' densities 1481 ppm (DNT1) and 1,793 ppm (DNT7) [32] – see Fig. 6, *a*. Analysis of the EPR spectra revealed that the singlet Lorentzian-like line observed consists of two main Lorentzian components: broad and narrow ones – see Fig. 6, *b* and Ref. [60]. It was suggested that broad and narrow signals are due to two types of $S = 1/2$ defects somehow differing by their both origin and location.

Modification of DND by grafting the DND surface with transition metal ions (for instance – divalent copper [60, 62] and trivalent gadolinium [63], being itself promising and useful method for design of DND with controlled characteristics [64], also appeared to be helpful in the attribution of broad and narrow lines [62]. Direct observation of Cu^{2+} and Gd^{3+} EPR signals allowed acceptable estimation of the number of transition metal ions attached to the DND surface. Thus, Cu^{2+} ions were used as paramagnetic probes which interact (by dipole-dipole and exchange channels) with the intrinsic $S = 1/2$ defects. Varying modification conditions one can control the strength of the said interactions which, in turn, allowed estimating distances between paramagnetic probes and different types of intrinsic defects. It was found that surface located Cu^{2+} ions cause broadening of the both types of EPR lines originated from $S = 1/2$ defects, but such a broadening is more pronounced for the broad lines and less – for the narrow lines [60, 62]. Such a behavior indicates that defects responsible for the broad lines are located closer to the DND surface than those ones responsible for the narrow line. The estimated depths of occurrence for two types of intrinsic $S = 1/2$ defects were found to be ~0.8 nm and ~1.5 nm from the DND surface for the shallow and deeper defects, respectively. It may be supposed that the intrinsic $S = 1/2$ defects in DND belong to at least two main groups differing first of all by their location inside the DND particle. The defects located at average distances of less than 1 nm from the surface are responsible for the broad Lorentzian component of the main EPR signal. Defects of another group, associated with the narrow Lorentzian component, are located deeper from the surface – at average distances ~1.5 nm. May defects of the first group be attributed to surface defects or are they “hidden” within the subsurface interface layers? EPR provides univocal answer to this question [58] reports on the experiments with evacuated DND samples.

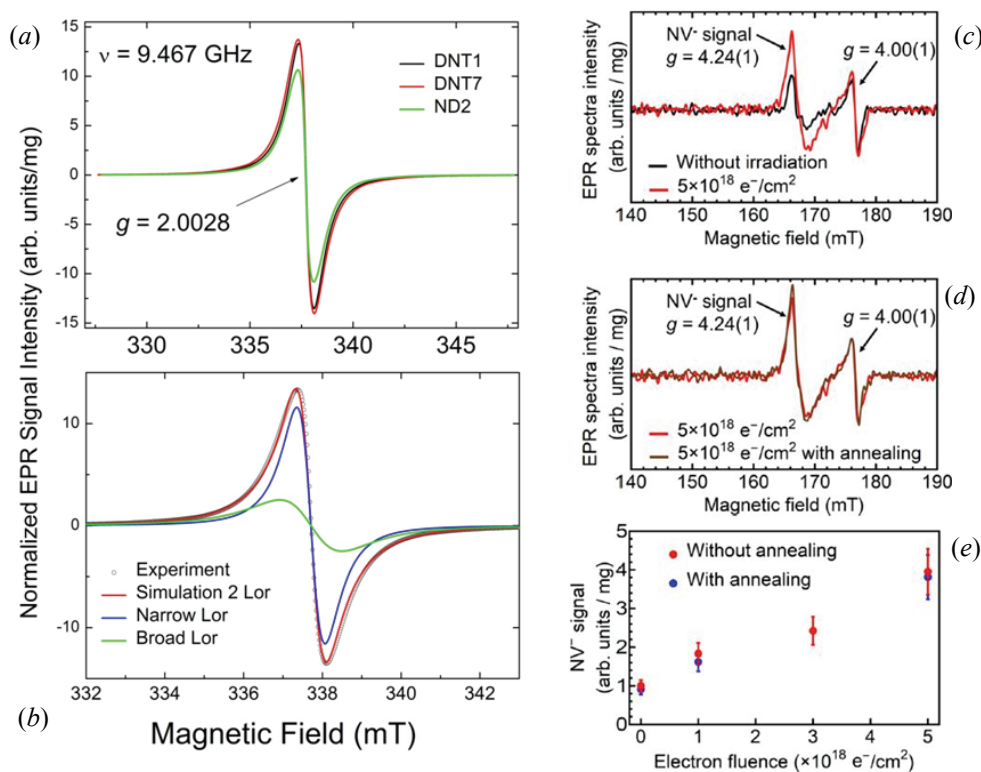


Fig. 6. EPR study of DND samples:

a – X-band EPR spectra of DND samples DNT1 (black traces), DNT7 (red trace) and ND2 (green trace) recorded at room temperature and $\nu = 9.466$ GHz [32]; *b* – deconvolution of the experimental EPR spectrum of DNT1 (black circles) into two Lorentzian lines with the same g -factor 2.0028: best least square fitting with 2 lines (red trace), narrow component with $\Delta H_{pp} = 0.72$ mT (blue trace), broad component with $\Delta H_{pp} = 1.58$ mT (blue trace); *c* – half-field EPR spectra of DND before (black trace) and after electron irradiation with fluence $5 \times 10^{18} \text{ e}^- \cdot \text{cm}^{-2}$ (red trace) recorded at room temperature and $\nu = 9.87$ GHz; *d* – half-field EPR spectra of electron irradiated DND samples before (black trace) and after annealing at 800 °C for 2 h under vacuum (red trace); *e* – dependence of the NV⁻ content in irradiated DND sample on the e-beam fluence [61]

Air evacuation increases doubly integrated intensity of the main EPR signal for about 10 % with no changes in its line shape, widths and positions of the signal. When the sample was open to air again, the intensity of the signal returned to its initial value. Such an effect may be understood in terms of exchange broadening of EPR lines of the defect's spins due to encounters with molecules of triplet oxygen (O₂), which is well known magnetic agent contained in air. Thus, there are some defects in the first group which are located on the surface of the DND particle or close enough to the surface for interacting with molecular oxygen. From the aforementioned 10 % reduction of the intensity it may be concluded that a single $S = 1/2$ defect may be located on the surface of a DND particle. Other defects in this group are well isolated from encounters with oxygen molecules because of their location inside subsurface interface layers. Following direct analogy with carbon-inherited defects, induced

in diamond particles by nanonization, this group of defects may be attributed to dangling bonds located within the distorted diamond structure of interface layers. Thesecond group of inherent defects in DND, which is located at least twice deeper inside the ND particle, is responsible for the narrow Lorentzian component of the EPR signal. The same narrow line is observed in EPR spectra of fine ND fractions obtained by nanonization of micron-sized type Ib HPHT diamonds [65]. There it was supposed that such a line originates from P1 centers strongly interacting with large amount of mechanically induced dangling bonds. It is logical applying the same model to DND. Indeed, typical P1 hyperfine split patterns have never been reliably observed in EPR spectra of DND. On the other hand, it is well known on the presence of high abundance of nitrogen in DND. Thus, the absence of characteristic P1 signals sounds quite puzzling. However, the hypothesis proposed in the Ref. [65] may

successfully solve the puzzle: namely, narrow Lorentzian component in EPR spectra of DND is due to nitrogen substitution defects (P1) which are located into the crystalline core of aDND particle and strongly interact with uncoupled electron spins of multiple dangling bonds located into interface layers. In such configuration (and there are no other configuration in small DND particles!) the conventional hyperfine split pattern cannot be observed at all [66].

X-band EPR study at $4 \leq T \leq 300$ K of well purified DND [58] revealed the presence within the half-field region two additional (to the main intense $S = 1/2$ signals) weak and narrow signals with $g_1 = 4.26(1)$, $\Delta H_{pp} = 2.9(1)$ mT and $g_2 = 4.00(1)$, $\Delta H_{pp} = 1.4(1)$ mT at $T = 4$ K), separated by the distance of 10.4 mT. Integral intensity of these signals was found to be several orders of magnitude lower than the same for the main signal. It was supposed that these doublet signals appear due to “forbidden” fine transitions between Zeeman states of some triplet centers. Further the same doublet signals were found in X- and Q-band (9.4 and 34 GHz, correspondingly) EPR spectra of a large variety of intact, purified and modified nanodiamonds obtained from various manufacturers and synthesized by different dynamic synthesis techniques (detonation, laser, “Du Pont”) [67]. Careful analysis of EPR spectra collected from multiple samples showed that these signals, in spite of having frequency dependent g -factors and splitting as well as sample dependent line widths and relative intensities ratios, always present in EPR spectra of DND and may be attributed to two different types of triplet paramagnetic centers: the X-band $g_1 = 4.26$ signal is characteristic for NV^- defects whereas the X-band $g_2 = 4.00$ signal is characteristic for exchange coupled $S = 1/2$ defects (multivacancies) – Figs. 6, *c*, *d*. Here it is worth mentioning that the ‘allowed’ lines, always accompanying ‘forbidden’ lines in EPR spectra of NV^- triplets recorded on bulky fluorescent diamonds and coarse fluorescent nanodiamond fractions, have never been observed in DND. Assumed nature of this phenomenon observed in fine fluorescent nanodiamond fractions is discussed in [67].

These two universal types of triplet centers are minor rare defects in all DND independently of the type of dynamic synthesis and precursors. The ultimate confirmation of the correctness of the above attribution was done by comparison of half-field EPR spectra of DND with similar spectra of fluorescent nanodiamonds obtained by nanonization of electron irradiated micron-sized HPHT diamonds [68].

Thus, it may be concluded that each DND sample contains certain amount of inherent (i.e. created by the synthesis itself, not induced by intentional high energy irradiation and/or nanonization) triplet NV^- and multivacancy defects. The actual content of each of these defects depends on a synthesis technique, starting materials and conditions as well as post-processing. The highest abundance of inherent NV^- defects, well compared with the same abundance in fine fluorescent (irradiated/annealed) nanodiamonds, was found in DND disregarding of their type of the conventional DND precursors – nitrogen-based explosives. It has been recently demonstrated [61] that the ability of DND particles for generating NV^- centers inside themselves is not limited to just those triplet centers born in the process of detonation synthesis: irradiation of conventional DND by high energy electron beam results in significant enhancement of the lower field line in the half-field EPR spectrum of the irradiated sample (see Fig. 6, *c*). This enhancement undoubtedly indicates enrichment of the DND particle by NV^- centers. Interesting, that, in contrast to irradiated HPHT nano- and micron-diamonds, annealing of the irradiated DND sample at 800 °C for 2 h under vacuum does not practically change the NV^- content (see Fig. 6, *c*). This puzzling feature is still within the focus of ongoing investigations. On the other hand, the fluence dependence (Fig. 6, *e*) is found to be in line with the same dependence found for HPHT crystallites [69].

5. Application of detonation nanodiamonds

5.1. Electrochemical metal-diamond coatings

5.1.1. The electrochemical deposition process of gold-diamond coatings

Composite coatings are divided into five groups – wear-resistant, antifriction, corrosion-resistant, frictional and coatings with surface strength, hardness and heat resistance.

The use of detonation diamonds (DND) in electroplated coatings is an illustration of their successful application. Composite electrochemical coatings (ECC) with DND have high hardness, strength and resistance to wear, corrosion and weathering. These properties are due to changes in the ECC structure caused by the inclusion of nanoparticles in the range from 0.1 to 1.0 %.

The doped (alloyed) nanodiamonds used in this work with phosphorus or boron were obtained by the explosion of a mixture of TNT with RDX in an aqueous shell; moreover, up to 5 wt.% was added to

the charge during molding, with thorough mixing. phosphorus or boron compounds – triphenyl phosphate (DND-32B), sodium tetraphenylborate (DND-27B), potassium tetraphenylborate (DND-36B) [70]. In addition, DND-STP were used – these are standard (classical) detonation nanodiamonds; DND-TAN is DND-STP, but subjected to treatment with NH_4OH at $\sim 225^\circ\text{C}$ and pressure up to 50 atm; DND (Japan) – DND-STP, from which prof. E. Osawa (Japan) nanoparticles less than 8 nm in size [71]; DND-FTI-1 – DND-STP, from which nanodiamond particles ~ 5 nm were isolated in the laboratory of prof. A.Ya. Vul (St. Petersburg, Russia) to a size of ~ 5 nm [72].

Gold coating of phosphate electrolyte when using DND-TAN and DND-FTI-2 (doped with boron) has a microhardness of $177\text{--}198 \text{ kgf}\cdot\text{cm}^{-2}$ at an application temperature of $20\text{--}25^\circ\text{C}$, which is close to the microhardness of films from citric acid electrolyte. The greatest increase in microhardness at density current of $3 \text{ mA}\cdot\text{cm}^{-2}$ is achieved with explosive injection into DND electrolyte (Japan) – up to $221 \text{ kgf}\cdot\text{mm}^{-2}$. DND-FTI-1 ($2 \text{ mA}\cdot\text{cm}^{-2}$) has similar values, an increase in microhardness by $25\text{--}30 \text{ kgf}\cdot\text{mm}^{-2}$ (up to 20 %).

The tests of gold coatings for wear resistance have shown that the greatest wear resistance is achieved in the case of using DND-FTI-2 (doped with boron) – 0.8 % wear per 22 hours of abrasion. The rest of the additives, explosively injected into the gold plating, gave almost the same wear – 2.1 % for 22 hours of abrasion.

The studies by atomic force microscopy, both glider methods and electron microscopy, have shown that the additives used affect the surface

microstructure, significantly reducing the grain size (Table 2).

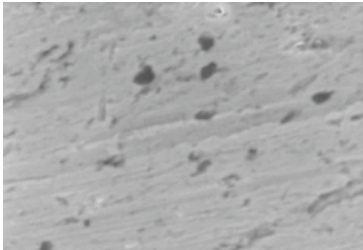
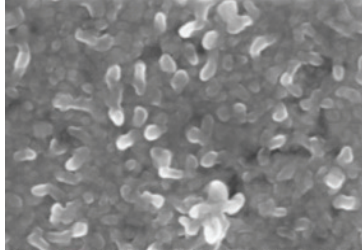
From Table 2 it follows that the recommended parameters for applying gold-diamond coating are in the ranges corresponding to the conditions of industrial coating. Thus: 1) the microhardness of gold coatings when using nanodiamonds with a concentration of $1\text{--}2 \text{ g}\cdot\text{L}^{-1}$ increases by 50–60 %, and in citric acid electrolyte – by 15–20 %; 2) the addition of DND-Ioffe-2 in citric acid gilding electrolyte gives a practically wear-free coating.

5.1.2. Chrome plating

The authors of [73] investigated the following electrolyte and coating modes: $\text{CrO}_3 - 250 \text{ g}\cdot\text{L}^{-1}$; $\text{H}_2\text{SO}_4 - 2.5 \text{ g}\cdot\text{L}^{-1}$; $t = 45^\circ\text{C}$, $i = 50\text{--}70 \text{ A}\cdot\text{dm}^{-2}$ (hard chrome plating mode); $t = 60^\circ\text{C}$, $i = 25\text{--}40 \text{ A}\cdot\text{dm}^{-2}$ (wear-resistant chromium plating mode).

Pre-modified DND (modified, MDND). For this purpose, NH_4NO_3 was added to the suspension containing DND-TAN, the resulting suspension solution was dried at 105°C until water was completely removed, then heated to 215°C and held for 2 hours. In this case, NH_4NO_3 decomposes to a mixture of nitrogen oxides, the latter interact with the nanodiamond surface, increasing the amount of oxygen-containing functional groups on the surface, and, as a consequence, the hydrophilicity of nanodiamonds. In addition, bonds between nanodiamond particles in aggregates are weakened as a result of exposure to high temperatures and oxidizing gaseous agents.

Table 2. Properties of gold plating with boron modified DND

| Characteristics | Electrolyte plated gold | |
|--|---|---|
| | Without additives | With the addition of DND 27-B (boron) – $1 \text{ g}\cdot\text{L}^{-1}$ |
| Micrograph of the gold surface (structure) |  |  |
| Microhardness, $\text{kgf}\cdot\text{mm}^{-2}$ | 180 | 214 |
| Wear, % | 1.7 | 1.0 |

Sodium hydrogen carbonate or monic acid was successively added to DND powder. When introduced into the water, a violent gas evolution and almost complete “dissolution” of DND occurs, a homogeneous stable suspension of DND in water is formed, which was added to the chromium electrolyte. MDND addition (calculated as pure DND) explosive was added to chromium electrolyte in the following concentrations: 0.1; 0.2; 0.5; 1.5; 5.0 g·L⁻¹. When MDND is explosively fed into the electrolyte in an amount of 1%, the content of nanodiamonds in the coating is 0.2 wt.%.

When MDND is added to the electrolyte, the microhardness of chromium coatings increases significantly – 1.3 times in the wear-resistant chromium plating mode and 1.6 times in the hard chromium plating mode compared to the microhardness values obtained in pure electrolyte (Fig. 7). With an increase in the content of nanodiamond additives over 1 g·L⁻¹ in the chromium plating electrolyte, the microhardness values reach a maximum and practically reach a plateau.

Wear resistance was measured only for chrome coatings obtained in the wear-resistant chromium plating mode. It sharply increases (~2 times) in comparison with the wear resistance of coatings obtained from pure chromium electrolyte. For a pure chrome coating, the friction coefficient during the experiment varied quite chaotically – from 0.15 to 0.7. The wear of the sample coated with pure chromium occurs very unevenly, with scuffing, which is not observed when the coating obtained with the addition of the nanodiamond additive MDND is worn.

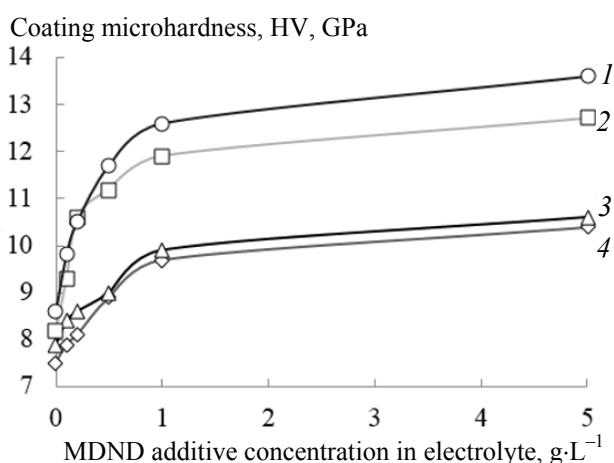


Fig. 7. Dependence of microhardness on the concentration of MDND additive at different current densities for hard chromium [73]:

1 – 13.6 GPa, $i = 70 \text{ A/dm}^2$; 2 – 12.7 GPa, $i = 65 \text{ A/dm}^2$;
3 – 10.6 GPa, $i = 60 \text{ A/dm}^2$; 4 – 10.4 GPa, $i = 50 \text{ A/dm}^2$

Thus: 1) a new composite dry DND powder (MDND) has been developed for use in the classic chromium plating electrolyte; 2) the microhardness of the chrome coating increased from 7.8 to 9.6 GPa (by 23 % (wear-resistant chromium plating mode)), and in the hard mode – from 10.4 to 13.6 GPa (by 31 %); 3) the coefficient of friction of the chromium-diamond coating decreases by 2 times.

5.1.3. Polymer-diamond composites

Heat generated by electronic devices and circuits must be dissipated to extend the life of the product. For this, in particular, lubricants (thermoplastic composites, TPC) based on polymers (silicones and epoxy resins) are used to connect the circuits (circuits) in the device itself. TPC have low coefficients of thermoplastic expansion than, for example, aluminum, which is important when TPC contacts with silicon or ceramic circuits. The use of polymeric materials, however, is limited due to their low thermal conductivity $\sim 0.2 \text{ W}\cdot\text{m}^{-1}\cdot\text{K}^{-1}$. As a polymer filler and heat-conducting additives, boron nitride or carbide, aluminum oxide, graphite are used. An increase in the thermal conductivity of TPC due to the extremely high content of the filler is impossible, since with an increase in the concentration of the filler, the mechanical properties of the cured product deteriorate.

So, in the patent [74], the thermal paste contains DND powder, thermal powder and polymer in the ratio of DND – from 5 to 30 % by volume, thermal powder from 40 to 90 % by volume, and polymer – from 5 to 30 % by volume DND.

The work [75] describes the production technology and properties of DND-containing TPA. It is shown that such a composite material contains from 0.01 to 80.00 wt.% DND particles, from 1 to 90 % of at least another filler and from 5 to 80 wt.% thermoplastic polymer. As the latter, acrylonitrile-butadiene-styrene, acryl, celluloid, cellulose derivatives, cyclic olefin copolymer, ethylene vinyl acetate, ethylene vinyl alcohol, fluoroplastics, or their combinations, a wide range of other polymers are proposed. The polymer can be in crystalline, semi-crystalline or amorphous form. The explosive size of the DNDs in TPC is preferably aggregates from 60 to 800 nm. In addition to purified DND, DS is used, preferably containing at least 10 wt.% non-diamond carbon. The second filler is metal, metal oxides, metal nitrides, carbon in various modifications, and ceramic materials. TPC molding is carried out at an elevated temperature, it is proposed for use in electronic devices and automobiles. Thus, when TPC was obtained from polyphenylene sulfide

(PPS), the following thermal conductivity results were obtained: pure PPS – $0.21 \text{ W}\cdot\text{m}^{-1}\cdot\text{K}^{-1}$, and with a mixture of nitride boron (40 wt.%) with DND (5 wt.%) thermal conductivity increased to $1.41 \text{ W}\cdot\text{m}^{-1}\cdot\text{K}^{-1}$, i.e. 7 times.

When preparing a thermal paste based on polyamide-66 (PA-66) with boron nitride and DND, it was found that even the combined addition of small amounts of DND (0.1 and 0.5 wt.%) to boron nitride makes it possible to raise the thermal conductivity from ~ 0.33 (PA-66 without additives) up to $4.72 \text{ W}\cdot\text{m}^{-1}\cdot\text{K}^{-1}$, i.e. 14 times.

5.1.4. DND application of in 3D printing

For 3D-printers, thermoplastic raw materials are used for layer-by-layer application of molten polymer filament when forming a product. The paper [76] describes the possibility of using DND as a reinforcing filler in such thermal pastes. Were obtained threads from acrylonitrile butadiene styrene (ABS) and from ABS modified with DND (ABS – DND). Modification of ABS with 0.05 wt.% nanodiamonds led to a decrease in friction during extrusion, which made it possible to increase the productivity of the filament manufacturing process. The use of DND additives increased the tensile strength and tensile load of ABS, and the rigidity and elastic modulus also increased. In addition, the thermal conductivity is improved and a higher glass transition temperature of the filament is achieved. The thread contains a thermoplastic polymer in an amount of 80 to 99.99 wt.% and nanodiamonds in an amount of 0.005 to 10 wt.%, and the thread has at least 15 % higher tensile strength than a thread without DND. The thermal conductivity of the DND filament is at least 8 % higher than the thermal conductivity of the nanodiamond-free filament.

Any suitable thermoplastic polymer can be used: acrylic, celluloid, cellulose acetate, cyclic olefin copolymer, ethylene vinyl acetate, ethylene vinyl alcohol, fluoroplastics such as polytetrafluoroethylene and perfluoroalkoxyalkanes, nylon (aliphatic or aromatic polyethylene (P)), PE), polyethylene terephthalate (PET) and polycarbonate (PC), most preferably polylactic acid. Detonation nanodiamonds can be monofunctionalized with amino, carboxyl, hydrogen, or hydroxyl groups. The DNDs used must have a zeta potential above + 30 mV or below – 30 mV. The zeta potential is measured in 0.5 wt.% of an aqueous dispersion of nanodiamond at pH = 7. The filament may additionally contain one filler other than DND selected from the group consisting of a metal, a metal oxide, a metal nitride, a metal

carbide, a carbon compound, a silicon compound, boron compounds such as boron nitride, ceramic materials, natural fibers or combinations thereof. The thermal conductivity of the article is at least 8 % higher than the thermal conductivity compared to the article without DND. The average tensile strength of the two PLLA (polylactic acid) reference samples is 26.182. The average tensile strength of the two nanodiamond samples is 36.142. The tensile strength of 3D-printed PLLA material with 0.05 wt.% amine-functionalized nanodiamond was improved by 38 %.

New 3D-printed products can be used in mechanical engineering, in the aerospace industry, in electronic devices, in the form of polymer compositions to replace existing metal products, as molds, medical devices and materials for the production of artificial bones, etc.

5.1.5. DND in fuel compositions

The prospective development of solid rocket propellants requires an increase in energy characteristics. This is achieved by explosive introduction of high-energy components (oxidants, polymeric combustible binders, plasticizers, fillers) into the compositions. Known mixed solid propellant, including an oxidizer - ammonium perchlorate (AP), polyvinyl isoprene rubber with end carboxyl groups, plasticizers – polyvinyl isoprene rubber, curing catalyst – zinc stearate, metallic fuel – dispersed aluminum [77, 78].

A diamond crystal, including detonation nanodiamond (DND), is an example of the densest packing of carbon with a density of $\sim 3.5 \text{ g}\cdot\text{cm}^{-3}$. In [79, 80], the possibility of using classical TNT-hexogen DNDs to increase the combustion rate of model rocket fuels was shown by calculation and experiment. The explosive use of DNDs in the composition of solid rocket fuels (SRF) gives a noticeable increase in the combustion rate of the composition [79, 80], and the effect of their application depends on the component base of the composition and the working pressure in the combustion chamber. A distinctive feature of compositions with DND is a high combustion rate at a low temperature of the combustion products of the composite propellant. In [80], the effect of DND on the combustion rate of a binary mixture of APC-DND with a DND mass content of up to 6% was studied.

In [81], a modified composite solid rocket fuel (CSRF) is considered, containing an active combustible binder and an oxidizer, while DND co-crystallized with AP is additionally explosive into the fuel with the following total ratio wt.%: active

combustible binder 15–30; oxidizing agent 84.5–60.0; detonation nanodiamond 0.5–10.0. The technical effect consists in increasing the density of the composition and the enthalpy of formation of the fuel and, as a consequence, the energy component, the absence of specific impulse losses for the two-phase flow compared to metal-containing compositions, an increase in gaseous combustion products, and the absence of burnout of the nozzle block in comparison with metal-containing compositions. Calculations performed on the effect of DND on the thermodynamic specific impulse of the reference fuel composition, consisting of 80% oxidizer – AP, and 20 % active fuel-binder (AFB) for standard conditions at $P_k/P_a = 40/1$ (P_k is the pressure in the combustion chamber, and P_a is the pressure at the nozzle exit) revealed its positive effect on the energy and mass characteristics of the fuel compositions. Explosive treatment in the reference DND composition was carried out by reducing the percentage of PCA, while the content of AFB remained unchanged. Analysis of the calculated data indicates an increase in the density of the composition and temperature in the combustion chamber and, as a consequence, leads to an increase in the specific impulse. With the explosive introduction of each 0.5 % DND into the fuel, the temperature in the combustion chamber increases by an average of 80 K, and the mass specific impulse increases by 2 kgf·s·kg⁻¹. A further increase in the DND content in the fuel composition leads to a decrease in specific impulse.

Thus, the main advantages of using DND in CSRFB compositions are: increasing the density of the composition; an increase in the enthalpy of formation of fuel and, as a consequence, the energy component; loss-free specific impulse due to the two-phase flow in comparison with metal-containing compositions; an increase in the amount of gaseous combustion products; no burnout of the nozzle block in comparison with metal-containing compositions.

5.1.6. Nanodiamonds in biology and medicine

The possibility of using DNDs in biology and medicine is determined by their unique properties: a large specific area of crystallites ~ 300 m² g⁻¹ [82], hence the high sorption activity; hydrophilic DND surface; chemical inertness of the diamond core and the activity of the peripheral shell; fluorescence of DND crystallites; the ability of crystallites to penetrate cells; availability of nanodiamonds [39, 83–85]. In addition, DND activity is predetermined by a large number of unpaired electrons (~ 40 per

crystallite ~ 4.8 nm) [86]. It has been shown that among the known carbon nanostructures, detonation nanodiamond has the least toxic effect [87, 88]. Therefore, in recent years, the interest of researchers has shifted from known carbon nanostructures to DNDs.

The DND surface covered with primary amino groups is a convenient platform for binding with biomolecules, enzymes, and peptide chains [89]. The relative simplicity of their modification opens up wide possibilities for the direct interaction of nanodiamond crystallites with biological molecules and biological structures, and an increase in the selectivity of DND [90, 91].

The most important for use in biology is the specific binding of DND to proteins, both covalent [92] and non-covalent [93]. The advantages of the covalent attachment of biological macromolecules to the nanodiamond surface are the high stability of the adduct, provided by strong covalent bonds rather than electrostatic interactions (for example, with peptides [94]). However, non-covalent modification also has its advantages, in particular, when creating drug delivery systems [95]. The modification of the DND surface with proteins opens up the possibility of creating biochips based on nanodiamond, since the actual immobilization of proteins on a diamond substrate is one of the critical stages in the creation of biochips [96–98], while the most important is the chemical and physical stability of diamonds, which ensures high strength of the substrate. Diamond particles containing color centers - fluorescent crystallographic defects embedded in the diamond lattice – outperform other classes of fluorophores, providing a combination of photostability, internal biocompatibility and significant mechanical and chemical resistance, emitting in the UV, visible and IR spectral regions with exceptional photostability even at high temperature. This exceptional combination of properties positions fluorescent diamond particles as unique fluorophores with new potential applications in a variety of fields, including bioimaging, supersensitive metrology at the nanoscale, fluorescent labels in industrial applications, and even potentially as contrast agents for magnetic resonance imaging.

One of the main areas of application of fluorescent nanodiamonds is focused on bioimaging and biosensors. In the field of bioimaging, there is still an unmet need for extremely bright, photostable, non-toxic particles of a few nanometers in size with radiation in the red (near infrared) range. DNDs containing nitrogen vacant centers exhibit strong fluorescence sufficient to observe a single particle in

a cell, and the fluorescence does not disappear within 300 s, for ordinary chemical dyes this time is 10 s [7]. The advantage of such DNDs is that they emit light in the red region of the spectrum (575–750 nm), which makes it possible to work outside the region where intrinsic cell fluorescence is observed (300–500 nm) [99]. Moreover, these emitters are photostable [100–102]. DND fluorescence can also be caused by the presence of vacant silicon complexes (SiV) [103, 104]. A convenient method for observing the behavior of DND is the method of radioactive labels. In [105], the preparation of tritium-labeled DNDs and their application in tissues and organisms are described.

The relative ease of DND penetration into cells has made it possible to successfully deliver various drugs immobilized on the surface into the cell, while the substances retain their natural activity [89, 92]. For example, due to ionic bonds, DNDs form adducts with the anticancer drug doxorubicin [106]. It was shown in [107] that neural stem cells can be successfully grown on the hydrophilic surface of DND.

Thus, the possible use of DNDs as fluorescent objects in cells is an alternative to toxic quantum dots. In addition, DNDs can be used in *in vitro* systems, for example, for the delivery of drugs into cells, with the creation of various diagnostic systems based on DNDs. The adsorption capacity of nanodiamonds opens up prospects for the creation of enterosorbents. The ability to deliver genes using DND allows them to be used for genetic engineering. Given the non-toxicity and biocompatibility of nanodiamonds, they are already used in compositions for external use, for example, in cosmetics.

Modern methods of cancer treatment have a number of limitations associated with the presence of serious toxic and side effects of chemotherapy, radiation therapy, and targeted therapy with antibodies at terminal stages of cancer development [1,7]. The use of DND opens up new possibilities for the simultaneous detection and treatment of cancer. The size of DND is comparable to biological macromolecules such as proteins, enzymes, and DND plasmids [4]. Consequently, DNDs can penetrate cell membranes, presumably during endocytosis [7], which allows them to act as drug carriers. The nanosized DNDs also allow them to penetrate and selectively accumulate in tumors at much higher concentrations than in surrounding healthy tissue.

The study [108] was devoted to the sorption / desorption of nuclear medical isotopes technetium, bismuth, yttrium, and radium on DND for potential use as carriers for their targeted delivery. For this purpose, the adsorption properties of Tc (VII, IV),

Bi (III), Y (III), and Ra (II) were studied using industrial DND samples. The choice of isotopes was determined not only by their wide range of applications, but also by the difference in their chemical properties. It was found that DND adsorb up to 90 % of Tc (VII), but its quantitative desorption occurs in physiological solution. Tc (IV) is efficiently sorbed by the oxidized DND surface by more than 90%, and its desorption in a solution of bovine serum albumin dissolved in phosphate-buffered saline (BSA in PBS) does not exceed 5 %. This allows the studied DNDs with oxygen-containing groups on their surface to be used for targeted delivery of Tc (IV). The adsorption of Bi (III) on the studied DNDs varied from 80 to 100 %, while its desorption in BSA in PBS for DND, DND-COOH did not exceed 10 %, and for DND without oxygen-containing groups - up to 30%. It was shown that the kinetics of sorption of Y (III) proceeds more slowly than for Bi (III). Desorption of Bi (III) in a BSA solution in PBS for 1 h rose to 35 % from the DND surface.

Within 48 h, the biodistribution of DND with a particle size of 2–8 nm and a purity of more than 95 % was investigated using the radioactive isotope ¹⁸⁸Re during intracheal explosive feeding of mice [109]. It was found that DNDs are distributed in the spleen, liver, bones and heart with maximum accumulation in the lungs.

For 28 days, the toxicity, accumulation and excretion from the lungs of DND (particle size 5 nm) and fragmented synthetic nanodiamond (particle size 50 nm) were studied during their intracheal explosive treatment [110]. Based on histopathological and ultrastructural studies, it was concluded that nanodiamonds did not have obvious negative effects on lung tissue during the entire study period. Their excretion from the lungs is associated with their absorption by alveolar macrophages and their subsequent clearance into the trachea and then into the pharynx.

DND is removed from all organs within almost 1 month. This opens up additional possibilities for the use of DND in pharmaceutical practice for the development of prolonged dosage forms. It is fundamentally important that DND particles penetrate the brain, overcoming the blood-brain barrier. Thus, there is a fundamental possibility of developing promising drugs based on DND for the treatment of diseases of the central nervous system.

The first researcher to suggest the use of DND in medicine was V.Yu. Dolmatov [111]. He found that DNDs are highly active against pathogenic viruses, microbes and bacteria and can be used as an

enterosorbent (adsorbent in vivo) [111]. The cytotoxicity of DND was also studied, which showed its good biocompatibility in such different cell cultures as human lung adenocarcinoma cells [112]; HeLa cells (human cervical carcinoma) [113]; neuroblastoma cells [114]; macrophages [114]; neutrophils [115].

Investigated [116] the effect of DND on 6 types of human cells (cells of the lungs, kidneys, colon, liver). It has been shown that DNDs with particle sizes of 20 and 100 nm enter cells efficiently and do not cause any cytotoxic or genotoxic effects up to a concentration of $500 \mu\text{g}\cdot\text{m}^{-1}$. By itself, nanodiamonds (oxidized form) are able to suppress the development of Alzheimer's disease (experiments on rats) [117].

In the only work [118], the acute toxicity of DND was studied and the LD50 value (mice, peros) was determined to be more than $7.5 \text{ g}\cdot\text{kg}^{-1}$.

The creation of anticancer dosage forms based on nanodiamond was studied in [119]. Two anticancer drugs have been investigated – paclitaxel (a mitosis blocker) and cetuximab, which enhances mitotic catastrophe and slows tumor growth in human colorectal cancer. Pure nanodiamond had no effect on the growth of cancer cells. The DND sample – paclitaxel - cetuximab was also effective in inhibiting the growth of tumor cells. Thus, it has been shown that nanodiamonds are a promising carrier for the development of new dosage forms in cancer therapy.

It was found that the system nanodiamond – cetuximab - cisplatin can significantly inhibit the growth of hepatocellular liver carcinoma cells, and the therapeutic activity of this system turned out to be better than that of the nonspecific nanodiamond – cisplatin conjugate.

The amount of adsorption of amikacin on DND depends on the nature of the surface functional groups. Thus, for oxidized and hydrogenated DND, the value of the maximum equilibrium adsorption of amikacin was 130 and $50 \text{ mg}\cdot\text{g}^{-1}$, respectively. In this case, the amount of irreversibly sorbed antibiotic was 48 and $22 \text{ mg}\cdot\text{g}^{-1}$, respectively.

DND-surface-bound paclitaxel, as well as unbound paclitaxel, is an effective inducer of lung carcinoma cell death, which confirms the preservation of drug efficiency after its immobilization on DND.

The covalent attachment to the surface of nanodiamond-anticancer drug amonafid was studied [120]. The resulting conjugates have been shown to be effective in the treatment of breast cancer.

It was noted [121, 122] that the use of DND suspension facilitates the condition of cancer patients, apparently due to a decrease in the level of intoxication of the body. In addition, DND has been

used as a means of correcting the processes of protein and lipid peroxidation during the growth of malignant neoplasms.

Currently, DNDs are the subject of intensive research aimed at improving the delivery of low molecular weight substances and biotechnological products, and especially chemotherapeutic agents.

6. Conclusion

In this review, the authors analyzed information on the synthesis and application of detonation nanodiamonds, namely:

- an assumption was made about the fractal principle of the formation of DND infrastructure in the zone of chemical reactions during the EM explosion;

- the distance of formation of DND particles from the beginning of the detonation wave front in EM is determined – $1/3$ – $3/4$ of the charge diameter;

- it was found that at the output of DND 6 wt.% and more for the formation of nanodiamonds is $(20 \pm 2) \%$ of carbon EM;

- an insignificant probability of the formation of nitrogen-free DNDs is shown, the optimal range of nitrogen concentration in EM molecules (23–28 wt.%) has been determined to obtain DND yield from 6 wt.% and more;

- the possibility of predicting the range of the DND output depending on the detonation velocity, specific power EM and pressure in the Chapman-Jouguet plane is shown;

- found that the most preferred individual EM for obtaining DND with a yield of 6–7 wt.% is tetryl, binary mixtures based on tetryl give a nanodiamond yield up to 7.3 wt.%, and ternary – up to 8.2 wt.%;

- the range of HNO_3 concentration and temperature for selective oxidation of the diamond charge to a given ratio of diamond and graphite phases at a temperature of 120–230 °C has been established;

- DND was characterized by IR-spectroscopy data;

- according to EPR and NMR data, it was shown that the size and structure of DND from tetryl is similar to nanodiamonds from an alloy of TNT with RDX or a ternary mixture of tetryl, RDX and TNT, which indicates a single mechanism for the formation of DND nanocrystallites;

- the features of EPR spectroscopy on non-oriented samples, which include diamond polycrystals, including DND samples, are described. The main parameters characterizing the lines in the EPR spectra are described. The sources of magnetism

in diamond samples are considered in detail. All known types of magnetic defects in DNDs are considered, including their origin and localization. Particular attention is paid to triplet centers in the DND, which include N-V centers and multivacancies detected at half magnetic field values (region $g = 4$). It was shown that EPR reliably indicates an increase in the content of triplet centers of the N-V-type in DND samples irradiated with electron beams.

– electrochemical gilding with DND leads to a practical absence of wear when using boron-doped DND, an increase in microhardness by 20–60 % (up to $220 \text{ kg}\cdot\text{mm}^{-2}$), it is recommended to reduce the thickness of the gold coating by 2–3 times;

– during joint electrochemical chromium plating in the presence of DND-TAN doped with phosphorus and boron DND, shiny, smooth uniform coatings are deposited, the microhardness increases from 855 to $1300 \text{ kg}\cdot\text{mm}^{-2}$;

– it is shown that the addition of DND from 0.1 to 5.0 wt.% in thermal paste can raise their thermal conductivity by 7–14 times (up to $4.72 \text{ W}\cdot\text{m}^{-1}\cdot\text{K}^{-1}$).

The possibility of using DND for polymer filaments of 3D-printers even in an amount of 0.05 wt.%, which leads to an increase in tensile strength by 38 % (polylactic acid), a friction decrease during extrusion (the productivity of filament deposition increased up to 10 times), raised rigidity and elastic modulus of the product. The explosive content of nanodiamonds in fuel compositions increases the amount of gaseous combustion products, there is no flare up of the engine nozzle, every 0.5 wt.% DNDs increase the temperature in the combustion chamber by 80K, and the mass specific impulse increases by $2 \text{ kg}\cdot\text{s}\cdot\text{kg}^{-1}$.

It has been shown that DNDs are an alternative to toxic quantum dots. Nanodiamonds can be used to deliver drugs to the cells of the body; they selectively accumulate in cancerous tumors in high concentrations. DNDs are also promising enterosorbents. When explosively ingested into the body, nanodiamonds are distributed in the spleen, liver, bones, heart, with the maximum amount in the lungs. DND particles penetrate into the brain, overcoming the blood-brain barrier. DNDs effectively enter human cells without causing any cytotoxic or genotoxic effects up to a concentration of $500 \text{ mg}\cdot\text{mL}^{-1}$.

7. Funding

This study was partially funded by the Russian Foundation for Basic Research within the framework of research project No. 18-29-19112.

8. Conflict of interests

The authors declare no conflict of interest.

References

1. Dolmatov VYu. *Detonation synthesis nanodiamonds: synthesis, structure, properties and applications*. St. Petersburg: NPO Professional; 2011. 536 p. DOI:10.1070/RC2007v076n04ABEH003643 (In Russ.)
2. Dolmatov VYu, Malygin AA, Dorokhov AO, Kozlov AS, Marchukov VA, Sushev VG, Myllymäki V, Vehanen A. Development of a process for producing detonation nanodiamonds from tetryl and binary compositions based on it. *Journal of Superhard Materials*. 2020;42(3):145–156. DOI:10.3103/S1063457620030053
3. Vul AYa, Shenderova O. (eds.) *Detonation nanodiamonds – science and applications*. New York: Jenny Stanford Publ.; 2014, 346 p. DOI:10.1201/b15541
4. Shenderova O, Gruen D. (eds.) *Ultranano-crystalline diamond, synthesis, properties, and application*. Kidlington-Norwich: William Andrew Publ.; 2006, 611 p.
5. Lisichkin GV, Olenin AYu, Kulakova II. *Modification of the surface of inorganic nanoparticles*. Moscow: Technosphere; 2020, 394 p. (In Russ.)
6. Khrapkovsky GM, Chachkov DV, Nikolaeva EV, Gaisin IS, Shamov AG. *Internet conference “Butlerov Readings”*. Available from: <http://butlerov.com/readings/> [Accessed 11 March 2019] (In Russ.)
7. Vul AYa, Shenderova OA (ed.) *Detonation nanodiamonds. Technology, structure, properties and applications: Collection of articles*. St. Petersburg: Ioffe Institute Publ.; 2016, 381 p. (In Russ.)
8. Kulakova II. Surface chemistry of nanodiamonds. *Physics of the Solid State*. 2004;46(4):636-643. DOI:10.1134/1.1711440
9. Danilenko VV. *Explosion: physics, engineering, technology*. Moscow: Energoatomizdat; 2010, 784 p. (In Russ.)
10. VanThiel M, Ree FH. Properties of carbon clusters in TNT detonation products: Graphite-diamond transition. *Journal of Applied Physics*. 1987;62(5):1761. DOI:10.1063/1.339575
11. Dremin AN, Pershin SV, Pyaternev SV, Tsaplin DN. Kink in the dependence of the detonation velocity on the initial TNT density. *Fizika goreniya i vzryva = Combustion, Explosion, and Shock Waves*. 1989;25(5):141-144. (In Russ.)
12. Antipenko AG, Pershin SV, Tsaplin DN. *In the book. IX All-union symposium on combustion and explosion*. Chernogolovka: FRCCP RAS Publ.; 1989. 104 p. (In Russ.)
13. Pershin SV, Tsaplin DN, Antipenko AG. On the possibility of diamond formation during tetryl

detonation. *In coll. of reports of V All-union detonation meetings*. Chernogolovka: IMTECH Publishing House; 1991. p. 233-236. (In Russ.)

14. Pershin SV, Tsaplin DN. Dynamic research of detonation synthesis of dense phases of matter. *In coll. of reports of V All-union detonation meetings*. Chernogolovka: IMTECH Publishing House; 1991. p. 237-244 (In Russ.)

15. Loboiko BG, Lyubyatinsky NS. Reaction zones of detonating solid explosives, *Combustion, explosion, and shock waves*. 2000;36(6):716-733. DOI:10.1134/S0010508214020166

16. Dremin AN, Shvedov KK. Determination of Chapman-Jouguet pressure and reaction time in a powerful explosive detonation wave. *Zhurnal prikladnoy mekhaniki i tekhnicheskoy fiziki = Journal of Applied Mechanics and Technical Physics*. 1964;2:154-159. (In Russ.)

17. Dolmatov VYu, Myllymaki V, Vehanen A. A possible mechanism of nanodiamond formation during detonation synthesis. *Journal of Superhard Materials*. 2013;35(3):143-150. DOI:10.3103/S1063457613030039

18. Aleshaev AN, Zubkov PI, Kulipanov GN, Luk'yanchikov LA, Lyakhov NZ, Mishnev SI, Ten KA, Titov VM, Tolochko BP, Fedotov MG, Sheromov MA. Application of synchrotron radiation for studying detonation and shock-wave processes. *Combustion Explosion and Shock Waves*. 2001;37(5):585-593. DOI:10.1023/A:1012353406187

19. Titov VM, Tolochko BP, Ten KA, Lukyan-chikov LA, Prueel ER. Where and when are nanodiamonds formed under explosion. *Diamond and Related Materials*. 2007;16(12):2009-2013. DOI:10.1016/j.diamond.2007.09.001

20. Dolmatov VYu, Dorokhov AO, Mullyumaki V, Vekhanen A, Marchukov VA. The zone of chemical reactions in the detonation synthesis of nanodiamonds in the phase diagram of carbon. *XXII Int. conference "Rock-cutting and metal-working tools – equipment and technology for its manufacture and application"*: Coll. of scientific papers. Kiev: V. Bakul Institute for Superhard Materials; 2019;22:199-204. (In Russ.)

21. Dolmatov VYu, Dorokhov AO, Kozlov AS, Marchukov VA, Myllymäki V, Vehanen A. Possibility of predictive estimation of DND yield from individual explosives. *Journal of Superhard Materials*. 2021;2:1-8.

22. Dolmatov VYu. On the possibility of obtaining nitrogen-free detonation nanodiamonds: effect of covalently bound nitrogen in explosive molecules on the yield of nanodiamonds. *Journal of Superhard Materials*. 2020;42(4):223-228. DOI:10.3103/S1063457620040036

23. Sattler KD. *Carbon nanomaterials sourcebook: graphene, fullerenes, nanotubes and nanodiamonds*. Vol. I. USA: CRC Press Taylor & Francis Group; 2016. 614 p.

24. Dolmatov VYu. The influence of detonation synthesis conditions on the yield of condensed carbon

and detonation nanodiamond through the example of using TNT-RDX explosive mixture. *Journal of Superhard Materials*. 2018;40(4):290-294. DOI:10.3103/S1063457618040093

25. Dolmatov VYu. *Diamond-carbon material and a method for the production thereof*. United States patent 7,862,792. 4 January 2011.

26. Nesvizhevsky V, Koster U, Dubois M, Batisse N, Frezet L, Bosak A, Gines L, Williams O. Fluorinated nanodiamonds as unique neutron reflector. *Carbon*. 2018;130:799-805. DOI:10.1016/j.carbon.2018.01.086

27. Kulakova II, Korol'kov VV, Yakovlev RYu, Lisichkin GV. The structure of chemically modified detonation-synthesized nanodiamond particles. *Nanotechnologies in Russia*. 2010;5:474-485. DOI:10.1134/S1995078010070074

28. Petrov EA, Baraboshkin KS, Bychin NV, Larionov BV., Bayramyan IV. Study of TNAB for the detonation synthesis of nanodiamonds. *VI Staverovsky readings: ultradispersed powders, nanostructures, materials: Proceedings of the All-Russian scientific and technical conference with international participation, dedicated to the 30th anniversary of the discovery of nanodiamonds*, 9-12 September 2012. Biysk, Gornyy Altay: Naukograd; 2012. p.14-15. (In Russ.)

29. Dolmatov VYu, Myllymäki V, Vehanen A, Dorokhov AO, Kiselev MN. Dependence of the detonation nanodiamond yield on the detonation process parameters. *Journal of Superhard Materials*. 2019;41(5):1-5. DOI:10.3103/S1063457619050071

30. Petrov EA. Investigation of physicochemical processes of detonation synthesis of nanodiamonds. *In Col. of report International scientific, technical and methodological conference*. Kazan: KNRTU Publ.; 2004. p. 881-888. (In Russ.)

31. Dorokhov AO, Dolmatov VYu, Malygin AA, Kozlov AS, Marchukov VA. Development of the detonation nanodiamond synthesis from tetryl based ternary mixtures. *Russian Journal of Applied Chemistry*. 2020;93(7):1083-1089. DOI:10.1134/S1070427220070204

32. Panich AM, Shames AI, Mogilyansky D, Goren SD, Dolmatov VYu. Detonation nanodiamonds fabricated from tetryl: Synthesis, NMR, EPR and XRD study. *Diamond and Related Materials*. 2020;108:107918. DOI:10.1016/j.diamond.2020.107918

33. Marchukov VA, Kolodyazhny AL, Makarov IA, Korolev KM, Suschev VG. *Method for cleaning detonation nanodispersed diamonds*. Russian Federation Patent 2,599,665. 10 October 2016. (In Russ.)

34. Sushchev VG, Dolmatov VYu, Malygin AA, Marchukov VA, Korolev KM, Dorokhov AO. Core-Shell composites based on partially oxidized blend of detonation synthesis nanodiamonds. *Russian Journal of Applied Chemistry*. 2020;93(5):660-670. DOI:10.1134/S1070427220050067

35. Yakovlev RY, Dogadkin NN, Kulakova II, Lisichkin GV, Leonidov NB, Kolotov VP. Determination of impurities in detonation

- nanodiamonds by gamma activation analysis method. *Diamond and Related Materials*. 2015;55:77-86. DOI:10.1016/j.diamond.2015.03.010
36. Volkov DS, Proskurnin MA, Korobov MV. Elemental analysis of nanodiamonds by inductively-coupled plasma atomic emission spectroscopy. *Carbon*. 2014;74:1-13. DOI:10.1016/j.carbon.2014.02.072
37. Korobov MV, Volkov DS, Avramenko NV, Belyaeva LA, Semenyuk PI, Proskurnin MA. Improving the dispersity of detonation nanodiamond: differential scanning calorimetry as a new method of controlling the aggregation state of nanodiamond powders. *Nanoscale*. 2013;5(4):1529-1536. DOI:10.1039/c2nr33512c
38. Volkov DS, Proskurnin MA, Korobov MV. Survey study of mercury determination in detonation nanodiamonds by pyrolysis flameless atomic absorption spectroscopy. *Diamond and Related Materials*. 2014;50:60-65. DOI:10.1016/j.diamond.2014.08.013
39. Dolmatov VYu, Ozerin AN, Kulakova II, Bochechka OO, Lapchuk NM, Myllymäki V, Vehanen A. Detonation nanodiamonds: new aspects in the theory and practice of synthesis, properties and applications. *Russian Chemical Reviews*. 2020;89(12):1428-1462, DOI:10.1070/RCR4924
40. Kulakova II, Korol'kov VV, Yakovlev RYu, Lisichkin GV. The structure of chemically modified detonation synthesized nanodiamond particles. *Nanotechnologies in Russia*. 2010;5(7-8):474-485. DOI:10.1134/S1995078010070074
41. Vereshcagin AL, Yur'ev GS. Structure of detonation diamond nanoparticles. *Inorganic Materials*. 2003;3(3):247-253. DOI:10.1023/A:1022621407325
42. Dolmatov VY. On the structure of detonation nanodiamond cluster. *Journal of Superhard Materials*. 2005;28.
43. Yur'ev GS, Dolmatov VYu. X-Ray diffraction study of detonation nanodiamonds. *Journal of Superhard Materials*. 2010;32(5):311-328. DOI:10.3103/S1063457610050035
44. Țucureanu V, Matei A, Avram AM. FTIR spectroscopy for carbon family study. *Critical Reviews in Analytical Chemistry*. 2016;46:502-520. DOI:10.1080/10408347.2016.1157013
45. Petit T, Puskar L. FTIR spectroscopy of nanodiamonds: Methods and interpretation. *Diamond and Related Materials*. 2018;89:52-66. DOI:10.1016/j.diamond.2018.08.005
46. Tsubota T, Urabe K, Egawa S, Hirabayashi O, Takagi H, Kusakabe K, Morooka H, Maeda H. Surface modification of hydrogenated diamond powder by radical reactions in chloroform solutions. *Diamond and Related Materials*. 2000;9:219-223. DOI:10.1016/S0925-9635(00)00234-X
47. Ando T, Rawles RE, Yamamoto K, Kamo M, Sato Y, Nishitani-Gamo M. Chemical modification of diamond surfaces using a chlorinated surface as an intermediate state. *Diamond and Related Materials*. 1996;5:1136.
48. Liang YJ, Ozawa M, Krueger A. A general procedure to functionalize agglomerating nanoparticles demonstrated on nanodiamond. *ACS Nano*. 2009;3:2288-2296. DOI:10.1021/nn900339s
49. Zheng WW, Hsieh Y-H, Chiu Y-C, Cai S-J, Cheng CL, Chen C. Organic functionalization of ultradispersed nanodiamond: synthesis and applications. *Journal of Materials Chemistry*. 2009;19(44):8432. DOI:10.1039/B904302K
50. Christiaens P, Vermeeren V, Wenmackers S. EDC-mediated DND attachment to nanocrystalline CVD diamond films. *Biosensors & Bioelectronics*. 2006;22(2):170-177. DOI:10.1016/j.bios.2005.12.013
51. Koscheev AP. Thermal desorption mass spectrometry in the light of solving the certification and unification problem of the surface properties of detonation nanodiamonds. *Rossiyskiy Khimicheskiy Zhurnal = Russian Journal of General Chemistry*. 2008;52(5):88-96. (In Russ.)
52. Weil JA, Bolton JR. *Electron paramagnetic resonance: elementary theory and practical applications*. New York: Wiley; 2007. 688 p.
53. Baranov PG, von Bardeleben H-J, Jelezko F, Wrachtrup J. *Magnetic resonance of semiconductors and their nanostructures: basic and advanced applications*. Austria: Springer-Verlag GmbH; 2019. 539 p.
54. Duer MJ. *Solid state NMR spectroscopy: principles and applications*. Oxford: Wiley; 2008. 592 p.
55. Shames AI, Osipov VYu, Boudou JP, Panich AM, von Bardeleben H-J, Treussart F, Vul' AYa. Magnetic resonance tracking of fluorescent nanodiamond fabrication. *Journal of Physics D: Applied Physics*. 2015;48(15):1-13. DOI:10.1088/0022-3727/48/15/155302
56. Casabianca LB, Shames AI, Panich AM, Shenderova O, Frydman L. Factors affecting DNP NMR in polycrystalline diamond samples. Magnetic resonance tracking of fluorescent nanodiamond fabrication. *Journal of Physical Chemistry C*. 2011;115(39):19041-19048. DOI:10.1021/jp206167j
57. Shames AI, Mogilyansky D, Panich AM, Sergeev NA, Olszewski M, Boudou J-P, Osipov VYu. XRD, NMR, and EPR study of polycrystalline micro- and nano-diamonds prepared by a shock wave compression method. *Physica Status Solidi A*. 2015;212(11):2400-2409. DOI:10.1002/pssa.201532154
58. Shames AI, Panich AM, Kempinski W, Alexenskii AE, Baidakova MV, Dideikin AT, Osipov VYu, Siklitski VI, Osawa E, Ozawa M, Vul' AYa. Defects and impurities in nanodiamonds: EPR, NMR and TEM Study. *Journal of Physics and Chemistry of Solids*. 2002;63(11):1993-2001. DOI:10.1016/S0022-3697(02)00185-3
59. Osipov VYu, Shames AI, Enoki T, Takai K, Baidakova MV, Vul' AYa. Paramagnetic defects and exchange coupled spins in pristine ultrananocrystalline diamonds. *Diamond and Related Materials*. 2007;16(12):2035-2038. DOI:10.1016/j.diamond.2007.06.003

60. Shames AI, Panich AM, Osipov VYu, Aleksenskiy AE, Vul' AYa, Enoki T, Takai K. Structure and magnetic properties of detonation nanodiamond chemically modified by copper. *Journal of Applied Physics*. 2010; 107(1):0143181,1-10. DOI:10.1063/1.3273486
61. Terada D, Segawa TF, Shames AI, Onoda S, Ohshima T, Ōsawa E, Igarashi R, Shirakawa M. Mono-disperse five-nanometer-sized detonation nanodiamonds enriched in nitrogen-vacancy centers. *ACS Nano*. 2019;13(6):6461-6468. DOI:10.1021/acsnano.8b09383
62. Shames AI, Osipov VYu, Aleksenskiy AE, Ōsawa E, Vul' AYa. Locating inherent unpaired orbital spins in detonation nanodiamonds through the targeted surface decoration by paramagnetic probes. *Diamond and Related Materials*. 2011;20(3):318-321. DOI:10.1016/j.diamond.2011.01.007
63. Panich AM, Shames AI, Sergeev NA, Osipov VYu, Alexenskiy AE, Vul' AYa. Magnetic resonance study of gadolinium-grafted nanodiamonds. *Journal of Physical Chemistry C*. 2016;120(35):19804-19811. DOI:10.1021/acs.jpcc.6b05403
64. Panich AM, Salti M, Goren SD, Yudina EB, Aleksenskii AE, Vul' AYa, Shames AI. Gd(III)-grafted detonation nanodiamonds for MRI contrast enhancement. *Journal of Physical Chemistry C*. 2019;123(4):2627-2631. DOI:10.1021/acs.jpcc.8b11655
65. Panich AM, Sergeev NA, Shames AI, Osipov VYu, Boudou J-P, Goren SD. Size dependence of ¹³C nuclear spin-lattice relaxation in micro- and nanodiamonds. *Journal of Physics: Condensed Matter*. 2015;27(7):072203,1-7. DOI:10.1088/0953-8984/27/7/072203
66. Zegrya GG, Samosvat DM, Osipov VYu, Vul' AYa, Shames AI. Size effect in electron paramagnetic resonance spectra of impurity centers in diamond nanoparticles. *arXiv*:1912.06330. 2019; Available from: <https://arxiv.org/abs/1912.06330>
67. Shames AI, Osipov VYu, von Bardeleben H-J, Vul' AYa. Spin $S=1$ centers: a universal type of paramagnetic defects in nanodiamonds of dynamic synthesis. *Journal of Physics: Condensed Matter*. 2012;24(22):225302,1-8. DOI:10.1088/0953-8984/24/22/225302
68. Shames AI, Osipov VYu, von Bardeleben H-J, Boudou J-P, Treussart F, Vul' AYa. Native and induced triplet nitrogen-vacancy centers in nano- and micro- diamonds: Half-field electron paramagnetic resonance fingerprint. *Applied Physics Letters*. 2014;104(10):063107,1-5. DOI:10.1063/1.4865205
69. Shames AI, Smirnov AI, Milikisiyants S, Danilov EO, Nunn N, McGuire G, Torelli MD, Shenderova O. Fluence-dependent evolution of paramagnetic triplet centers in e-beam irradiated microcrystalline Ib type HPHT diamond. *Journal of Physical Chemistry C*. 2017;121(40):22335-22346. DOI:10.1021/acs.jpcc.7b06514
70. Dolmatov VYu, Rudenko DV, Burkat GK, Aleksandrova AS, Vul' AYu, Aleksenskii AE, Kozlov AS, Myllymäki V, Vehanen A, D'yakov IA, Dorokhov AO, Kiselev MN. A study of the process of gold plating from citrate and phosphate electrolytes in the presence of modified detonation nanodiamonds. *Journal of Superhard Materials*. 2019;41(3):169-177. DOI:10.3103/S1063457619030043
71. Ōsawa E. Recent progress and perspectives in single-digit nanodiamond. *Related Materials*. 2007;16:2018-2022. DOI:10.1016/j.diamond.2007.08.008
72. Aleksenskiy AE, Vul' AYa, Didykin AT. *A method for producing an aqueous suspension of detonation nanodiamonds*. Russian Federation patent 2,446,097. 14 September 2010. (In Russ.)
73. Dolmatov VYu, Burkat GK, Svir KA, Marchukov VA, Dorokhov AO, Vehanen A, Myllymäki V, Kozlov AS, Almazova NS. Study of electrochemical deposition process of chromium in the presence of composite diamond-containing compound. *Tooling materials science, Collection of Scientific Papers*. 2020;23:187-194.
74. Lu H-T, Uvarov S. *Nanodiamond thermal grease*. United States patent 2010/0022423 A1. 28 January 2010.
75. Myllymäki V, Syren J. *Nanodiamonds containing thermoplastic thermal composites*. United States patent 20150259591. 17 September 2015.
76. Myllymäki V, Larson Sch. *A filament and 3D printed item*. Patent EP 3,502,324. 26 July 2019.
77. Kutsenko GV, Okhrimenko EF, Khimenko LL, Fedotov IA, Kozintseva LG, Pyankova EE. *Mixed solid propellant*. Russian Federation patent 2,430,902. 10 October 2011. (In Russ.)
78. Egorychev VS, Kondrusev VS. *Chemical rocket engine fuels*. Samara: Samara University Publ.; 2007. 72 p. (In Russ.)
79. Golubev AA, Gorbachev VA, Shevchenko NV, Ubeiy-Volk EYu. Detonation nanodiamond as prospective component of composite solid propellants. *Izvestiya Vysshikh Uchebnykh Zavedenii, Seriya Khimiya i Khimicheskaya Tekhnologiya = ChemChemTech*. 2016;59(8):96-100. DOI:10.6060/tcct.20165908.37y (In Russ.)
80. Shevchenko NV, Gorbachev VA, Ubej-Volk EYu, Danilenko VV, Blank VD, Golubev AA, Deribas AA. Influence of detonation nanodiamonds on the combustion of energy-intensive rocket fuel compositions. *Konstruktsii iz kompozitsionnykh materialov = Composite structures*. 2014;3(135):33-39. (In Russ.)
81. Gorbachev VA, Ubej-Volk EYu, Shevchenko NV. *Fuel composition*. Russian Federation patent 2,649,573. 04 April 2018. (In Russ.)
82. Jee A-Y, Lee V. Surface functionalization and physicochemical characterization of diamond nanoparticles. *Current Applied Physics*. 2009;9:144-147. DOI:10.1134/S1070363212130117

83. Krueger A. Diamond nanoparticles: jewels for chemistry and physics. *Advanced Materials*. 2008;20:2445-2449. DOI:10.1002/adma.200701856
84. Mochalin V, Osswald S, Gogotsi Y. Contribution of functional groups to the Raman spectrum of nanodiamond powders. *Chemistry of Materials*. 2009;21:3728-3735. DOI:10.1021/cm802057q
85. Osswald S, Yushin G, Mochalin V, Kusheyev SO, Gogotsi Y. Control of sp²/sp³ carbon ratio and surface chemistry of nanodiamonds powders by selective oxidation in air. *Journal of the American Chemical Society*. 2006;128(35):11635-11642. DOI:10.1021/ja063303n
86. Fang XW, Mao JD, Levin EM, Schmidt-Rohr K. Nonaromatic core-shell structure of nanodiamond from solid-state NMR spectroscopy. *Journal of the American Chemical Society*. 2009;131(4):517-526. DOI:10.1021/ja8054063
87. Piotrovsky LB, Kiselev OI. *Fullerenes in biology*. St. Petersburg: Rostock; 2006. 335 p.
88. Keservani RK, Sharma AK. (eds.) *Nanoparticulate drug delivery systems*. Toronto: Apple Academic Press; 2019. p. 4-5.
89. Chao J-I, Perevedentseva E, Chung PH, Liu KK, Cheng CY, Chang CC, Cheng CL. Nanometer-sized diamond particle as a probe for biolabeling. *Biophysical Journal*. 2007;93:2199-2208. DOI:10.1529/biophysj.107.108134
90. Spitsyn BV, Davidson JL, Gradoboev MN, Galushko TB, Serebryakova NV, Karpukhina TA, Kulakova II, Melnik NN. Inroad to modification of detonation nanodiamond. *Diamond and Related Materials*. 2006;15:296-299. DOI:10.1016/j.diamond.2005.07.033
91. Tsubota T, Tanii S, Ida S, Nagata M, Matsumoto Y. Chemical modification of diamond surface with various carboxylic acids by radical reaction in liquid phase. *Diamond and Related Materials*. 2004;13:1093-1097. DOI:10.1016/j.diamond.2003.10.065
92. Cheng CY, Perevedentseva E, Tu JS, Chung PH, Cheng CL, Liu KK, Chao JI, Chen PH, Chang CC. Direct and in vitro observation of growth hormone receptor molecules in A549 human lung epithelial cells by nanodiamond labeling. *Applied Physics Letters*. 2007;90:163903. DOI:10.1063/1.2727557
93. Chung PH, Perevedentseva E, Tu JS, Chang CC, Cheng CL. Spectroscopic study of bio-functionalized nanodiamonds. *Diamond and Related Materials*. 2006;15:622-625. DOI:10.1016/j.diamond.2005.11.019
94. Krueger A, Liang YJ, Jarre G, Stegk J. Surface functionalization of detonation diamond suitable for biological applications. *Journal of Materials Chemistry*. 2006;16:2322-2328. DOI:10.1039/B601325B
95. Huang H, Pierstorff E, Osawa E, Ho D. Active nanodiamond hydrogels for chemotherapeutic delivery. *Nano Letters*. 2007;7(11):3305-3314. DOI:10.1021/nl071521o
96. Drummond TG, Hill MG, Barton JK. Electrochemical DND sensors. *Nature Biotechnology*. 2003;21:1192-1199. DOI:10.1038/nbt873
97. Lee Y-S, Mrksich M. Protein chips: from concept to practice. *Trends in Biotechnology*. 2002;20:s14-s18. DOI:10.1016/s1471-1931(02)00200-8
98. Zhu H, Snyder M. Protein chip technology. *Current Opinion in Chemical Biology*. 2003;7:55-63. DOI:10.1016/s1367-5931(02)00005-4
99. Fu C-C, Lee H-Y, Chen K, Lim T-S, Wu H-Y, Lin P-K, Tsao P-H, Chang H-C, Fann W. Characterization and application of single fluorescent nanodiamonds as cellular biomarkers. *Proceedings of the National Academy of Sciences*. 2007;104(3):727-732. DOI:10.1073/pnas.0605409104
100. Chang IP, Hwang KC, Chiang C-S. Preparation of fluorescent magnetic nanodiamonds and cellular imaging. *Journal of the American Chemical Society*. 2008;130(46):15476-15481. DOI:10.1021/ja804253y
101. Faklaris O, Garrot D, Joshi V, Boudou JP, Sauvage T, Curmi PA, Treussart F. Comparison of the photoluminescence properties of semiconductor quantum dots and non-blinking diamond nanoparticles and observation of the diffusion of diamond nanoparticles in living cells. *Journal of the European Optical Society-Rapid Publications. Rap.* 2009;4:09035. DOI:10.2971/jeos.2009.09035
102. Neu E, Agio M, Becher C. Photophysics of single silicon vacancy centers in diamond: implications for single photon emission. *Optics Express*. 2012;20:19956-19971. DOI:10.1364/OE.20.019956
103. Neugart F, Zappe A, Jelezko F, Tietz C, Boudou JP, Krueger A, Wrachtrup J. Dynamics of diamond nanoparticles in solution and cells. *Nano Letters*. 2007;7(12):3588-3591. DOI:10.1021/nl0716303
104. Wang C, Kurtsiefer C, Weinfurter H, Burchard B. Single photon emission from SiV centres in diamond produced by ion implantation. *Journal of Physics B: Atomic, Molecular and Optical*. 2006;39:37-41. DOI:10.1088/0953-4075/39/1/005
105. Girard HA, El-Kharbachi A, Garcia-Argote S, Petit T, Bergonzo P, Rousseau B, Arnault J-C. Tritium labeling of detonation nanodiamonds. *Chemical Communications*. 2014;50:2916-2918. DOI:10.1039/C3CC49653H
106. Huang H, Pierstorff E, Liu K, Osawa E, Ho D (ed.). *Nanodiamond-mediated delivery of therapeutics via particle and thin film architectures. Nanodiamonds: applications in biology and nanoscale medicine*. USA: Springer; 2010;7:151-174. DOI:10.1007/978-1-4419-0531-4
107. Chen Y-C, Lee D-C, Hsiao C-Y, Chung Y-F, Chen H-C, Thomas JP, Pong W-F, Tai N-H, Lin I-N, Chiu I-M. The effect of ultrananocrystalline diamond films on the proliferation and differentiation of neural stem cells. *Biomaterials*. 2009;30(20):3428-3435. DOI:10.1016/j.biomaterials.2009.03.058
108. Kazakov AG, Garashchenko BL, Yakovlev RYU, Vinokurov SE, Kalmykov SN, Myasoedov BF. An experimental study of sorption / desorption of

selected radionuclides on carbon nanomaterials: a quest for possible applications in future nuclear medicine. *Diamond and Related Materials*. 2020;104:107752. DOI:10.1016/j.diamond.2020.107752

109. Zhang X, Yin J, Kang C, Li J, Zhu Y, Li W, Huang Q, Zhu Z. Biodistribution and toxicity of nanodiamonds in mice after intratracheal instillation. *Toxicology Letters*. 2010;198(2):237–243. DOI:10.1016/j.toxlet.2010.07.001

110. Yuan Y, Wang X, Jia G, Liu J-H, Wang T, Gu Y, Yang S-T, Zhen S, Wang H, Liu Y. Pulmonary toxicity and translocation of nanodiamond in mice. *Diamond and Related Materials*. 2010;19(4):291-299. DOI:10.1016/j.diamond.2009.11.022

111. Dolmatov VYu, Kostrova LN. Detonation-synthesized nanodiamonds and the feasibility to develop a new generation of medicines. *Journal of Superhard Materials*. 2000;3:79-82.

112. Liu K-K, Wang C-C, Cheng C-L, Chao J-I. Endocytic carboxylated nanodiamond for the labeling and tracking of cell division and differentiation in cancer and stem cells. *Biomaterials*. 2009;30(26):4249-4259. DOI:10.1016/j.biomaterials.2009.04.056

113. Vaijayanthimala V, Tzeng Y-K, Chang H-C, Li C-L. The biocompatibility of fluorescent nanodiamonds and their mechanism of cellular uptake. *Nanotechnology*. 2009;20(42):425103. DOI:10.1088/0957-4484/20/42/425103

114. Schrand AM, Huang H, Carlson C, Schlager JJ, Sawa EO, Hussain SM, Dai L. Are diamond nanoparticles cytotoxic? *Journal of Chemical Physics B*. 2007;111(1):2-7. DOI:10.1021/jp066387v

115. Karpukhin AV, Avkhacheva NV, Yakovlev RY, Kulakova II, Yashin VA, Lisichkin GV, Safronova VG. Effect of detonation nanodiamonds on phagocyte activity. *Cell Biology International*. 2011;35(7):727-733. DOI:10.1042/CBI20100548

116. Paget V, Sergent JA, Grall R, Altmeyer-Morel S, Girard HA, Petit T, Gesset C, Mermoux M, Bergonzo P, Arnault JC, Chevillard S. Carboxylated nanodiamonds are neither cytotoxic nor genotoxic on liver, kidney, intestine and lung human cell lines. *Nanotoxicology*. 2014;8(1):46-56. DOI:10.3109/17435390.2013.855828

117. Alawdi SH, El-Denshary ES, Safar MM, Eidi H, David M-O, Abdel-Wahhab MA. Neuroprotective effect of nanodiamond in Alzheimer's disease rat model: a pivotal role for modulating NF- κ B and STAT3 signaling. *Molecular Neurobiology*. 2017;54(3):1906-1918. DOI:10.1007/s12035-016-9762-0

118. Dolmatov VYu. *Ultrafine detonation synthesis diamonds. Obtaining, properties, application*. St. Petersburg: Peter the Great St. Petersburg Polytechnic University Publ.; 2003. 343 p. (In Russ.)

119. Liao W-S, Ho Y, Lin Y-W, Raj EN, Liu K-K, Chen Ch, Zhou X-Z, Lu K-P, Chao J-I. Targeting EGFR of triple-negative breast cancer enhances the therapeutic efficacy of paclitaxel- and cetuximab-conjugated nanodiamond nanocomposite. *Acta Biomaterialia*. 2016;86(1):395-405. DOI:10.1016/j.actbio.2019.01.025

120. Zhao J, Lu M, Lai H, Lu H, Lalevee J, Barner-Kowollik Ch, Stenzel MH, Xiao P. Delivery of amonafide from fructose-coated nanodiamonds by oxime ligation for the Treatment of Human Breast Cancer. *Biomacromolecules*. 2018;19(2):481-489. DOI:10.1021/acs.biomac.7b01592

121. Dolmatov VYu. *Biologically active ultrafine detonation synthesis diamonds*. Russian Federation patent 2,203,068. 27 April 2003. (In Russ.)

122. Dolmatov VYu, Kostrova LN. Detonation-synthesized nanodiamonds and the possibility to develop a new generation of medicines. *Journal of Superhard Materials*. 2000;3:79-82.

Информация об авторах / Information about the authors

Долматов Валерий Юрьевич, доктор технических наук, начальник научно-исследовательской лаборатории, ФГУП «Специальное конструкторско-технологическое бюро «Технолог», Санкт-Петербург, Российская Федерация; ORCID 0000-0001-8643-0404; e-mail: diamondcentre@mail.ru

Шамес Александр Исаакович, Ph.D., старший исследователь, Университет им. Бен Гуриона в Негеве, Беэр-Шева, Израиль; ORCID 0000-0002-0574-1911; e-mail: sham@bgu.ac.il

Эйджи Осава, профессор, президент, NanoCarbon Institute Co., Ltd., Японский национальный университет в префектуре Нагано, Уэда, Япония; ORCID 0000-0002-1147-0898; e-mail: osawa@nano-carbon.jp

Аско Веханен, Ph.D., директор, Carbodeon Ltd. Oy, Вантаа, Финляндия; AuthorID (Scopus) 6701383667; e-mail: asko.vehanen@carbodeon.com

Valerii Yu. Dolmatov, D. Sc. (Engineering), Head of research laboratory, Special Construction and Technology Bureau “Technolog”, St. Petersburg, Russian Federation; ORCID 0000-0001-8643-0404; e-mail: diamondcentre@mail.ru

Alexander I. Shames, Ph.D., Senior Researcher, Ben-Gurion University of the Negev, Beer-Sheva, Israel; ORCID 0000-0002-0574-1911; e-mail: sham@bgu.ac.il

Eiji Osawa, Professor, President of NanoCarbon Research Institute Limited, Shinshu University, Ueda, Japan; ORCID 0000-0002-1147-0898; e-mail: osawa@nano-carbon.jp

Asko Vehanen, Ph.D., Director, Carbodeon Ltd. Oy, Vantaa, Finland; AuthorID (Scopus) 6701383667; e-mail: asko.vehanen@carbodeon.com

Веса Мюлльмяки, Ph.D., главный исполнительный директор, Carbodeon Ltd. Oy, Вантаа, Финляндия; AuthorID (Scopus) 55627561500; e-mail: vesa.myllymaki@carbodeon.fi

Дорохов Александр Олегович, главный инженер, АО «Завод «Пластмасс» Копейск, Российская Федерация; AuthorID (Scopus) 57209505072; e-mail: aldor7174@icloud.com

Марчуков Валерий Александрович, кандидат химических наук, ведущий инженер-конструктор, ФГУП «Специальное конструкторско-технологическое бюро «Технолог», Санкт-Петербург, Российская Федерация; AuthorID (Scopus) 7801670746; e-mail: marvalal@yandex.ru

Козлов Анатолий Сергеевич, кандидат химических наук, начальник НПК-2, ФГУП «Специальное конструкторско-технологическое бюро «Технолог», Санкт-Петербург, Российская Федерация; AuthorID (Scopus) 7402290001; e-mail: tool999@yandex.ru

Нарыжный Сергей Юрьевич, инженер-конструктор I категории, ФГУП «Специальное конструкторско-технологическое бюро «Технолог», Санкт-Петербург, Российская Федерация; e-mail: sergei.nar@bk.ru

Смирнова Анастасия Захаровна, инженер-исследователь 3 категории, ФГУП «Специальное конструкторско-технологическое бюро «Технолог», Санкт-Петербург, Российская Федерация; e-mail: 1nasty5smir1@mail.ru

Vesa Myllymäki, Ph.D., CEO, Carbodeon Ltd. Oy, Vantaa, Finland; AuthorID (Scopus) 55627561500; e-mail: vesa.myllymaki@carbodeon.fi

Alexander O. Dorokhov, Chief Engineer, JSC “Plant” Plastics”, Kopeysk, Russian Federation; AuthorID (Scopus) 57209505072; e-mail: aldor7174@icloud.com

Valerii A. Marchukov, Cand. Sc. (Chemistry), Leading Design Engineer, Special Construction and Technology Bureau “Technolog”, St. Petersburg, Russian Federation; AuthorID (Scopus) 7801670746; e-mail: marvalal@yandex.ru

Anatoly S. Kozlov, Cand. Sc. (Chemistry), Head of NPK-2, Special Construction and Technology Bureau “Technolog”, St. Petersburg, Russian Federation; AuthorID (Scopus) 7402290001; e-mail: tool999@yandex.ru

Sergey Yu. Naryzhny, 1^{cat.} Design Engineer, Special Construction and Technology Bureau “Technolog”, St. Petersburg, Russian Federation; e-mail: sergei.nar@bk.ru

Anastasia Z. Smirnova, 3^{cat.} Research Engineer, Special Construction and Technology Bureau “Technolog”, St. Petersburg, Russian Federation; e-mail: 1nasty5smir1@mail.ru

Received 13 January 2021; Accepted 26 February 2021; Published 21 April 2021



Copyright: © Dolmatov VYu, Shames AI, Ōsawa E, Vehanen A, Myllymäki V, Dorokhov AO, Martchukov VA, Kozlov AC, Naryzhny SYu, Smirnova AZ, 2021. This article is an open access article distributed under the terms and conditions of the Creative Commons Attribution (CC BY) license (<https://creativecommons.org/licenses/by/4.0/>).

Территория распространения – Российская Федерация, зарубежные страны.
Distributed in the Russian Federation and foreign countries.

Оригинал-макет подготовлен в Издательском центре ФГБОУ ВО «ТГТУ»,
392032, Тамбовская обл., г. Тамбов, ул. Мичуринская, д. 112А

Подписано в печать 31.03.2021. Дата выхода в свет 21.04.2021

Формат 60×90/8. Усл. печ. л. 10,0. Уч.-изд. л. 10,32. Тираж 100 экз. Цена свободная. Заказ № 016.

СМИ журнал “Journal of Advanced Materials and Technologies”

(Журнал современных материалов и технологий) выпуск 2021. Том 6, № 1.

Материалы журнала доступны по лицензии Creative Commons “Attribution” («Атрибуция») 4.0 Всемирная (CC BY 4.0)

All the materials of the “Golden Horde Review” are available under the Creative Commons License “Attribution” 4.0 International (CC BY 4.0)

